INSIGHTS

Industry challenges demand technical insight

Managing geological risk in deepwater drilling

Schlumberger

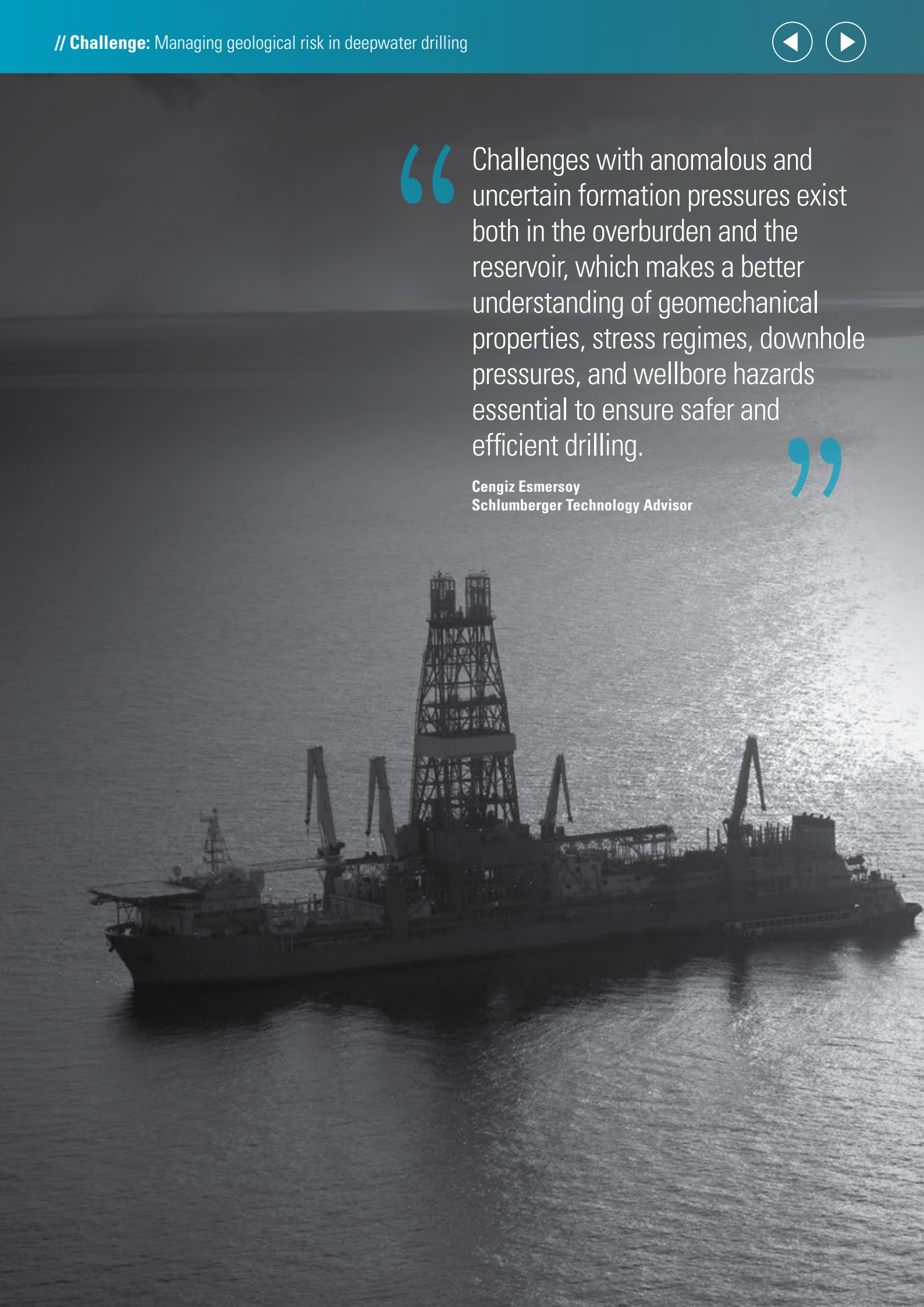

> Challenges with anomalous and uncertain formation pressures exist both in the overburden and the reservoir, which makes a better understanding of geomechanical properties, stress regimes, downhole pressures, and wellbore hazards essential to ensure safer and efficient drilling.

Cengiz Esmersoy
Schlumberger Technology Advisor

Welcome to *Insights*, a journal created to provide insights on specific industry challenges by bringing together a selection of recent complementary papers and articles by various Schlumberger technical experts. This issue focuses on some of the challenges in planning for and managing geological risk in deepwater drilling.

Deepwater field developments represent the most complex and capital-intensive projects undertaken by the industry, with a unique set of challenges linked to drilling operations. Costs of drilling deepwater wells can be more than triple those of shallow-water wells. More advanced and sophisticated measurement and drilling tools and technologies are needed to reduce risk in all aspects of operations, from drilling to production.

Deepwater and ultradeepwater projects often involve complex subsurface structures such as salt bodies or overlying basalt layers that can obscure reservoir features. In addition, the costs involved often contribute to limiting the offset well information to adequately constrain the subsurface interpretations. At the same time, challenges with anomalous and uncertain formation pressures exist both in the overburden and the reservoir, which makes a better understanding of geomechanical properties, stress regimes, downhole pressures, and wellbore hazards essential to ensure safer and efficient drilling.

Using advanced seismic data and expertise to plan well trajectories and locations is subject to uncertainties in the interpretation, particularly below complex overburden. Faster and accurate modeling and data processing enable MWD to form a constraint on the interpretation and facilitate rapid reimaging of the surface seismic data to redefine the target, hazards, and pore pressures ahead of the bit. This enables decisions to be made based on new information from the well being drilled—essentially using the new well as a perfect "offset well" for well control in seismic processing and interpretation.

Traditional methods—often applied in siloed workflows—are increasingly failing to deliver the necessary constraint in the earth models to improve safety while successfully and efficiently positioning wells in the right place for the entire life of the reservoir. An integrated approach—bringing together the multidisciplinary services, measurements, and expertise required for successful deepwater operations—is shown to be crucial to overcoming these limitations. Experience has shown that such integrated projects with a well-coordinated point of control benefit from lower NPT and considerable project AFE savings.

In this issue of *Insights* we have selected some recently published papers that address the challenge of managing geological risk in deepwater drilling.

Inside *Insights*

In this issue of *Insights* we have selected some recently published papers that address the challenge of planning for, and managing, geological risk in deepwater drilling.

Target selection and well planning

The first paper (page 4) addresses the reduction of deepwater exploration risk offshore Brazil by examining the benefits of integrating seismic and deep-reading electromagnetics data.

The following paper (page 8) shows how a 3D mechanical earth model is developed in order to evaluate the stresses caused by an overlying salt structure in the Gulf of Mexico. The model is used to minimize risks associated with deepwater well location planning, drilling and casing design.

The article on page 18 provides an overview of how software platforms can be used for all planning phases, including well location selection and predrill planning.

The paper on page 20 provides an insight to planning and drilling an inclined ultradeep water well based on a 1D mechanical earth model that has been derived from formation evaluation information from other wells in the area. A case study for a deepwater well offshore India highlights the value of a real-time geomechanics workflow.

Well planning optimization during operations

The following paper (page 30) illustrates how sonic and borehole seismic data acquired on wireline and while drilling are used to achieve higher accuracy in planning salt exit points, particularly important for casing setting and drilling depth prediction.

The paper on page 34 highlights a Gulf of Mexico case study where a seismic-guided drilling workflow is used to update the predrill earth model in real time based on data acquired during drilling operations. The objective is to reduce drilling uncertainties and improve prediction ahead of the bit.

The paper on page 40 discusses how contingency plans—coupled with an evaluation of pore pressure uncertainties—are used in conjunction with a ream-on-demand system to avoid unnecessary bottomhole assembly trips in a deepwater well in the Gulf of Mexico.

The final paper (page 46) discusses how predrill planning coupled with real-time assessment was crucial in drilling an exploratory well around and beneath a complex salt body.

Find out more at slb.com/deepwater

Contents

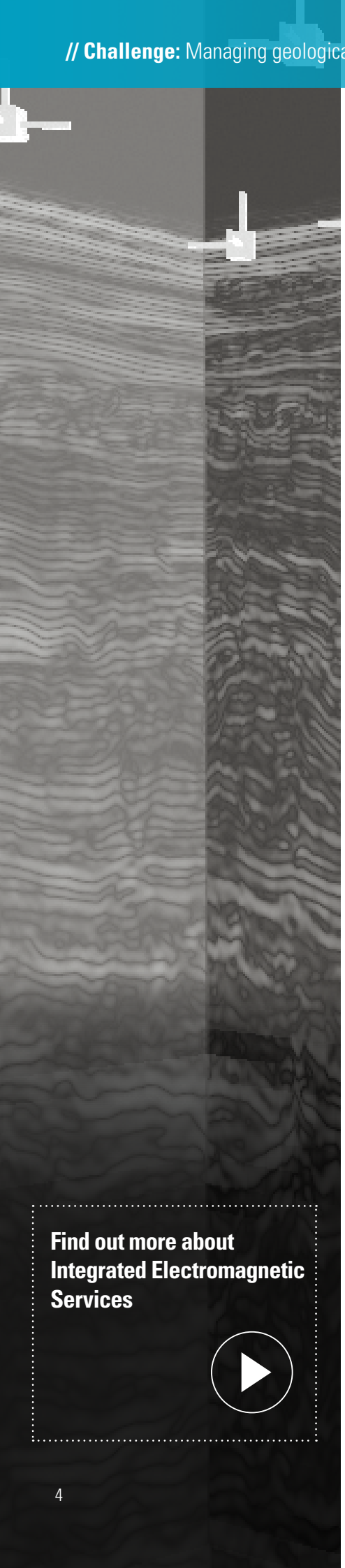

Seismic: Deep-Reading Electromagnetics Integration

takes on deepwater risk.

Deep water is a complex high-risk environment with no shortcuts to success. Formidable risks must be addressed and mitigated to meet deepwater objectives. Cooperative joint inversion (CJI) and simultaneous joint inversion (SJI) of seismic and deep-reading electromagnetics (EM) provide a powerful tool for the risk mitigation process. This work gives case examples for the application of seismic deep-reading EM integration to locate the most promising deepwater prospects, to reduce uncertainties, and minimize timescale and costs. It underlines the importance of using all available seismic and EM information in the integration of the data, including a rock physics framework to be either numerically derived or empirically calibrated at well locations.

We show that 'state-of-the-art' CJI and SJI of seismic and EM data are consistently proving to lower exploration risk while maximizing knowledge of the prospects in the deep Brazilian offshore where challenges, logistics, and costs can be formidable.

Today's agenda: Deepwater oil and gas

Exploration is moving into deeper waters, and while rich potential is driving the search ever deeper, the challenges and risks involved are also being amplified dramatically. The oil and gas industry has long realized that information is the greatest tool in mitigating risk. By understanding more about what lies beneath the surface, the risk of drilling a dry hole is reduced. With deepwater marine drilling costs topping USD 1 million per day, anything that can increase the margin of success is welcomed. A balance must be struck between the cost of gathering more information and the impact this information will have on decisions made further along in the process. The latest developments in high-tech seismic vessels and 'mega' channel counts have driven a revolution in seismic data quality and accuracy, as have the post-processing and interpretation tools at the industry's disposal. TTI reverse time migration (RTM) and full waveform inversion (FWI) are enabling geoscientists to image large volumes of reservoir quality rocks, even in complex geologies. The availability of low-frequency, long-offset full-azimuth datasets and increased compute power has now allowed FWI to become the preferred method for building detailed velocity models. Still, even with all these advanced techniques, certain exploration challenges remain.

Integration to create value and cut costs

Today, workflows are being developed to integrate technologies that reduce the exploration risk in demanding deepwater environments.

Find out more about Integrated Electromagnetic Services

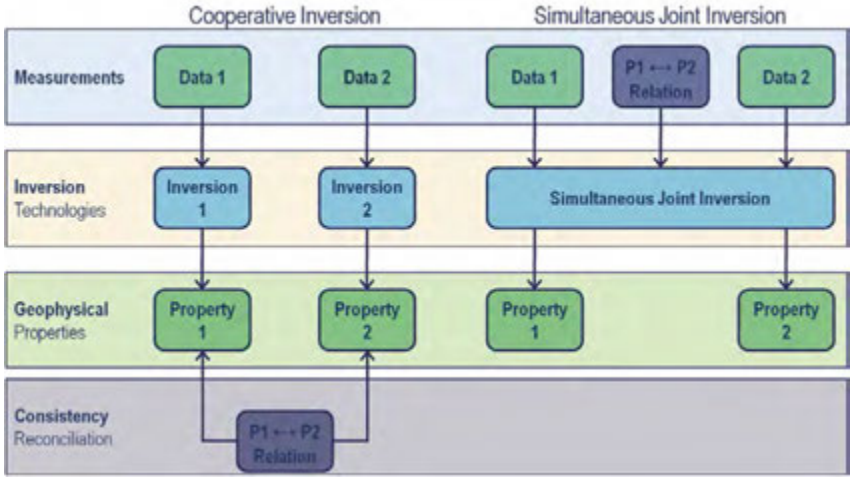

Figure 1: Cooperative and simultaneous joint inversion approaches.

Using all available seismic and deep-reading electromagnetics data to consistently lower exploration risk while maximizing knowledge of prospects in deep water offshore Brazil.

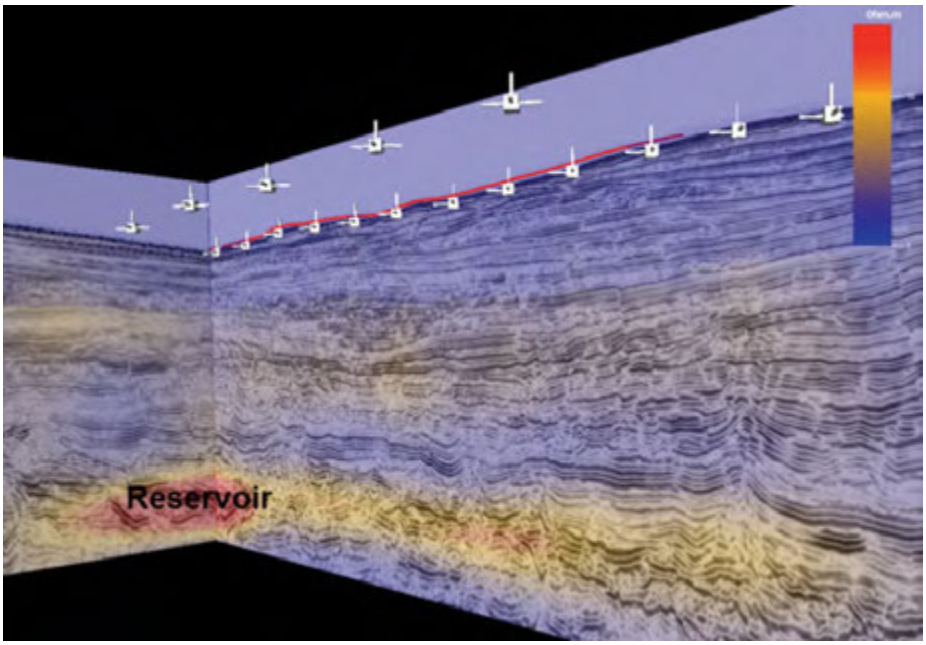

Figure 2: 3D integrated inversion of seismic—CSEM data from the Potiguar basin. Resistivity features are correctly located in depth and indicate the presence of hydrocarbon within the structures to help improve exploration decisions.

The approach is to develop geologically-sound earth models consistent with all of the available data types, then enhance the model by the application of complementary measurements until exploration risk is reduced to acceptable levels.

While all of the seismic tools mentioned above tell a large part of the exploration story, many information gaps may be filled in with deep-reading EM methods. Seismic techniques may predict the presence of hydrocarbons in a formation, but one of the biggest predrill knowledge gaps is formation resistivity. Formation resistivity is one of the most reliable indicators of hydrocarbon saturation levels within a formation structure. Previously this information has only been available through well logs, but now deep-reading EM is providing subsurface resistivity information before drilling.

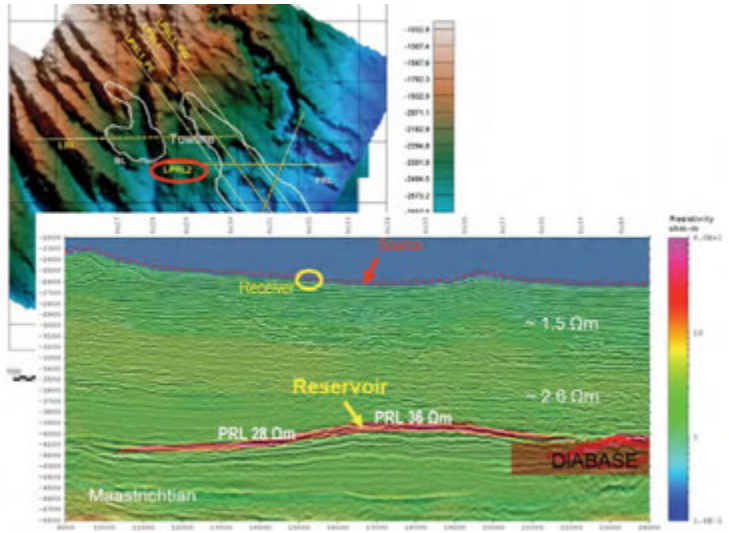

Figure 3: Cooperative inversion of seismic—CSEM data from the Sergipe-Alagoa basin. Vertical resistivity depth-section corendered with seismic. Seismic interpretation used to structurally constrain the inversion. Resistivity features are correctly located in depth and indicate the presence of hydrocarbon within the structures to help improve exploration decisions.

CSEM: A coming-of-age tool for risk reduction

Controlled source electromagnetics (CSEM) is an active deep-reading EM technology that images resistive structures beneath the seafloor. Resistivity changes caused by the displacement of high-resistivity hydrocarbons by far less resistive salt water are generally greater in relative terms, than the sound velocity changes (Eidesmo et al., 2002 and Ellingsrud et al., 2002). Therefore, CSEM data can provide additional information to determine the hydrocarbon saturation more accurately.

CSEM uses a manmade source to control and fine-tune the measured field to the target being imaged. The fine-tuning of the source allows the survey to be designed precisely so that it can illuminate rocks that are suspected of bearing hydrocarbons. The CSEM data reveals information about subsurface resistivity. When correlated with seismic, resistive structures can be imaged and discriminated from host rocks. After integration into the geologic model, CSEM data can reduce the uncertainty of promising drilling targets.

Using models developed from seismic, CSEM data are used to help prioritize the prospects. The combination of seismic and CSEM clearly delineates the resistive structures within the prospects enabling structures of interest to be prioritized and to assist in the task of ranking potential drilling leads.

Multimeasurement-constrained imaging: Clearer delineation of prospects

Several approaches can be adopted to exploit the electrical properties for a) deepwater prospect identification and evaluation; and b) building a velocity model that bridges the gap between the low frequencies and long offsets acquired in the data. In a CJI approach, seismic and EM model building are carried out in parallel and the results mutually utilized in an iterative fashion to constrain both datasets.

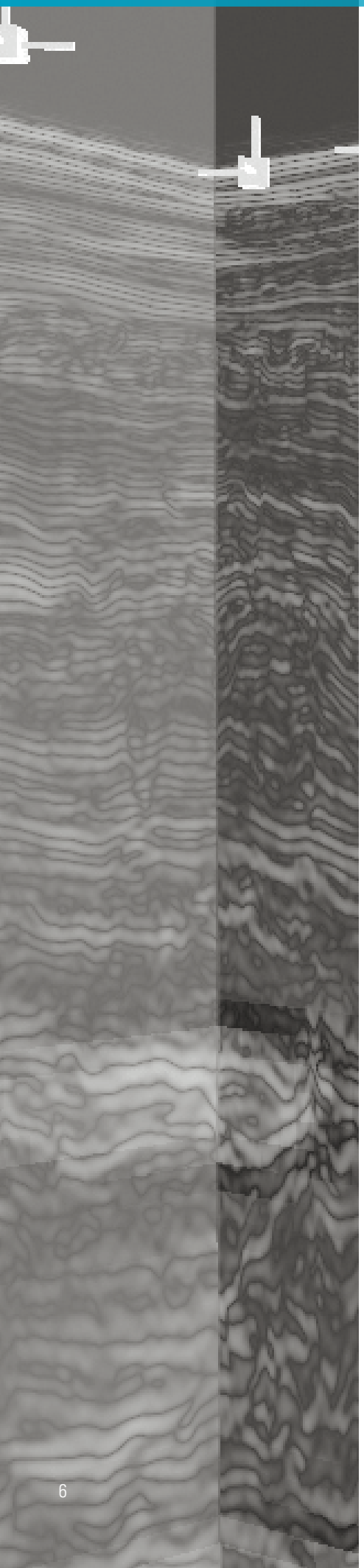

Another approach is the so-called SJI approach. In this case, with respect to the cooperative approach, the two datasets, seismic, and EM, are inverted together: The inversion process will not only minimize the misfit between observed and model-predicted synthetic data for both datasets, but will also minimize the differences between different properties of a single multi-property earth model, according to geometrical or petrophysical relationships between the geophysical properties (Figure 1) [Colombo, De Stefano (2007), De Stefano et al., (2011)].

In SJI, each inverted method is used to stabilize the others. In fact, all the methods illuminate the same subsurface formations but they are characterized differently in terms of penetration and resolution, and more importantly in terms of noise. Therefore, a particular portion of the subsurface that may be scarcely recovered by one method may be, on the other hand, recovered reliably by another. Combining the complementary information from the various methods allows the recovery of an underlying earth model with reduced uncertainty.

In the case studies we present, we show how these approaches enable a quicker and more robust method to build a reliable earth model that can be used to produce better images. The SJI multi-property model also provides the interpreters consistent co-located multiple properties of the subsurface that are keys for clearer delineation of prospects and better potential for hydrocarbon saturation and volume estimations.

A necessary condition for the applicability of the SJI technique is the existence of patterns linking seismic properties and resistivity. These patterns are expressed in terms of structural relations by means of the cross-gradient function and/or numerically derived or empirical functions that can be derived directly from well log analysis. A valuable result of SJI is also a multiple property earth model which benefits from resistivity characteristics for reservoir-scale formations while maintaining the resolution of seismic, which in turn yields information on pore fluid.

Seismic: EM cooperative joint inversion (CJI) and SJI at work—The Brazilian deepwater experience

Seismic EM integration through CJI and SJI has been applied extensively by Petrobras over several distinct geological settings of the deep Brazilian offshore. In this work we present the potential of this integration over selected case histories and demonstrate the value of the integrated interpretation based on the joint inversion of seismic and CSEM data (Figure 2 through 6).

We show that these new integrated workflows lead to location of the most promising deepwater prospects, then minimize the technical and economic risks. Specific challenges and limitations such as ambiguities in reconstructing a prospect's depth, resolving stacked objectives, and imaging uncertainties for prospects in the proximity of salt or in rough bathymetry are addressed. Models with remarkable structural resemblance and improved estimates of electrical resistivity and seismic properties are reconstructed, significantly reducing the artifacts observed in the resistivity and seismic models obtained from the standalone interpretation. The most promising deepwater prospects are accurately delineated showing more geometrical similarity between the resistivity images and the seismic images, as well as reproducing the true features, electrical resistivities, and seismic properties.

We show that 'state-of-the-art' CJI and SJI of seismic and EM data are consistently proving to lower exploration risk while maximizing knowledge of the prospects in the deep Brazilian offshore where challenges, logistics, and costs can be formidable.

Conclusions

We have shown case examples for the application of seismic deep-reading EM integration to locate the most promising prospects in the deep Brazilian offshore, to reduce uncertainties, and to minimize timescale and costs.

We have underlined the ability of 'state-of-the-art' cooperative and simultaneous joint inversion to leverage seismic and accommodate complex geologies, ensuring robust and reliable models and improved property modeling.

'State-of-the-art' joint inversion of seismic and EM data is defining new strategies for deepwater prospect identification and evaluation, thereby enhancing the role of non-seismic methods. Applications relevant for the later stages of petroleum operations are being addressed in quantitative reservoir characterization studies on real data and in feasibility studies for reservoir monitoring.

Acknowledgements

The authors thank Petrobras and Schlumberger for their support and willingness to share these results with the geophysical community. We also thank Paulo de Tarso Menezes, Luiz Felipe Rodrigues, and Celso Moura Jardin of Petrobras E&P for helpful discussions.

Main References

Buonora, M.P., Reddig, R., Zerilli, A., 2006. Marine Controlled Source Electromagnetics: The Campos Basin Experience, 2006 Offshore Technology Conference, 1–4 May, Reliant Center, Houston, Texas, U.S.A.

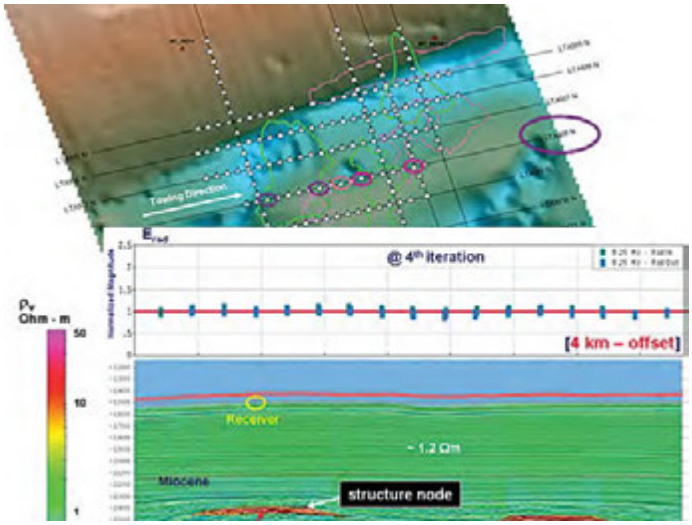

Figure 4: Cooperative inversion results of line LTAM08 Santos basin. Vertical resistivity depth section corendered with seismic. Seismic interpretation used to structurally constrain the inversion. The image shows a consistent background resistivity trend and reveals resistivity anomalies (red) within the reservoir's boundaries fixed in x and z at the seismic interpretation locations (closed structures nodes). The upper graph shows normalized magnitude at 0.25 Hz and +/- 4-km offset to final inversion model. The normalized graph shows that the data are well fit.

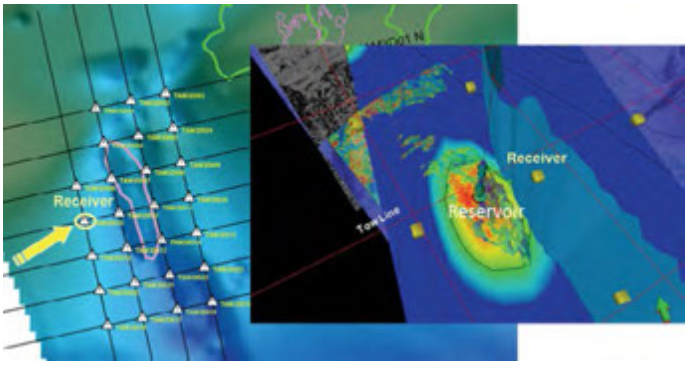

Figure 5: 3D integrated inversion of full-azimuth CSEM data from the Santos basin. Radial vs. azimuthal ratio confirming the presence of a hydrocarbon reservoir.

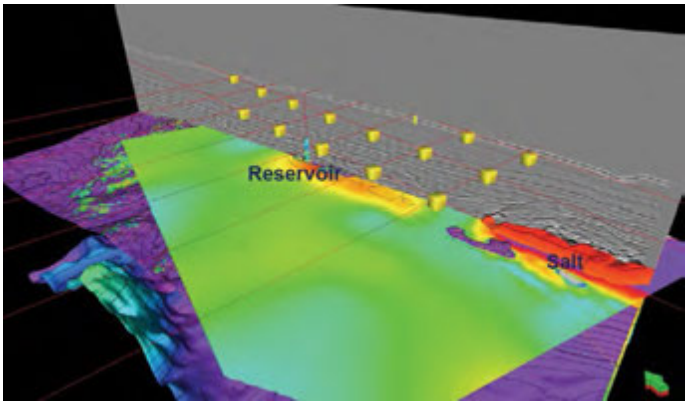

Figure 6: 3D integrated inversion of full-azimuth CSEM data from the Santos basin. Vertical resistivity slice quantifying resistivities, depth, and lateral extent of the reservoir.

Buonora, M.P., Zerilli, A. Labruzzo, T., 2006. Marine Controlled Source Electromagnetics: New Insights in Data Interpretation, "Deepwater Challenges in Exploration, Development and Production", Society of Exploration Geophysicist D&P/SBGf/ULG Deepwater Forum, Rio de Janeiro, Brazil.

Buonora, M.P., Zerilli, A., Labruzzo, T., Rodrigues, L.F., 2008. Advancing Marine Controlled Source Electromagnetics in the Santos Basin—Brazil, European Association of Geophysical Engineers, 70th Meeting and Technical Exhibition, Rome, Italy.

Buonora, M.P., Zerilli, A., Labruzzo, T., Rodrigues, L.F., 2008. Detecting Hydrocarbon Reservoirs From Marine CSEM in the Santos Basin—Brazil, 33rd IGC International Geological Congress, Oslo, August 6–14.

Buonora, M.P., Zerilli, A., Labruzzo, T., Menezes, P.T., Crepaldi, J., 2011. Hunting for Oil Under the Deep Brazilian Offshore Using mCSEM, AAPG International Conference & Exhibition, 23–26 October, Milan, Italy.

Colombo, D. and De Stefano, M., 2007, Geophysical Modeling via Simultaneous Joint Inversion of Seismic, Gravity, and Electromagnetic Data: Application to Prestack Depth Imaging, The Leading Edge, 26, 326–331.

De Stefano, M., Andreasi, F.G., Re, S., Virgilio, M., Snyder, F., 2011, Multiple-Domain, Simultaneous Joint Inversion of Geophysical Data with Application to Subsalt Imaging, Geophysics, 76, 69–80.

Eidesmo, T., S. Ellingsrud, L. M. MacGregor, S. Constable, M. C. Sinha, S. Johansen, F. N. Kong, and H. Westerdahl, 2002, Sea Bed Logging (SBL), A New Method for Remote and Direct Identification of Hydrocarbon-Filled Layers in Deepwater Areas: First Break, 20, 144–152.

Ellingsrud, S., M. C. Sinha, S. Constable, L. M. MacGregor, T. Eidesmo, and S. Johansen, 2002, Remote Sensing of Hydrocarbon Layers by Seabed Logging (SBL): Results from a Cruise Offshore Angola: The Leading Edge, 21, 972–982.

Zerilli, A., Labruzzo, T., Buonora, M.P., Menezes, P.T.L., Rodrigues, L.F., 2009. Advances in marine Controlled Source Electromagnetic: The Santos Basin Project—Brazil, Society of Exploration Geophysicist 79th Annual Meeting and Exposition, 25-30 October, Houston, Texas, 845–849.

Zerilli, A., Buonora, M.P., Labruzzo, T., Rodrigues, L.F., 2009. Integrated mCSEM Interpretation—Success Stories from the Brazilian Deep Waters, AAPG International Conference and Exhibition, Rio de Janeiro, Brazil, 15–18 November.

Zerilli A., 2010. Integration of Seismic and Electromagnetic Methods in Deep Water Exploration, SPE Applied Technology Workshop "Deep Sea Subsalt Reserves Potential and Associated Risks", Sharm El Sheikh, Egypt, 27–30 June.

Zerilli, A., Labruzzo, T., Buonora, M.P., Menezes, P. T .L. Rodrigues, L.F., Lovatini, A., 2010. 3D Inversion of Total Field mCSEM Data: The Santos Basin Case Study, Society of Exploration Geophysicist 80th Annual Meeting and Exposition , 17–22 October , Denver, Colorado, 629-633.

Zerilli, A., Buonora, M.P., Labruzzo, T., 2011. Enhancing the Resolution of mCSEM Data Using a Hybrid-Based Inversion Workflow, European Association of Geophysical Engineers, 73rd Conference & Exhibition, Vienna, Austria, 23–26 May.

Zerilli, A., 2012. Deep-Reading Electromagnetics for Reservoir Characterization and Monitoring, Special Session, Technological Development in Reservoir Characterization and Monitoring, Rio Oil and Gas Expo and conference 2012, Rio de Janeiro, September 17–20.

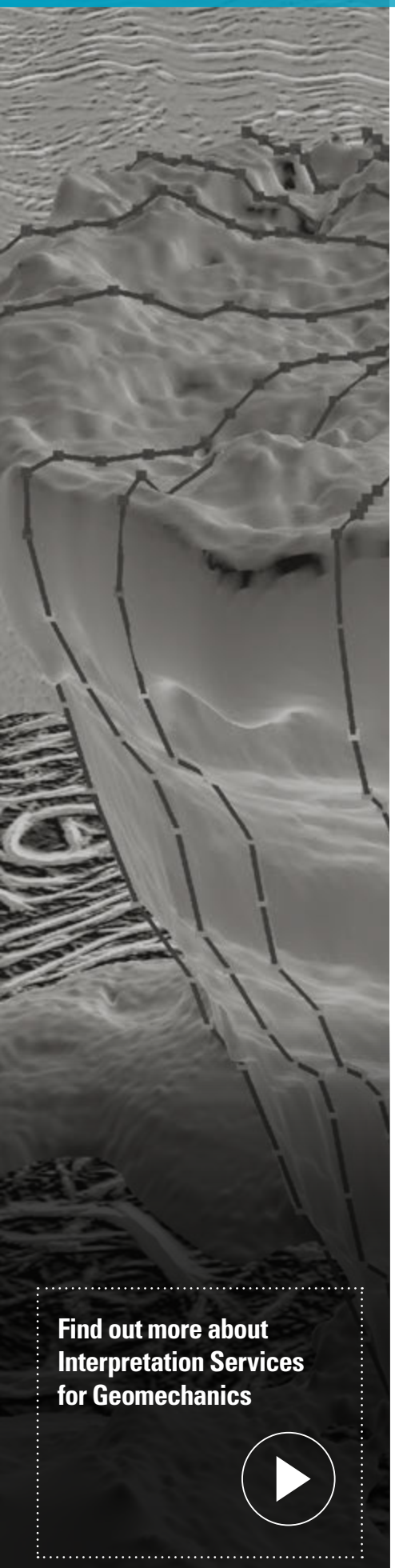

Find out more about Interpretation Services for Geomechanics

Iterative 3D Geomechanical Modeling

to determine distribution and impact of stresses in deepwater Gulf of Mexico subsalt and near-salt environments.

A 3D finite-element model (FEM), covering an area of 300 km^2 in the deepwater Gulf of Mexico, was used to determine the stress distribution around salt structures, and to study the impact on well design decisions. A 3D model was necessary to accurately determine the full stress tensor (i.e., changes of stress magnitude and orientation around the salt body). An iterative workflow to fine-tune properties and stresses has been developed to validate wellbore failure and to explain drilling events. The 3D FEM was built using a geological model, high-quality seismic velocity data, and results from 1D mechanical earth models.

The model indicates that the stress magnitude and orientation are modified by salt morphology. In particular locations at the salt/sediment interface, this phenomenon resulted in significant stress rotation and high von Mises stress. In these circumstances, the safe drilling mud weight window can quickly disappear, forcing the operator to manage both wellbore instability and mud loss, and with no choice but to sidetrack or select a new well location.

The described case study illustrates the application of the 3D FEM, which was able to explain drilling events (including an abandoned wellbore), provide input for calculating the mud weight window (range between shear failure and minimum stress), and guide well design.

The significance of this study is that, as more well trajectories are drilled in these complex environments, robust, predictive 3D FEMs will be necessary to assess potential risk prior to drilling and to improve well planning.

Introduction

Many major discoveries in the deepwater Gulf of Mexico are located beneath thousands of feet of salt. This salt environment (supra- and subsalt) is characterized by complex geological structures and represents significant drilling challenges for operators. Many of these challenges have been described [1], and include drag zones composed of deepwater shales, low-strength strata and reactive shales, subsalt "rubble-" or breccia-like zones, and active or relict translation surfaces (faults and "gouge-zones"). These challenges are mostly associated with the sedimentary strata in the vicinity of the salt and sediment contact (e.g., fractured carapace facies in the suprasalt or at the lower salt interface), which is characterized by relatively low minimum stress and fracture gradient, perturbed vertical and horizontal stresses, horizontal stress anisotropy, and stress-arching [2-4].

The conventional industry-standard approach to estimate the stresses along a trajectory planned to reach a subsalt target mostly includes 1-dimensional (1D) analytical calculation of properties, pressures, and stresses. The intrinsic properties, formation pressures, and stress gradients are often migrated, from the existing offset wells to the planned well location, along geological markers. These simple assumptions and results do not explain and cannot predict drilling events around complicated salt environments because the assumptions that the largest compressive principal stress (P1) is vertical, that rotation of stresses around the salt body can be ignored, or that rock properties are laterally constant are generally erroneous.

Three-dimensional (3D) numerical simulation techniques have been developed for solving a complex set of equations with appropriate boundary conditions needed to estimate stresses and fluid pressures in salt environments [2, 5-8]. Detailed description and comparison of the modeling techniques is included in Luo et al. [4]. Numerical simulation to solve complex geomechanical problems has proven suitable; however, it has not become a routine practice due to the perceived lack of well information or lack of quality subsalt seismic velocity data prior to drilling, which makes the results uncertain. Furthermore, basin-wide models usually have low spatial resolution, so these models are considered to be mostly impractical by many for wellbore-centric studies. Finally, it is difficult to validate the results of a 3D model with wellbore data; therefore, the 3D results are often considered qualitative only.

In this paper, we describe a modeling approach in which 3D numerical simulation covering 300 km^2 (115.8 mi^2) was used to predict stresses around a salt body in a deepwater field in the Gulf of Mexico (Figure 1). While recent publications in which authors describe attempts to overcome the

3D stress modeling offers a quick-look tool to predict potential safe and unsafe drilling conditions for well location and casing design evaluation.

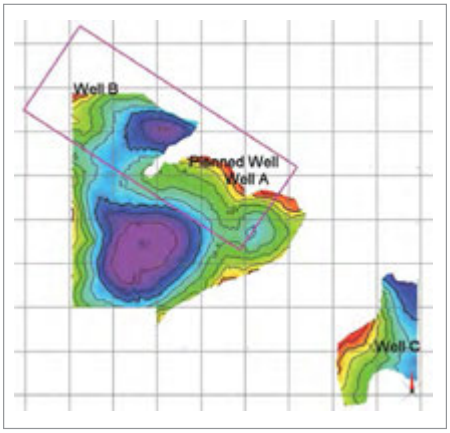

Figure 1: Location map of the study area (magenta rectangle) in the deepwater Gulf of Mexico showing available offset wells, A, B, and C, and the reservoir top surface in the background. Scale: 1 US offshore block is 4.8 km × 4.8 km (3 × 3mi).

shortcomings associated with spatial resolution or data quality by incorporating local gridding techniques [8, 9]; or well data and high-quality processed seismic interval velocity, respectively; we show examples that validate the 3D model by using wellbore data to explain drilling events. The calibrated iterative model was used to estimate the mud weight window for a planned well in the same prospect. The combined 3D models generated from well log-derived and locally-calibrated elastic properties, strength, pressures, and stresses provide a more realistic earth model in contrast to the past published stress models, which are mostly uncalibrated and are built on spatially constant properties (layer-cake).

2. Methodology: Iterative 3D modeling

2.1. Wellbore-centric modeling

1D mechanical earth models (MEMs) were constructed for three existing offset wells (A, B and C) in the area of interest (Figure 1). The MEM is defined as a mathematical representation of rock properties, pore pressure, and in situ stresses as a function of the depth for a particular interval. The development of the earth model followed a detailed workflow, which comprises ten steps [10]. Input data used to construct the models includes formation evaluation logs (compressional and shear velocity, gamma ray, density, neutron porosity, and checkshots) from wireline or logging-while-drilling operations; formation markers and lithology descriptions, drilling data with list of drilling events from offset wells, fluid and mud logging information, and petrophysical interpretations (porosity and volume of clay). Proprietary correlations for mechanical properties based on laboratory measurements on cores were adapted from a nearby field.

Pore pressures and stresses were derived from available wellbore density and sonic data, and calibrated against in-situ formation measurements and well events (kicks, results of leakoff test (LOT), and mud losses).

2.2. Field-centric modeling

Factors considered while building the 3D geological model for the study area included the structural complexity of the salt (overhangs), orientations (pinchout) of the reservoir sands relative to the base of salt, and the positions of existing offset wells. In addition to the 3D interpreted water bottom surface, the top and base of salt and the reservoir sand surfaces were used to generate the structural framework. In the framework model, truncation rules (e.g., erosional, base, discontinuous, and conformable) were accurately represented, as interpreted from the available seismic image data. A 3D MEM was generated on the basis of well-log-derived rock properties (1D MEMs) and the available 3D seismic data. In sections where well logs were not available due to the absence of logging operations, such as in the overburden, correlations were used to predict the required properties from the seismic velocity. The 3D MEM, which incorporated reservoir geometry and mechanical properties was exported from the geological model and imported into the finite element stress modeling routine of proprietary geomechanics modeling software [11]. The geological model was extended by adding sideburdens on the four vertical sides and the underburden (below the reservoir). This improved the model's aspect ratio and ensured a reasonable transfer of stresses within the reservoir and from the overburden in the preproduction stress phase of the modeling. The embedded model consisted of 148 × 72 × 358 I,J,K cells, for a total of 3.81 million cells.

Properties in the sideburden section were assumed constant for each layer and reflected average layer values. Properties in the underburden section were extended downward from the model bottom.

The initial stress state of the field was determined with the finite element geomechanics software [11]. Inelastic constitutive laws for sediments surrounding the salt were applied in multiple modeling runs, while the fluid pressures were derived from 3D seismic interval velocity data, using a velocity-to-pore-pressure transform. The Mohr-Coulomb plastic yield criterion was used to model intact rock behavior. Effective stresses were used during simulations, and then were added to pore pressure to obtain the total stresses according to the effective stress principle. The salt formation was modeled as a linear elastic perfectly-plastic material (with high Poisson's ratio, low Young's modulus, very low cohesion, and zero pore pressure) to ensure isotropic principal stresses within the salt formation.

The stress initialization process, similar to that used by Fredrich and colleagues [2], was performed in several discrete steps. First, rollers on the sides (allowing the model to move freely in the vertical plane) were introduced, while vertical motion of the base was prevented.
The model was subjected to gravity loading, with the appropriate pore pressure for sediments calculated separately. This loading induced a reaction at the base of the model. Second, the model was fixed at corner points and the stress from the first run was applied at the base. While the loads were applied, stresses were calculated on the sides of the model on the basis of the prescribed boundary conditions (ratio of the far field stresses S_h/S_H, where S_h is minimum horizontal stress, and S_H is maximum horizontal stress). Third, the boundary conditions were adjusted iteratively until a good match was achieved between the minimum principal stress (P3) and field data (mud losses and LOT data) at well locations within the model. The 3D stress model computes the six Cartesian components of the stress tensor (σ_{xx}, σ_{yy}, σ_{zz}, σ_{xy}, σ_{yz}, σ_{xz},) in each cell, from which the three orthogonal principal stresses and stress directions were determined (P1, P2, and P3).

Computed stresses inside the salt converged to an isotropic condition after relaxation.
This was verified by evaluating the ratio between the deviatoric stress q and the mean stress p inside the salt.

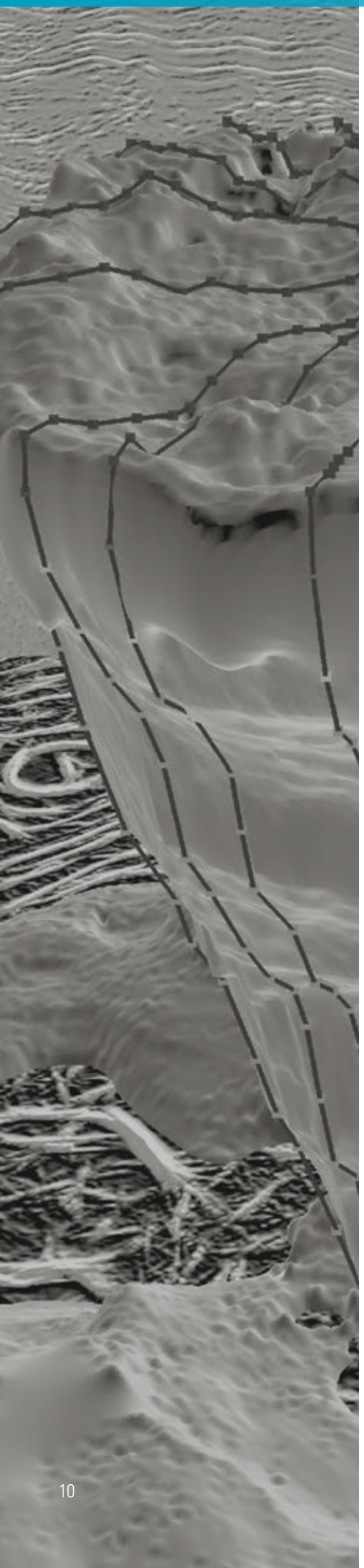

2.3. Iterative workflow

The stresses in the initial 1D MEMs were calculated assuming that the orientation of the largest principal stress was vertical and orthogonal to the intermediate and minimum principal stresses (i.e., P1 = S_V, P2 = S_H, and P3 = S_h) (Figure 2). Because of the absence of strength measurements from cores in the study area and there is no way to directly measure S_H, the unconfined compressive strength (UCS) and the horizontal stress ratio (S_h/S_H) were fine-tuned so that the calculated shear and tensile failure were consistent with oriented (four-arm) caliper, image logs, and reported drilling events (results of shoe tests and mud losses). The values of UCS and S_h/S_H had considerable uncertainty when imported into the stress model with the other properties, which include density (ρ), pore pressure (*Pp*), static Young's modulus (*E*), tensile strength (*T*), friction angle (ϕ), and Poisson's ratio (ν). The main outputs of the 3D stress model include the stress and strain tensors, from which principal stresses (effective and total), displacements, and deviatoric stresses were calculated (Figure 2). The six-component stress tensor, extracted from the 3D model along the wellbore trajectory, allowed the recalculation of the wellbore stresses (and shear and tensile failure) in a new 1D MEM, using inclined far-field stresses (P1', P2', and P3'). In this new 1D iteration, the far field stresses were fixed (P3' = P3) because it was calibrated by well events, and the UCS was further adjusted until the shear failure matched the profile of the oriented (four-arm) caliper, image logs, and was consistent with reported drilling events (tight hole, drag, and overpull). The last step of the workflow included the export of this updated UCS to the stress model (Figure 2).

3. Case study background

The area of interest is located in the deepwater Gulf of Mexico and covers 300 km^2 (115.8 mi^2) that includes approximately 13 US offshore blocks (Figure 1).

Drilling of the recent exploratory well, Well A, resulted in a serious well-control incident followed by mud losses, and finally loss of the wellbore before entering the salt body. The existing two other offset wells, Wells B and C, 17.7 km (11 mi) and 32.2 km (20 mi) away, respectively, successfully reached subsalt targets after considerable non-productive time. The planned well is located approximately 4.8 km (3 mi) to the northwest from Well A, and the play is defined by a three-way salt closure. There is a significant thickness variation of the suprasalt sedimentary sequence in the study area, varying from 370 m (1,200 ft) at Well B to 1,830 m (6,000 ft) at the planned well and Well A. Well A was drilled on the top of a local salt high that plunges steeply toward a minibasin to the southeast, which is filled with up to 4,900 m (16,000 ft) of thick suprasalt sedimentary rocks that onlap the salt body. The thickness of the salt varies from 500 to 8,000 m (1,400 to 26,000 ft) and is characterized by a high width-to-height aspect ratio within the study area and has no significant salt overhangs (therefore simplifying the construction of the geological model).

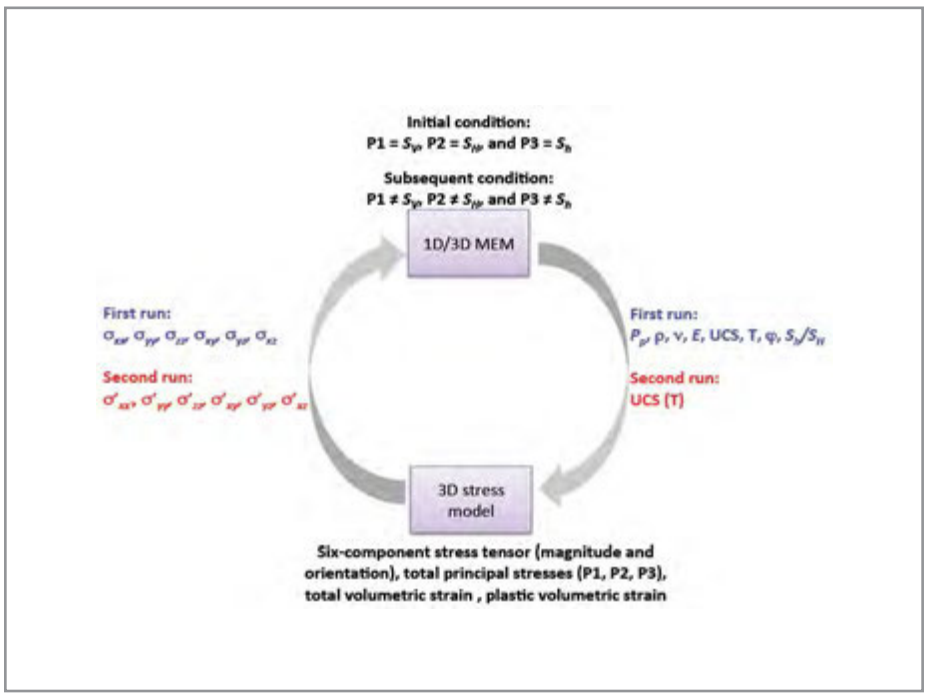

Figure 2: Schematic workflow showing the iterative approach applied during the execution of the study. See text for explanation of symbols.

4. Results

1D properties, pressures, and sand stresses were calculated from well log data. In sections in which well logs were not available due to the absence of logging operations, such as in the overburden, correlations were used to predict the required properties from the seismic velocity data. These properties were calibrated using available wellbore data, and validated within the geological model for consistency, as described below.

4.1. Mechanical properties

As with all mechanical properties, local correlations from core are preferred for calibrating log mechanical properties. For this study, however, no core data were available for calibration; therefore a proprietary correlation, defined for an adjacent field, was used to establish the static Young's modulus:

$$E_{sta} = (a - b\phi)E_{dyn} \quad \textbf{1.}$$

where E_{sta} is the static Young's modulus, a and b are calibration parameters, ϕ is total porosity, and E_{dyn} is the dynamic Young's modulus. The dynamic Young's modulus is obtained from the density ρ, the compressional wave velocity V_p, and the shear wave velocity V_s:

$$E_{dyn} = \rho V_s^2 \left(\frac{3\,V_p^2/V_s^2 - 4}{V_p^2/V_s^2 - 1} \right) \quad \textbf{2.}$$

where the density and velocities are in consistent units. To calculate the static Poisson's ratio ν from the sonic data, the following correlation was used:

$$\nu = a \times \nu_{dyn} \quad \textbf{3.}$$

where a is a locally derived calibration parameter. In the above equation, ν_{dyn} is the dynamic Poisson's ratio, obtained using the compressional velocity and the shear wave velocity according to

$$\nu_{dyn} = \frac{V_p^2 - 2V_s^2}{2(V_p^2 - V_s^2)} \quad \textbf{4.}$$

The same correlations for Young's modulus and Poisson's ratio were used for both sands and shales. Because no laboratory measurements of rock strength were available in any of the offset wells, a proprietary correlation, defined for an adjacent field, was used for sands and shales. For rock strength, Horsrud-type [12] equations were defined for sand and shales and expressed as

$$UCS_{sand\,/shale} = a + bV_p^C \quad \textbf{5.}$$

where the unit of UCS is expressed in psi units, Vp is in ft/s, and a, b, and C are calibration parameters for sand and shale. Because the original equation was defined in units of MPa and Vp in km/s, unit conversion parameters were used for consistency.

The friction angle φ was according to the method in Plumb [13], which is valid for both grain-supported and clay-supported rocks; whereas the tensile strength was estimated as 10% of the UCS for both sand and shale. The results of the mechanical property profiles (elastic properties and rock strength) along the trajectories of Well A and Well B are shown in Figure 3 and Figure 4, respectively.

The salt lithology was assumed to be made up exclusively of halite and was modeled with properties published previously [8, 14].

The 3D MEM containing key elastic properties and rock strength was generated on the basis of well log-derived rock properties, and the available 3D seismic interval velocity volume was used where log data were not available. Poisson's ratio for the suprasalt sands and shales was correlated with V_p and expressed as

$$\nu = -0.0004 \times V_p + 0.62493 \quad \textbf{6.}$$

where V_p is in ft/s, and ν is dimensionless.

Static Young's modulus for the suprasalt sands and shales was correlated with V_p and expressed as

$$E = 0.003 \times e^{0.00082 \times V_p} \quad \textbf{7.}$$

where E in Mpsi, V_p is in ft/s.

4.2. Pore pressure

The pore pressure model was built for the area of interest using the seismic interval velocity from the E-Wave* advanced imaging project volume provided by WesternGeco [e.g., 15]. The accuracy of the seismic velocity was investigated at the available offset well locations as described in the Appendix.

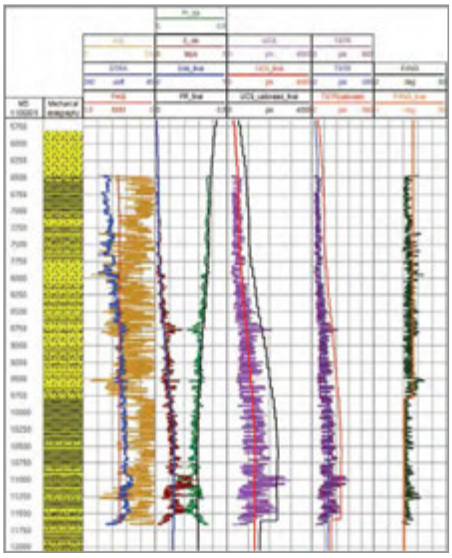

Figure 3: Profiles of elastic properties and rock strength calculated from compressional and shear velocities and density logs in Well A. Track 3: input data; Track 4: static Young's modulus and Poisson's ratio; Track 5: UCS; Track 6: tensile strength; Track 7: friction angle. The extractions of the same static properties from the 3D MEM (thick blue, red, black and orange curves in Tracks 4–7) are shown for quality check.

The velocity-to-pore pressure transform was calibrated using available pressure measurements—MDT pressures, mud weight and equivalent circulating density (ECD) data—and drilling events from the existing offset wells.

In this study, the method of Eaton [16] was employed, which estimates the vertical component of effective stress σ obtained from the P-wave seismic interval velocity, v, according to the relation:

$$\sigma = \sigma_{normal}\ (V/V_{normal}\ )^n \quad \textbf{8.}$$

where σ_{normal} and V_{normal} are the vertical effective stress and seismic velocity that would occur if the sediment was normally pressured, and n is an exponent controlling the sensitivity of velocity to effective stress; in the current study $n = 3$. To use Eaton's method, the deviation of velocity from V_{normal} and the velocity of normally pressured sediments must be estimated. This was obtained by fitting the sonic log to an analytical function of the form proposed by Galperin [17]:

$$V(z) = V_0(1 + bz)^{1/a} \quad \textbf{9.}$$

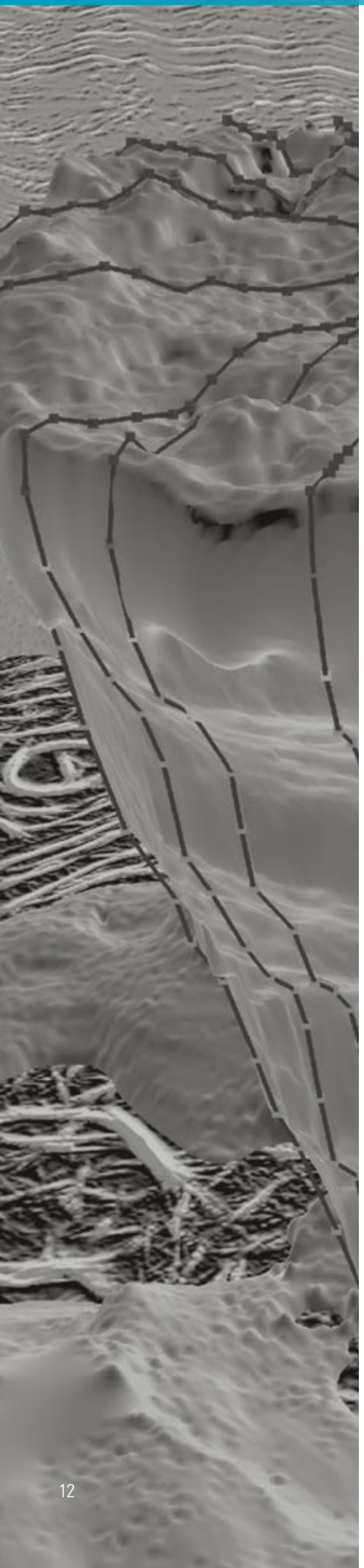

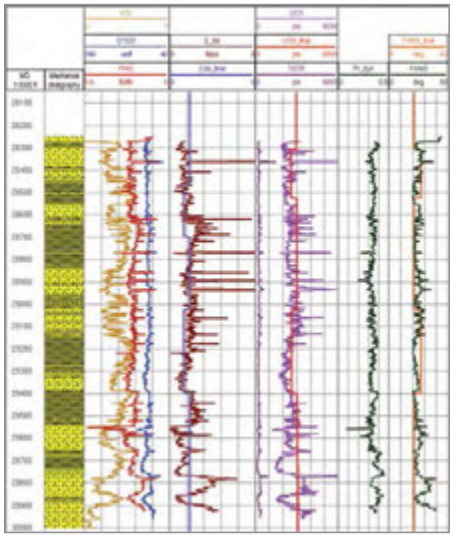

Figure 4: Profiles of elastic properties and rock strength calculated from compressional and shear velocities and density logs in Well B. Track 3: input data; Track 4: static Young's modulus; Track 5: UCS and tensile strength; Track 6: Poisson's ratio; Track 7: friction angle. The extractions of the same static properties from the 3D MEM (thick blue, red and orange curves in Tracks 4, 5, 7) are shown for quality check.

A composite pore pressure transform was used to estimate the pore pressure distribution in the area of interest, and consisted of fitting parameters for the subsalt reservoir section and for the supra- and subsalt shales. This calculated pore pressure, as also observed for Well C, indicated a significant pressure reversal below the salt. The phenomenon has been widely described in the deepwater Gulf of Mexico [e.g., 18].

4.3 Vertical stress

The vertical component of the total stress, S_V, at any point was assumed to be given by the combined weight of the rock matrix and the fluids in the pore space overlying the interval of interest. This may be calculated from an integral of density:

$$S_V(z) = g\int_0^z \rho_b(z)dz + \rho_w g z_w \quad \textbf{10.}$$

where S_V is the overburden stress (psi units), g is the acceleration due to gravity, ρ_w is the sea water density (assumed to be 1.03 g/cm^3), z_w is the water depth, z is the true vertical depth (TVD, ft) below mud line ($z = TVD - z_w - z_a$), and z_a is the height of kelly bushing above the sea surface. In the absence of a density log, ρ_b in the suprasalt section was estimated using the Amoco equation [19]. This can be expressed as

$$\rho(z) = \rho_0 + a \times z^b \quad \textbf{11.}$$

where the unit for ρ_b is g/cm^3; $\rho_0 = 1.6$ g/cm^3, $a = 0.053$, $b = 0.28$, and z is TVD below the mudline.

4.4. Horizontal stresses

The magnitude of the minimum horizontal stress (S_h) in the 1D MEMs was calculated using the poro-elastic equation including the effect of tectonic strains, which can be expressed as [20]

$$S_h - \alpha P_p = \frac{\nu}{1-\nu}(S_V - \alpha P_p) + \frac{E}{1-\nu^2}\varepsilon_h + \frac{E\nu}{1-\nu^2}\varepsilon_H \quad \textbf{12.}$$

$$S_H - \alpha P_p = \frac{\nu}{1-\nu}(S_V - \alpha P_p) + \frac{E}{1-\nu^2}\varepsilon_H + \frac{E\nu}{1-\nu^2}\varepsilon_h \quad \textbf{13.}$$

where α is Biot's coefficient, P_p is the pore pressure, and ε_h and ε_H are strain components in the direction of the minimum and maximum horizontal stress, respectively. The Young's modulus (E) and Poisson's ratio (ν) were calculated from the correlations described in Eqs. 1, 3, 6 and 7. A value of $\alpha = 1$ was used for the Biot's coefficient.

Given the tectonic setting of the Gulf of Mexico area, we first considered that the strains ε_h and ε_H should be not only small, but very close to each other. This essentially produced stress ranges similar to that used by Fredrich et al. [2] (varying from $S_h = S_H = 0.7S_V$ to $S_h = S_H = S_V$). The magnitude of the maximum horizontal stress (S_H) is difficult to quantify because of the lack of any technique to measure it directly.

An iterative method was employed to reduce the error in estimating S_H; by changing ε_h and ε_H in the poro-elastic equation during the iterations, the correct S_H should reproduce, as closely as possible, the observed response of wellbore failure indicated by the oriented caliper data and wellbore events.

4.5. Model validation

One of the challenges of the 3D approach is the definition of the model accuracy when trying to validate it with wellbore data. To this end, we compared output data calculated in the 1D and 3D models for the magnitude and the azimuth of the minimum principal stress (S_h and P3) in particular. We acknowledge that the 3D stress model does not calculate S_h, and because P3 = S_h is certainly not always the case; the comparison of these outputs may not be fully valid. This certainly would be the case where stresses are perturbed such as in the zone adjacent to the salt. However, since the location of comparison is approximately 1,140 m (3,750 ft) below the salt (discussed in Section 4.5.2.), we predict that the minimum principal stress is mainly aligned in the horizontal plane; therefore, P3 = S_h. In addition, the validity of the magnitude and location of failure calculated in the 1D model provided a consistency check of the six-component stress tensors.

4.5.1. Minimum stress magnitude

In the absence of reliable LOTs or minifrac data, a novel approach introduced by Edwards et al. [21] was used in the study to estimate the magnitude of the S_h. Mud loss occurred in the subsalt section of Well B, during which while-drilling service was recording the downhole annular pressure and flow rate. The wellbore breathing was characterized by mud losses when the pumps were turned on, followed by mud gains when the pumps were turned off. This effect is caused by opening and closing of fractures and simulates an extended-LOT, which yielded an accurate value for S_h. Examples of annular pressure signatures before and after mud losses observed in Well B are shown in the Appendix. Mud losses also occurred in the suprasalt section of Well A when the mud weight in the hole was increased due to well control issues. Excessive ECD most likely caused the fracturing and the loss of drilling fluid to the formation. The location of the loss zone and the downhole conditions, interpreted from the while-drilling pressure log, were used to calibrate S_h (Figure 5).

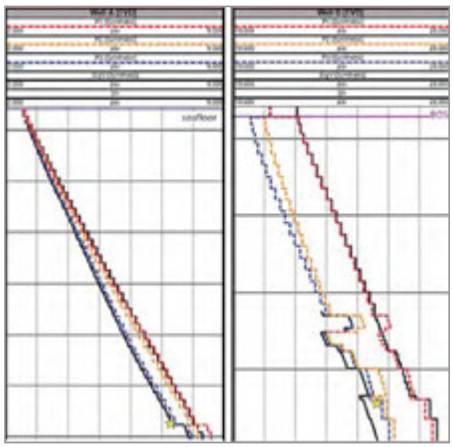

Figure 5: 1D profiles of wellbore (S_h and S_V – solid black) and principal (far-field) stresses (P1-red, P2-orange, P3-blue) in Wells A and B. The profiles were calibrated with mud losses (yellow star) in both wells. Note the good match between the stresses calculated by the different models. Horizontal lines are drawn at every 1,000 ft for vertical scale.

In the 3D stress model, boundary conditions were adjusted iteratively during the stress initialization process until a good match was achieved between the minimum principal stress (P3) and the mud losses event in Well B.

Since the mud loss events are located in different stratigraphic intervals and are distant from each other, they provide an adequate calibration to validate the stress profile calculated in the 1D and 3D stress models, as shown in Figure 5.

4.5.2. Azimuth of minimum stress

Breakout occurs when the stresses around the wellbore exceed those required to cause compressive failure of the borehole wall. Around a vertical or near-vertical wellbore, stress concentration is greatest in the direction of S_h; therefore, breakouts are oriented approximately perpendicular to S_H [22]. The direction of S_h was estimated using oriented caliper information (C1-3 and C2–4 from oil-based mud imaging tool) acquired in the subsalt section of Well B to identify the breakouts and their direction [23]. The analysis indicated that the azimuth of the elongations varies slightly between 120 (+180) and 150 (+180) degrees. This direction of elongation is considered the azimuth of S_h. The orientation of S_H was further investigated from the analysis of shear wave anisotropy measured in the subsalt section of Well B. A shear-wave splits into a fast and slow shear wave when traveling through a formation that has intrinsic stress anisotropy. In a vertical well, the fast shear will have polarization in the direction of the maximum horizontal stress, while the slow shear will have polarization parallel to the direction of minimum horizontal stress [24]. The fast shear azimuth in Well B varies little with depth and is approximately oriented at ~65 to 80 degrees.

The azimuth of the minimum principal stress (P3) was calculated in each cell of the 3D model from the components of the stress tensor (σ_{xx}, σ_{yy}, σ_{zz}, σ_{xy}, σ_{yz}, σ_{xz}). Figure 6 shows the azimuth for the layer located at the approximate depth at which elongation data from the wellbore was also available. The P3 azimuth from the 3D model agrees with the S_h azimuth interpreted from the caliper enlargement; therefore, the consistency between the 1D MEM and the 3D stress model was verified.

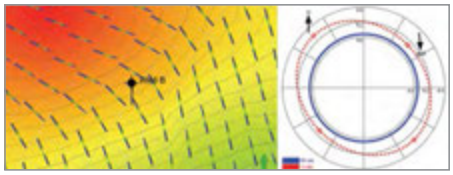

Figure 6: Map view showing the orientation of the minimum principal stress (P3) just above the first reservoir sand in Well B as shown in data derived from the 3D model (left) and from wellbore data (right). Note that the orientation of P3 (blue arrow) is NW-SE, which is similar to the elongation interpreted from the wellbore (blue: bit size, red: hole size).

5. Discussion

5.1. Migration of abnormally high pore pressure at the salt flank

A major well-control event occurred in the suprasalt section of Well A when drilled into an unexpected overpressured shale. A velocity slow-down anomaly was observed in the seismic velocity data (Figure 7a), which is attributed to high pressure that has migrated through permeable formation from the mini-basin from southeast of Well A. This pressure charged the adjacent shales that onlapped the salt flank or pinched out against the fault seated at the salt, and caused the unexpected abnormal pressure in Well A (Figure 7b). Located at the structural apex, this fault acted as a trap, whereas the suprasalt shale and silty shales acted as a seal for abnormal pressure migrating from the minibasin. A pressure buildup can also be seen at the footwall side of this fault.

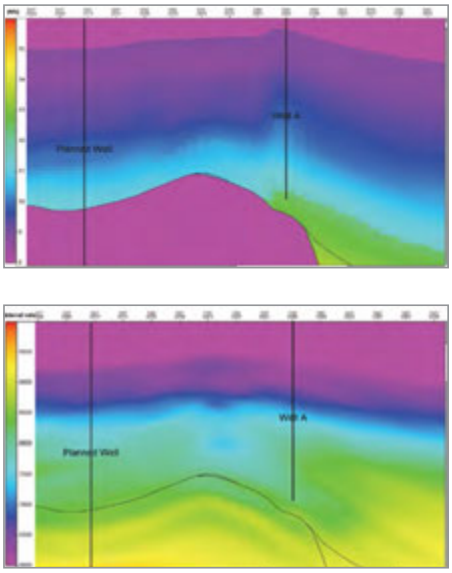

Figure 7: NW-SE cross-section through Well A and the planned well showing the distribution of seismic interval velocity in ft/s (a) and pore pressure converted to mud weight equivalent units of pound per gallon (ppg) (b). Velocity slowdown (pressure charge) extends down the salt flank but this charge is not evident at the planned well location.

5.2. Stress orientation, rotation, and stress anisotropy adjacent to the salt body

The changes in vertical, horizontal, and shear stresses cause principal stress directions to be perturbed and become reoriented adjacent to a salt body [2, 8]. The isotropy of the stresses inside the salt should induce rotation of the principal stresses at the rock/salt interfaces [2, 4, 14]. Similar observations were made in the study area with the principal stresses in the sediment near the salt oriented parallel and perpendicular to the salt/sediment interface. Visualization of the stress orientation calculated from the six-component tensor is presented with arrow(s) pointing in the direction of principal stresses within each cell. Note that the presentation of orientations includes out-of-plane directions, which may not be truthfully represented on cross-section.

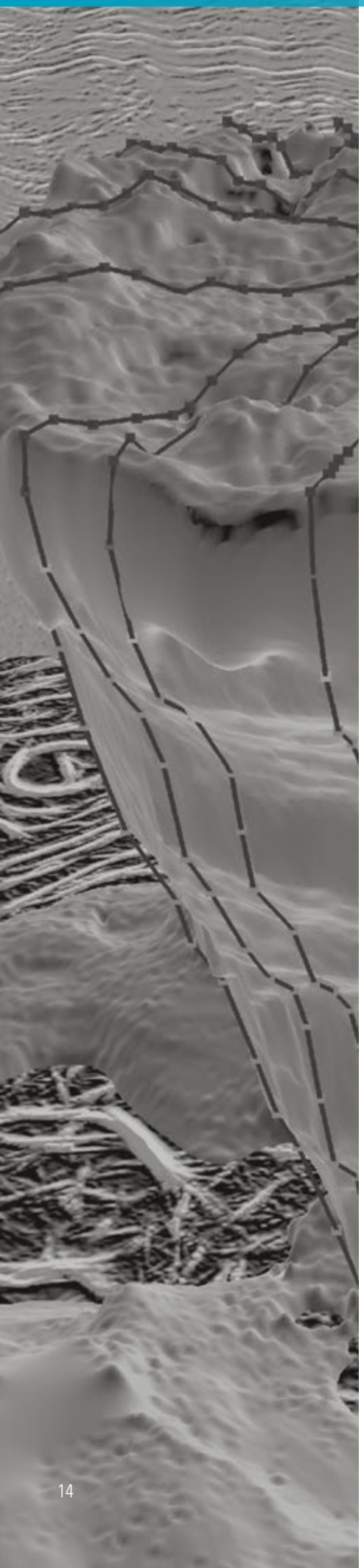

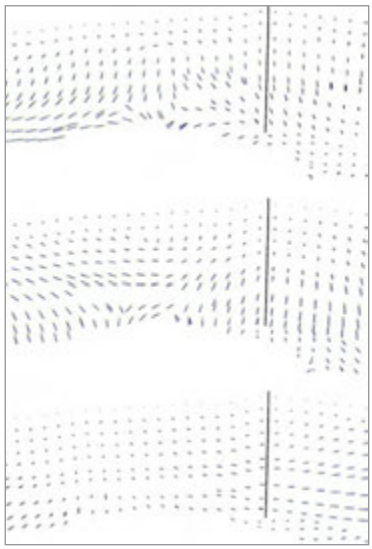

Figure 8: Orientation of the principal stresses along a NW-SE cross-section in the vicinity of Well A; maximum (P1) (top), mid (P2) (middle) and minimum (P3) (bottom). For clarity purposes, only the stresses in the suprasalt sediments are shown (top of salt is at bottom). The size of the vectors is proportional to the stress magnitude.

The 3D model shows that the stress perturbation in the vicinity of the salt flank at Well A caused the maximum principal stress (P1) to be nearly horizontal (Figure 8, top), whereas the mid principal stress (P2) is close to vertical (Figure 8, middle). The maximum principal stress (P1) in the subsalt section at Well B is oriented orthogonal to the base of salt surface (Figure 9, top), whereas the mid (P2) and minimum principal stresses (P3) are rotating in and out of the plane (Figure 9, middle and bottom).

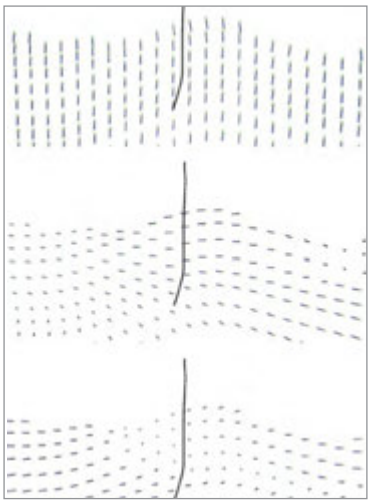

Figure 9: Orientation of the principal stresses along a NE-SW cross-section in the vicinity of Well B, subsalt section; maximum (P1) (top), mid (P2) (middle) and minimum (P3) (bottom). For clarity purposes, only the stresses in the subsalt sediments are shown (base of salt is at top). The size of the vectors is proportional to the stress magnitude.

Fredrich et al., [2] found up to 35% horizontal stress anisotropy adjacent to the salt body despite that S_h and S_H were defined equal in the far field. Others [3] postulated that the stress regime is associated with thrusting in this region, where S_V = P3, though, fault elements near the salt body are rare. Small thrust faults with NE-SW compressional features have been interpreted at the top of the salt to the west of Well A (not presented in this paper). Although, it is not clear in the seismic image data; nevertheless, it seems to follow the salt-ridge with a NE-SW trend and perpendicular to the main extensional faults. This stress reorientation (with a constant wellbore trajectory) may have caused significant increase in the shear failure limit, while showing a decrease in tensile failure limit in Well A. Actually, the stress rotation caused the tensile failure in this zone to be lower than S_h, which was calculated in the 1D MEM. As a consequence, the change in failure limits, i.e., mud weight window, combined with the applied casing design, resulted in simultaneous wellbore instability and mud losses to drilling-induced fractures, and ultimately in loss of the well.

The von Mises stresses are good indicators of the locations of the maximum horizontal stress anisotropy, and can be used as a well design tool during the planning phase. Locations of high von Mises stresses coincide with narrow mud weight window [2, 4]; therefore it is a useful tool for evaluating drillability or casing design schemes. The trajectory of Well A penetrated the zone of high von Mises stresses (Figure 10), and the well became undrillable due to wellbore instability and mud losses.

5.3. Application of the model to the planned well design

Detailed mapping of the suprasalt section in the study area showed numerous normal faults, which are the consequence of vertical extension in the suprasalt section during stress relaxation throughout geologic time [4]. The planned well

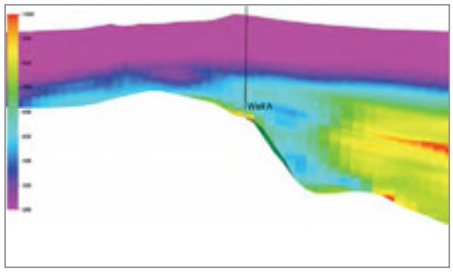

Figure 10: NW-SE cross-section of von Mises stresses (in psi) indication of stress perturbation (high von Mises stresses) at the salt/sediment interface in the vicinity of Well A.

is positioned at a favorable location, since the trajectory will bypass most of these faults. In addition, no velocity slowdown is present above the salt or at the salt/sediment interface (Figure 7a). Furthermore, the extensional faults at the salt flank form a structural apex that seems to contain the pressure and prevent it from diffusing through this topographic high, as evidenced by the pressure change (~0.5 to 1.5 mud weight equivalent in ppg) across this zone (Figure 7b).

The results of 3D stress modeling can provide a "quick-look" means to predict potential drilling problems—a volume of the difference between P3 and pore pressure (in ppg) identifies areas of the model that have a narrow mud weight window and, therefore, will be more difficult to drill. A cross-section of such a volume is shown in Figure 11, where the red color indicates a narrow mud weight window. As pointed out by others' work [8], this representation is somewhat incomplete, since this excludes trajectory-dependent limits such as shear and tensile failure. Nevertheless, it illustrates the effect of the salt geometry on the mud weight window and the drillability of the formation. In Figure 11, there is a gradual decrease in width of the window adjacent to the steeply dipping salt flank, and it practically becomes zero as the salt/sediment interface is reached. Because Well A was drilled into the top of this structure, it experienced serious drilling problems related to the narrow mud weight window. In contrast, the mud weight window at the planned well location is larger and allows a more achievable casing design and safer drilling operation.

In a more regional context, the drillability profile (Figure 11) demonstrates that a drilling operation is predicted to be more difficult if approaching a convex (i.e., salt bulging outward) salt/sediment interface, whereas a concave geometry provides a relatively larger drilling window [e.g., 8]. This is a result of horizontal extension and contraction caused by the salt geometry during stress relaxation [4]. The caveat of this approach is that high pressure that develops locally, as shown in this study, overprints the stress signature (e.g., in the embayment adjacent to the steep salt flank).

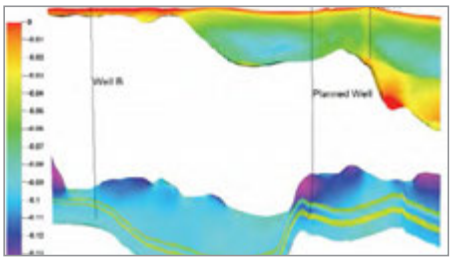

Figure 11: Cross-section of the study area showing difference between the minimum principal stress (P3) and pore pressure (in ppg), which identifies regions characterized by a narrow mud-weight window. For clarity purposes, the salt has been removed from the plot. Red color indicates areas with a narrow window (< 0.5 ppg); blue color indicates areas with a wide window (> 2 ppg) for safe drilling. 2x vertical exaggeration.

6. Conclusions

Regardless of obvious drawbacks in terms of the amount of available data and model resolution to calculate failure along a single trajectory, we successfully used the combination of 1D/3D static geological and geomechanical models and 3D finite-element model to characterize stress state adjacent to a salt body located in the deepwater Gulf of Mexico. During the modeling approach, several iterations were performed in the 1D and 3D domain to fine-tune the values for UCS and the S_h/S_H in order to validate wellbore data and to explain drilling events. The following main conclusions are drawn from this modeling study:

- Reliable wellbore-centric results generated from 1D and 3D mechanical earth models (MEMs) that utilize wellbore data, high-quality 3D seismic data, and a geological framework model prove to be a more realistic representation of the properties of an area than uncalibrated, layer-cake type models published in the literature.
- In this study, one of the key findings is that the 3D seismic velocity model clearly shows an over-pressured zone above the salt at the Well A location that is pressure-connected to the adjacent minibasin. The velocity and pore pressure model also shows that the overpressure is trapped by extensional faults and is pressure-separated from the planned well location, reducing the drilling risk for the planned well.
- Not only does the complexity of the salt geometry impact the stress magnitudes, but rotation of the principal stresses is shown at the rock/salt interface. Visualization of the stress orientation demonstrates that reoriented stresses exist at the reservoir level in Well B, which agrees with the azimuth of borehole enlargement.
- Similar to previous works, this study demonstrates that salt geometry plays a significant role during stress relaxation. Horizontal extension occurs at a convex salt/sediment interface and causes a narrow mud weight window and challenging drilling conditions, whereas horizontal contraction at a concave interface provides a relatively larger drilling window and safer drilling conditions. Contrary to this, we illustrated that the embayment adjacent to the steep salt flank is an example in which high pressure had developed locally and overprinted the stress signature.
- The 3D stress modeling results offer a quick-look tool for predicting potential safe and unsafe drilling conditions, and thereby, the application contributes to evaluating well locations and realistic casing design. The difference (in ppg) between minimum principal stress (P3) and pore pressure, when applied to the study area, predicted an ever-narrowing mud weight window at Well A upon approach to the salt/sediment interface on the steeply dipping salt flank, which, in hindsight, explained the serious drilling problems encountered in that well. The same method showed that those unsafe drilling conditions were not present in the planned well location.

Acknowledgements

The authors acknowledge the support from WesternGeco, allowing us to use the seismic volume from the E-Wave advanced imaging project dataset. We thank, in particular, Eldin Burns for all the discussions and support, and thank Denise Comeaux, Scott Cornish, Jennifer Chesterman, and Cynthia Swenceski (all WesternGeco) for preparing the data for this study. We thank Joyce Evans (Schlumberger) and an anonymous reviewer (ARMA) for improving the earlier version of the document.

The data for this publication was released by YPF Services USA Corp., and Schlumberger.

References

1. Wilson, S.M., and J.T. Fredrich 2005. Geomechanics Considerations for Through- and Near-Salt Well Design. In Society of Petroleum Engineers Annual Technical Conference and Exhibition, Dallas, Texas, 9–12 October 2005, PE 95621.

2. Fredrich, J.T., D. Coblenz, A.F. Fossum, and B.J. Thorne 2003. Stress Perturbations Adjacent to Salt Bodies in the Deepwater Gulf of Mexico. In Society of Petroleum Engineers Annual Technical Conference and Exhibition, Denver, Colorado, 5–8 October 2003, SPE 84554.

3. Dusseault, M.B., V. Maury, F. Sanfilippo and J.F. Santarelli 2004. Drilling Around Salt: Risk, Stress, and Uncertainties. Gulf Rocks 2004, In 6th North America Rock Mechanics Symposium (NARMS), Houston, Texas, 5–9 June 2004, ARMA/NARMS 04–647.

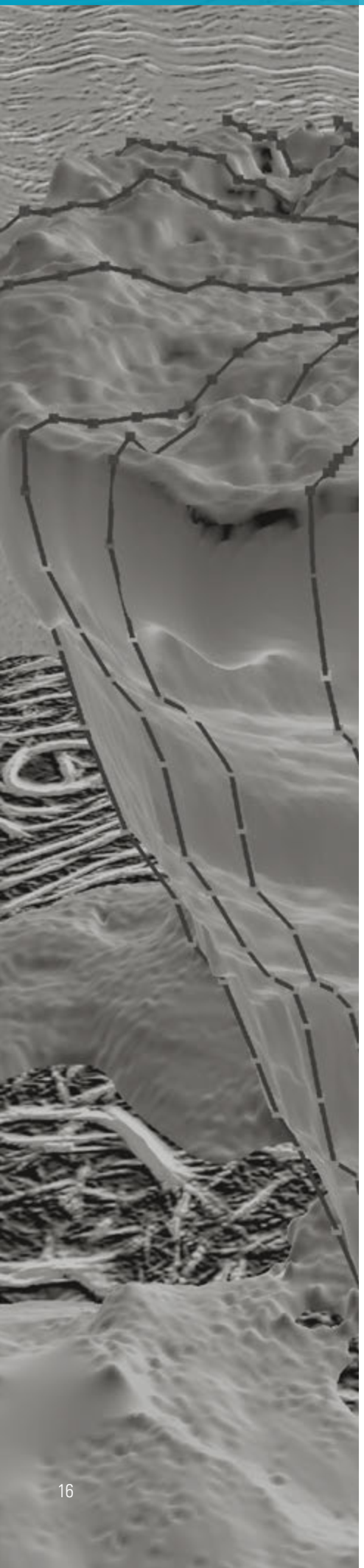

4. Luo, G., M.A. Nikolinakou, P.B. Flemings and M.R. Hudec 2012. Geomechanical Modeling of Stresses Adjacent to Salt Bodies: Part 1–Uncoupled models. AAPG Bulletin, 96: 43–64.

5. Fredrich, J.T., B.P. Engler, J.A. Smith, E.C. Onyia and D.N. Tolman 2007. Predrill Estimation of Subsalt Fracture Gradient: Analysis of the Spa Prospect to Validate Nonlinear Finite Element Stress Analysis. In 2007 SPE/IADC Drilling Conference, Amsterdam, The Netherlands, 20–22 February 2007, SPE/IADC 105763.

6. Koupriantchik, D., S.P. Hunt, P.J. Boult and A.G. Meyers 2005. Geomechanical Modeling of Salt Diapirs: 3D Salt Structure from the Officer Basin, South Australia. In Proceedings to the 11th International Conference on Computer Methods and Advances in Geomechanics, Torino, Italy, 19 June 2005.

7. Mackay, F., N. Inoue, S.A.B. da Fontoura and F. Botelho 2008. Analyzing Geomechanical Effects While Drilling Subsalt Wells Through Numerical Modeling. In 2008 Indian Oil and Gas Technical Conference and Exhibition, Mumbai, India, 4–6 March 2008, SPE 113216.

8. Adachi, J.I., Z.R. Nagy, C.M. Sayers, M.F. Smith and D.F. Becker 2012. Drilling Adjacent to Salt Bodies: Definition of Mud Weight Window and Pore Pressure Using Numerical Models and Fast Well Planning. In SPE Annual Technical Conference and Exhibition, San Antonio, Texas, 8–10 October 2012, SPE 159739.

9. den Boer, L.D., C.M. Sayers, Z.R. Nagy, P.J. Hooyman and M.J. Woodward 2006. Pore Pressure Prediction Using Well-Conditioned Seismic Velocities. First Break, 24: 43–49.

10. Plumb, R., S. Edwards, G. Pidcock and D.W. Lee 2000. The Mechanical Earth Model Concept and its Application to High-Risk Well Construction Projects. In 2000 IADC/SPE Drilling Conference, New Orleans, Louisiana, 23–25 February 2000, IADC/SPE 59128.

11. VISAGE 2009. Introduction to Geomechanics and VISAGE 2009.1 Software. Software Solution Training Manual, Schlumberger Information Solutions, 2009.

12. Horsrud, P. 2001. Estimating Mechanical Properties of Shale from Empirical Correlations. SPE Drilling & Completion, June 2001, pp 68–73, SPE 56017.

13. Plumb, R.A. 1994. Influence of Composition and Texture on the Failure Properties of Clastic Rocks. In EUROCK, Delft, The Netherlands 29–31 August 1994, SPE/ISRM 28022.

14. Fossum, A.F. and J.T Fredrich 2002. Salt Mechanics Primer for Near-Salt and Subsalt Deepwater Gulf of Mexico Field Developments. Sandia National Laboratory, Report SAND 2002–2063.

15. den Boer, L.D., C.M. Sayers, S. Noeth, A. Hawthorn, P.J. Hooyman, and M.F. Smith 2011. Using Tomographic Seismic Velocities to Understand Subsalt Overpressure Drilling Risk in the Gulf of Mexico. In Offshore Technology Conference, Houston, Texas, 2–5 May 2011, OTC 21546.

16. Eaton, B. A. 1975. The Equation for Geopressure Prediction from Well Logs. In 50th Annual Fall Meeting of SPE-AIME, Dallas, TX, Sept 28 Oct. 1975, SPE 5544.

17. Galperin, E. 1974. Vertical Seismic Profiling, Society of Exploration Geophysicists Special Pub. no. 12, Society of Exploration Geophysicists, Tulsa, Oklahoma.

18. Zhang, J., W. Standifird and C. Lenamond 2008. Casing Ultradeep, Ultralong Salt Section in Deep Water: A Case Study for Failure Diagnosis and Risk Mitigation in Record-Depth Well. SPE Annual Technical Conference and Exhibition, Denver, Colorado, 21–24 September 2008, SPE 114273.

19. Traugott, M. 1997. Pore Pressure Fracture Pressure Determinations in Deepwater, Deepwater Technology Supplement to World Oil. August 1997.

20. Thiercelin, M.J., and R.A. Plumb 1991. A Core-Based Prediction of Lithologic Contrast in East Texas Formations. At Rocky Mountains Meeting and Low-Permeability Reservoirs Symposium, Denver, Colorado, 15–17 April 1991, SPE 21847.

21. Edwards, S.T., T.R. Bratton and W.B. Standifird 2002. Accidental Geomechanics—Capturing In-Situ Stress from Mud Losses Encountered While Drilling. In 2002 SPE/ISRM Rock Mechanics Conference, Irving, Texas, 20–23 October 2002, SPE/ISRM 78205.

22. Plumb, R.A and S.H. Hickman 1985. Stress-Induced Borehole Elongation: A Comparison Between the Four-Arm Dipmeter and the Borehole Televiewer in the Auburn Geothermal Well. Journal of Geophysical Research, 90-B7: 5513–5521.

23. Plumb, R.A. and J.W. Cox 1987. Stress Directions in Eastern North America Determined to 4.5 km from Borehole Elongation Measurements. Journal of Geophysical Research, 92-B6: 4805–4816.

24. Plona, T.J., K.W. Winkler, B.K. Sinha and R. D'Angelo 1998. Measurement of Stress Direction and Mechanical Damage Around Stressed Boreholes Using Dipole and Microsonic Techniques. In SPE/ISRM Eurock '98, Trondheim, Norway, 8–10 July 1998, SPE 47234.

Appendix

A.1. Quality check of seismic velocities

The seismic interval velocity model used in this study was obtained using tilted transversely isotropic, full wave inversion (TTI FWI). The accuracy of the velocities was investigated at the offset wells by comparing with the interval velocities obtained by upscaling available sonic logs for these wells. Figure A-1 compares the velocity from the sonic log with the velocity obtained from the seismic velocities. Very good agreement is observed between the upscaled sonic data and seismic-derived velocity data.

A.2. Estimating mud losses using annular pressure data

The signature of annular pressure in the recorded-mode log is characteristic of mud losses [21]. The pressure signal during the last connection without losses was square shaped (Figure A-1a) in the subsalt section in Well B. After the losses occurred, the pumps were turned on and off many times while several connections were made until the total depth was reached.

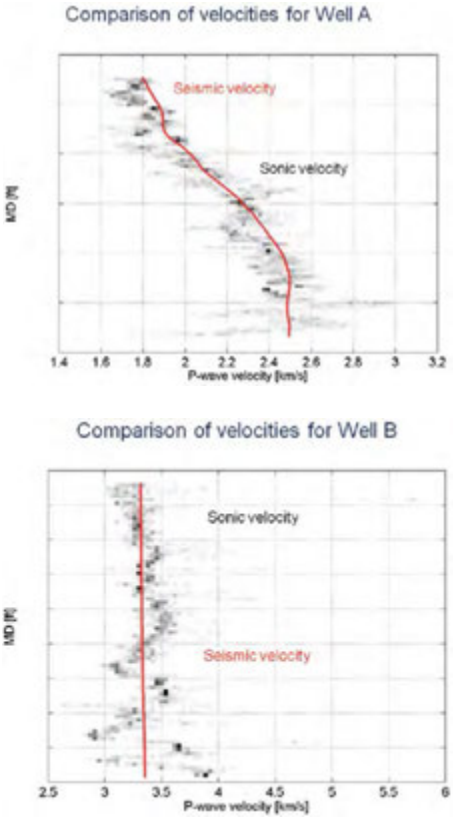

Figure A-1: Comparison of P-wave velocity from the seismic cube (red curves) with the P-wave velocity from the suprasalt well (top) and subsalt well (bottom). The wellbore (sonic) velocity is represented in a 2D histogram.

The fracture opened and closed with each cycle of the mud pumps. Careful choice of opening and closing pressures was determined on the time dataset to estimate the closure pressure.

Location of the "thief zone" is important because it is required for calibrating the stress model. One method compares the oil-based mud invasion profile using time-lapse resistivity data acquired across the zone of losses. Since this data was not available, the resistivity data acquired during logging-while-drilling services and, following that, on wireline tools were used.

This analysis, however, did not clearly indicate the zone of losses.

Review of the drilling report and the annular pressure time-data indicated that the point of losses is likely to have occurred on-bottom while drilling the sand/shale interface at the reservoir section.

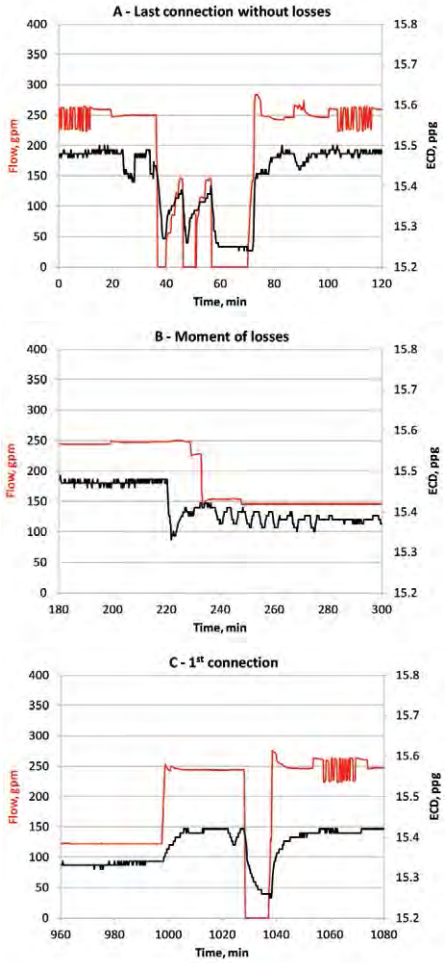

Figure A-2: Signature of annular pressure during the mud-loss event in Well B. Legend: Black curve is downhole pressure (converted to mud weight equivalent in ppg); Red curve is flow rate in gallons per minute (gpm). From top to bottom: A shows last connection without losses; B shows the moment of losses at 220 minutes. Note the characteristic drop in ECD from 15.48 ppg to 15.34 ppg while pump rate remained constant (250 gpm); C shows first connection after the losses with sigmoid-shaped curve characteristic of fracture closure and reopening; D, E shows second and third connections after the losses with only fracture closure interpreted; F, G shows fourth and fifth connections after the losses with fracture closure and reopening.

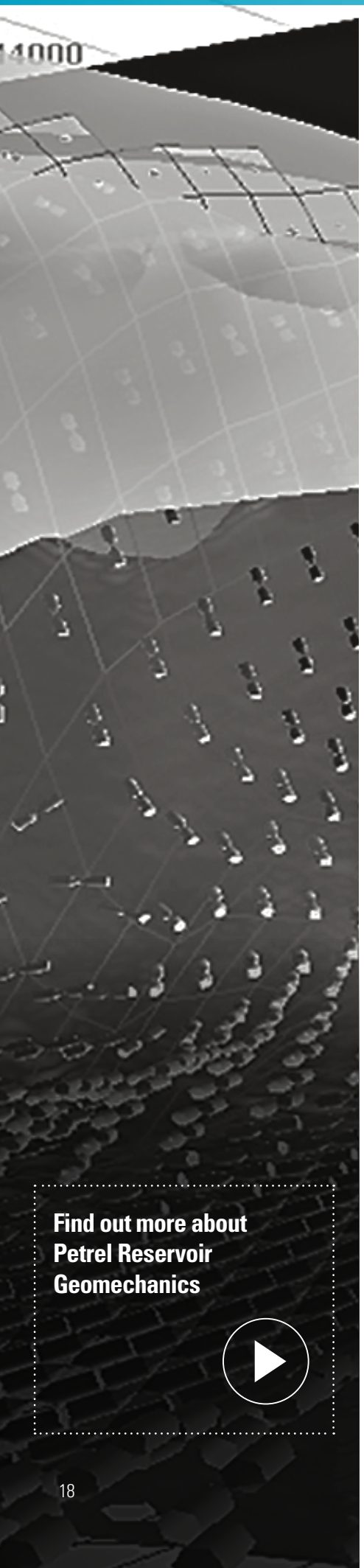

Find out more about Petrel Reservoir Geomechanics

Making Deep Water Pay

by first drilling wells digitally.

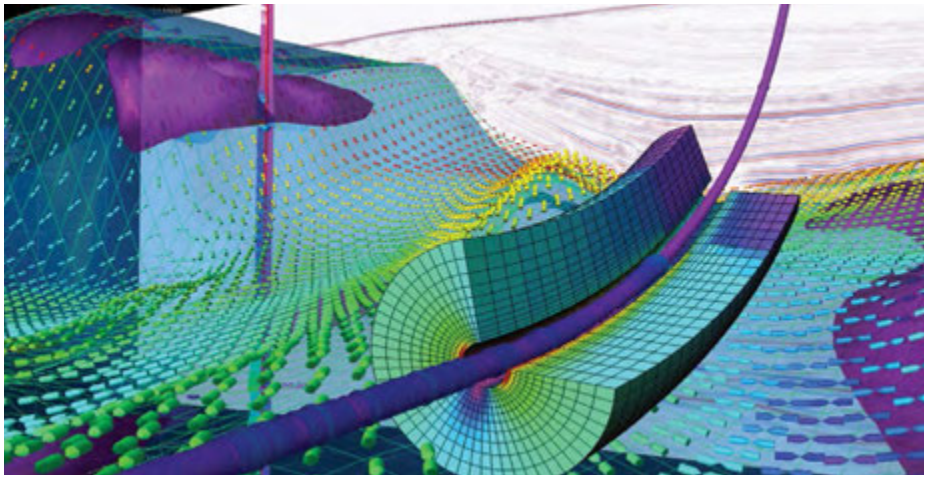

Figure 1: Geomechanics risks for drilling, well construction, and well survivability can be assessed and mitigated in the E&P software platform.

With a million-dollar-per-day average spread rate, deepwater operations demand that risk and uncertainty are properly quantified. Operators would probably agree that optimal use of integrated software mitigates risk; however, they may disagree as to when software can have the most impact on the deepwater process.

Validating deepwater prospects in an integrated E&P software platform is essential for success. Petroleum systems modeling software is used to evaluate basin history and understand its chronostratigraphic and structural development—the thermal maturation of the source rock, expulsion of hydrocarbons over time, and their eventual entrapment.

Prospect assessment is undertaken to model geologic complexity and quantify risk, as well as examine the full range of possible risked prospect volumes. Using exploration economics software to simulate exploratory drilling, appraisal, and development activities delivers the range of expected after-tax economic value. This enables oil and gas companies to choose their best prospects and drilling options, with a clear understanding of geological and economic chance of success.

Enhancing seismic data to reveal the best drilling targets is key, given the complex geological environment and salt geometries which often mask potential deepwater targets and affect image quality. The seismic also provides overburden information, as well as foresight into possible geomechanical issues—which account for 40% of all drilling incidents. Wider azimuth surveys image subsalt, advanced ray tracing algorithms return energy sources correctly, and prestack gathers help interpret poorer data quality areas to illuminate subtle targets and further reduce uncertainty.

This basin-to-prospect assessment is accomplished within the Petrel E&P software platform, which supports integration of basin analysis, prestack interpretation, geomechanical information, and economic analysis in a single environment.

Offset well information is then analyzed within the wellbore software platform to provide context for well planning. The velocity model used for interpretation and modeling is refined, and continues in real time while drilling the first exploratory wells.

Due to the pore pressure anomalies and irregular drilling conditions expected, a huge focus is placed on the geomechanical model. Even at this early stage the engineering team begins to create a concept design of how the field, if proven, will be developed.

Earth model uncertainties are analysed in the E&P software platform using specific reservoir simulation software.

Optimization and experimental design techniques allow rapid analysis of multiple realizations to evaluate numerous development alternatives—with a clear understanding of the uncertainty related to reservoir properties, volumes, and the potential number of wells required.

Today's software platforms can be employed to optimize deepwater operations every step of the way—long before the rig arrives on location.

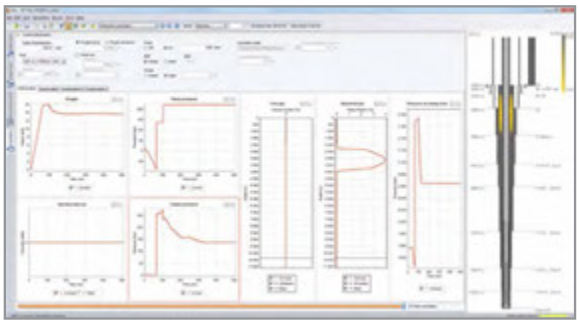

Figure 2: Drilling operations software simulates dynamic pressure and flow rate conditions to optimize well control procedures, such as managing kick incidents.

Using integrated Microsoft communication technology, the drilling team joins the collaboration space in the E&P software platform environment to discuss and review potential well plan options.

Well and network planning

The earth model's geomechanical components allow the well-planning team to easily establish the optimal geometry for initial wells. The trajectory is optimized based on pore pressure information to maximize the safe drilling window, and optimize well and casing design. Pore pressure information combined with lithology, stresses, and fluids behaviors establishes the expected rate of penetration (ROP)—allowing users to better understand whether ROP fluctuations are due to lithology changes or drillbit failure.

Real-time information enables drillers to geosteer and monitor formations to adhere to the optimized trajectory and honor formation changes as they drill.

Predictive capabilities using look-ahead drilling tools assist when crossing high-risk areas—like over-pressured zones, or areas of high instability.

The collaborative model is automatically updated with real-time formation data and properties are redistributed and calibrated using seismic attribute data. The reservoir engineering team can now establish the required number of wells—and their locations—to successfully develop the field using optimization routines.

Offshore deepwater operations now legally require relief-well contingency plans and kick-tolerance models. Drillbench drilling operations software, as well as dynamic multiphase flow simulators, are used to design and model wellbore and mud system dynamics.

Well integrity planning includes an evaluation of realistic potential blowout scenarios, blowout flow simulations, and relief well constraints for intersection and kill operations. Drilling operations software can be used to design these plans, as well as evaluate potential technical and logistical problems.

The production team creates multiple models for the wells and flowlines to evaluate design alternatives. Initial casing design, flowline sizes, routings, and associated facility requirements are estimated based on expected production rates, fluid types, and production system constraints. Nodal analysis is run on each well to design the preliminary lift system specifications.

Ensuring flow in deepwater environments means designing and operating facilities within given tolerances, such as temperature, pressure, fluid composition, and seabed topography changes.

This allows users to plan for all likely eventualities, not just intervene when a problem occurs.

OLGA flow assurance simulation software allows detailed flow modeling, incorporating dynamic flow phenomena.

Understanding dynamic fluids behavior is critical in subsea environments, given long multiphase flowlines exposed to extreme temperatures to inhibit hydrates or other solids formation, and is imperative in the overall system design.

Production advantages and beyond

Production operations software gathers, cleanses, and aggregates all operational data types and events—including measurements from real-time SCADA systems. It transforms data into visual information, allowing engineers to monitor operations: from well tests and allocated volumes, to the performance of electric submersible pumps (ESPs), to the levels of potentially erosive sand production, and indicators on the condition of wells and equipment. Flow models built in multiphase flow simulation software during the development phase are continuously updated with high frequency measurements by the production operations platform to reliably identify the causes of production problems. The same data can be visualized in oilfield management software—production engineers can assign appropriate well decline rates, and decide when artificial lift or secondary recovery methods are required. Sensitivity tools in flow-simulation software define the number of ESP stages required to optimize production. Multiple scenarios are modeled to produce the optimal pump configuration. Performance can then be monitored and modeled to predict failures and issues.

Accurate monitoring and forecasting allows for the appropriate allocation of capital and operational expenditure through the life of the field in dedicated planning, risks, and reserves software. Actual production data are brought back into the E&P software platform to update the history match of the reservoir model.

Approaching a deepwater project from exploration to production using a fully integrated software system with predictive modeling significantly mitigates the inherent risks. From the first tentative exploration stages, to planning artificial lift requirements and optimizing production long-term, software can be used every step of the way to ensure operators get it right, the first time.

Keith Tushingham (Schlumberger), Ayn Becze (Schlumberger)

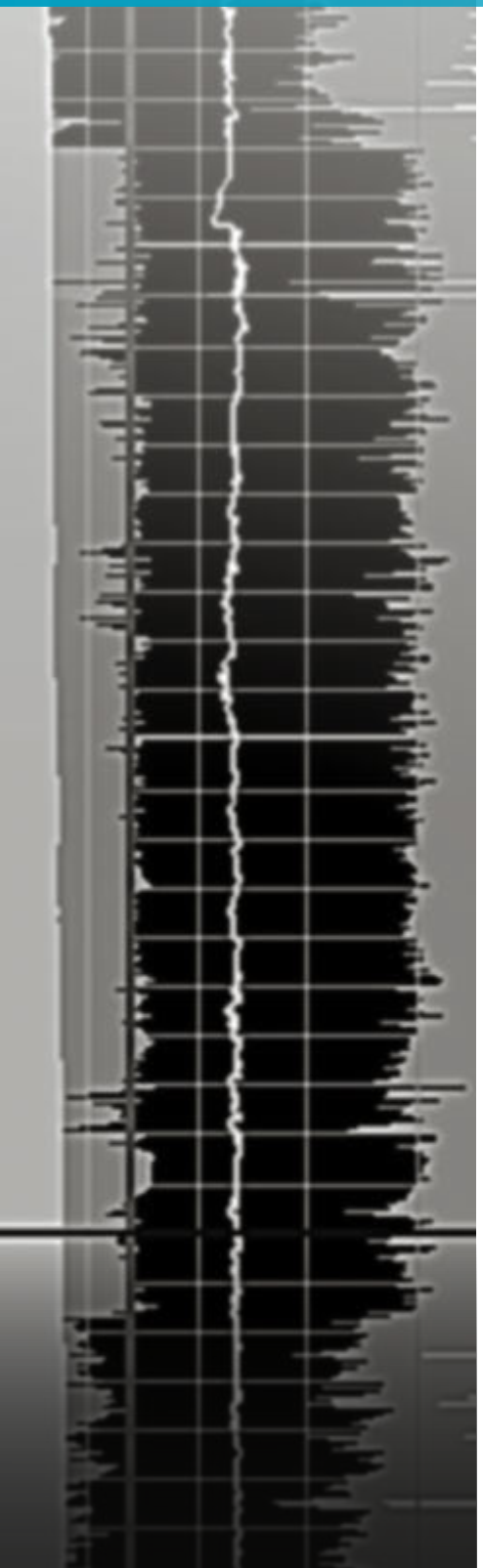

Find out more about Wellbore Quality Services

Real-Time Drilling Geomechanics:

Successful application in an inclined well in ultradeep water off the east coast of India.

Assurance of wellbore stability (WBS) is of utmost concern and a key challenge in drilling an inclined well in ultradeep water off the east coast of India. The WBS analysis requires accurate modeling of earth stresses and rock mechanical properties. These processes are primarily based on sonic logs (compressional and shear slowness), bulk density, and lithological distribution. To understand and address drilling complications in the study area, post-drill (offset well analysis), and real-time drilling geomechanics is carried out in this well.

A 1D mechanical earth model (MEM) and a WBS model are constructed for offset wells, which are calibrated with a caliper log, pressure test, and leakoff datasets. WBS analysis suggested drilling with lower mud-weight in the zones of shear failure and pack-off. Disparity in resistivity values is also observed when wireline logs and LWD logs are analyzed. This might be due to mud invasion or fluid-shale interaction in the open hole, as it is resolved by changing the mud system from water-based mud (WBM) to synthetic oil-base mud (SOBM). The post-drill analysis of offset wells established parameters for the upcoming inclined well.

The planned well was the first inclined well (horizontal drift more than ~2000 m) in ultradeep water off the east coast of India to avoid drilling risks; real-time drilling geomechanics were put into operation for the first time. Required sonic and density data was received in reasonable time intervals to perform real-time analysis. Timely updates on rock mechanical properties were provided to the client, which helped in optimizing drilling parameters. As a result, the first inclined well in ultradeepwater off the East Coast of India was drilled successfully.

Introduction

The significance of real-time pore pressure monitoring has already been recognized in the petroleum industry and over time it has been introduced to the domain of real-time geomechanics during drilling. Successful real-time geomechanics depends on the availability of data and the feasibility of data acquisition. Wireline or LWD data, in conjunction with other datasets, can be used for modeling during predrilling to understand the regional and local drilling complexities. Recent advances in LWD techniques provide reasonable quality data for quantitative analysis in real time. This paper discusses the workflow and a case study of an inclined well drilled off the east coast of India.

Real-time geomechanics: Approach and workflow

The conventional approach of pore-pressure prediction and wellbore stability provide a safe mud-weight window between pore pressure and fracture gradient and a stable mud-weight window between the collapse and fracture gradients (Plumb et al., 2000). Apart from this, the predrill wellbore stability study only predicts the shearing of rock in the wellbore wall. However, borehole enlargement, or breakout, is significantly influenced by the drilling process. The predrill wellbore stability study cannot model the effect of the drilling process and therefore cannot predict wellbore degradation. The situation becomes more complex in inclined deepwater wells where the stable mud-weight window becomes very narrow in deeper sections of smaller hole sizes (sometimes less than 1 ppg). Any reduction in uncertainty will help mud-weight tuning and effective circulating density (ECD) limits so that pore pressure and wellbore stability can be managed (Plumb et al., 2004).

In such cases, the predrill model often needs to be supplemented with additional data to drill the well efficiently.

At the same time, it is important to understand how the wellbore is responding to the drilling process; which zones are starting to degrade and what is causing it. This not only helps manage the wellbore geometry for tripping, casing, and cementing, but also controls the volume of solids being released into the wellbore that require additional time to clean. Real-time geomechanics allows the operator to make pore pressure and wellbore stability decisions during drilling by providing the most current information about the wellbore condition, right up to setting casing (Bradford et al., 2000). Hazards identified for a specific well trajectory and geological setting

Real-time analysis provides information on current wellbore conditions and enables remedial actions to avoid NPT.

are identified and consolidated through the overburden and into the reservoir with a predrill MEM. The service collects and aggregates all available data, which may include drilling measurements, LWD, mud logging, seismic, and hydraulics. Through continuous, 24/7 monitoring it makes sure that deviations from the plan are quickly recognised so that immediate action can be taken by the operator. Real-time geomechanics provides continuously updated forecasts of pore pressure and wellbore stability through real-time enabled software. This ensures that the predictions remain applicable for drilling ahead (Figure 1). Finally, end of well summary of the pore pressure and wellbore stability analysis is prepared and submitted for input to future well planning and drilling.

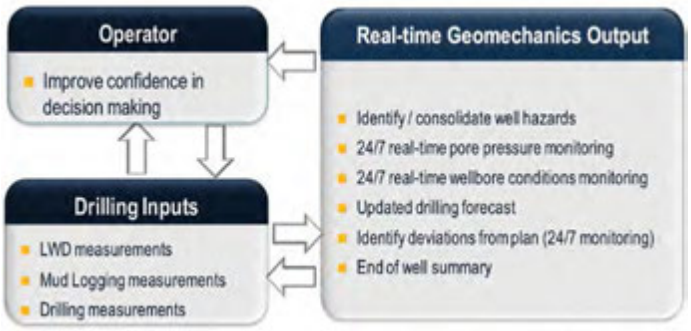

Figure 1: Real-time geomechanics inputs and outputs, showing interactive approach between geomechanics and drilling operations.

The real-time geomechanics workflow can be simplified into three phases, i.e., predrill, drilling, and end of well. The predrill phase includes data audit to review available field and offset well data. In this phase, hazards are identified from geomechanical analysis, drilling records, and discussions with the drilling team. Pore pressure and wellbore stability plans are constructed and delivered to the operator, with some level of uncertainty because of the offset input data. However, expected hazards are identified and it is possible to set limits for drilling parameters. This defines the basis to measure and interpret the actual behaviour of the wellbore during drilling.

During drilling, a continuous feed of all data from the well is monitored and compared. If the well data moves out of the predefined boundaries, then the predrill model is updated with the new data and the operator is notified. Any deviation from the plan is interpreted to establish the root cause. Once the root cause is established, the operator can confidently apply

Figure 2: Simplified real-time geomechanics workflow.

the best remedial action. Apart from this, 24-h look-ahead is issued on a daily basis, for specific drilling hazards during the next period, and will include any updates and changes to the plan resulting from new data or changes in well condition.

At the end of the well, a summary is prepared including a revised model for the well based on the new data. This also includes analyzed drilling events and the effectiveness of the response to develop a set of lessons learned and to build best practices for the field (Figure 2).

Case study

The study area is located in deep water off the east coast of India (Figure 3), with a water depth of more than 2,000 m. The operator has drilled three vertical offset wells in the same block. All the wells have reported problems during drilling. The upcoming well was the side track (L-shape) from an offset well. In offset well drilling, challenges are broadly categorised into two domains: mud engineering and wellbore stability. Direction control was an additional concern in the upcoming extended-reach drilling (ERD) well. Of these, assurance of wellbore stability is essential at every stage (planning/drilling/production) of the well's life.

Predrill phase: Offset well analysis

The predrill phase commences from offset well data analysis to identify and characterize the drilling problems experienced in the region. These drilling problems can then be cross-referenced to the geomechanical study to highlight areas of concern, to support and confirm findings and hypotheses based on the geomechanical analysis, and to help understand root causes of observed instability or drilling problems. Tight hole was found to be the major drilling risk, whereas other problems such as breakouts, mud loss, differential sticking, fluid influx, and pack-offs were also reported from lower Pliocene and Miocene formations (Table 1).

Stratigraphy	Section	Drilling Risks					
		Mud Loss	Tight hole/ Over pull	Breakouts	Differential Sticking	Influx	Pack-Off
Pleistocene	36”		Yes				
Upper Pliocene	26”		Yes				
Lower Pliocene	17.5”	Yes	Yes	Yes	Yes		
Miocene	12.25” and 8.5”		Yes	Yes		Yes	Yes

Table 1: Summary of drilling complications review from offsets wells. Overpull was reported in every stratigraphic section. Lower Pliocene and Miocene report drilling complications of mud loss, tight hole, break outs, differential sticking, influx, and pack off.

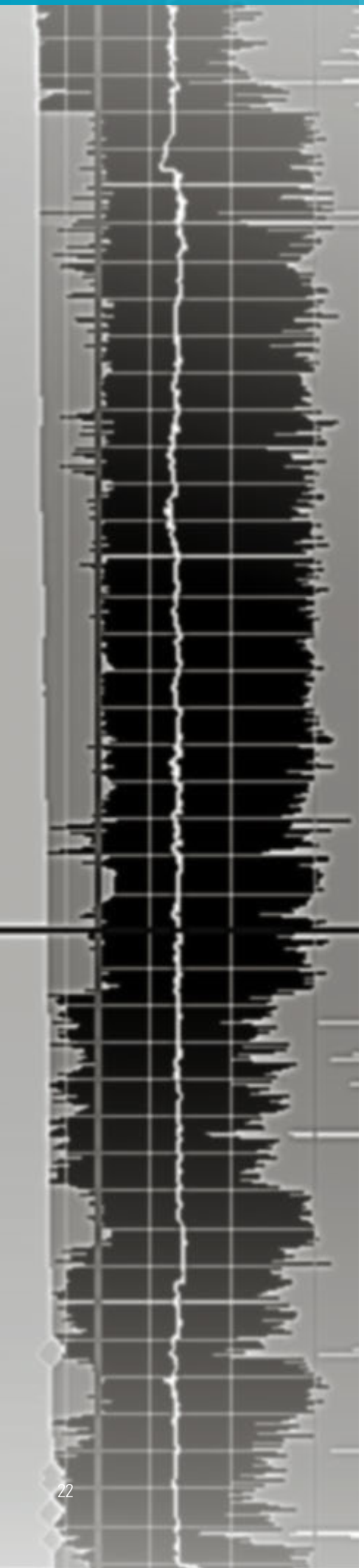

Figure 3. Location map of study area.

Mechanical earth model

The 1-D MEM—a numerical representation of the state of in-situ stress and rock mechanical properties—was constructed for the offset wells. The MEM was calibrated with a leakoff test (LOT), pressure test (modular dynamic test or MDT) and caliper log data for history matching and to understand the well profile in terms of geomechanics. Typical workflow of MEM construction is shown in Figure 4.

Overburden stress and pore pressure

Overburden stress (vertical stress) was computed using the formation density log. For missing intervals, power law has been used to extrapolate density values from the depth of the available density log to mudline. Sonic and resistivity logs were used to identify pore pressure trends in shale and the estimated pore pressure was calibrated using the mud weight used during drilling and well test/MDT results. MDT results in the region show that pore pressure was close to hydrostatic.

Horizontal stresses: Magnitude and direction

A poro-elastic, bi-axial strain model was used to compute horizontal stresses. Unlike minimum horizontal stress (σh), direct measurement of maximum horizontal stress (σH) is not possible. However, it was inferred through modeling similar to σh, but using additional constraints from wellbore failure as indicated by caliper logs or images. Further calibration of minimum horizontal stress profile was done using the LOT/FIT data and the maximum horizontal stress is adjusted until the predicted failures were in good agreement with the observed borehole failures indicated by the caliper log/images. Horizontal stress orientation was determined based on the breakout direction in the FMI image log.

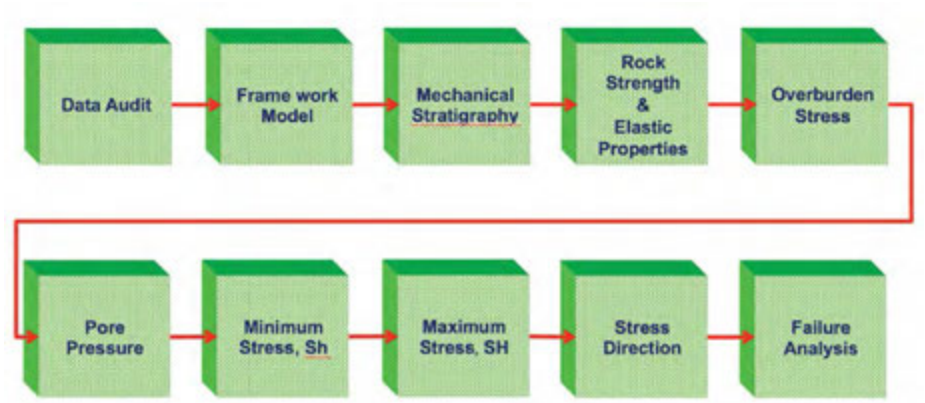

Figure 4: Workflow for constructing an MEM.

Elastic and rock strength properties

Elastic properties (Young's modulus, shear modulus, and Poisson's ratio) were calculated using sonic data (compressional slowness and shear slowness) along with density data. Rock strength parameters included unconfined compressive strength (UCS), friction angle, and tensile strength. Since there was no laboratory core test data available for this study, the rock elastic and strength properties were estimated by using various Schlumberger proprietary correlations. Since the tensile strength (TSTR) of rock is usually in the order of 1/12th to 1/8th of its UCS value, and in the absence of any other data, the tensile strength of the rock was assumed to be 1/10th of UCS.

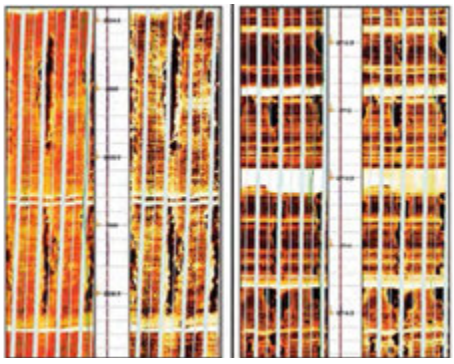

Figure 5. Breakouts observed in offset well using the FMI fullbore formation microimager.*

FMI for offset (8.5-in section) has borehole breakout in N-S direction which is inferred to be minimum horizontal stress azimuth (Figure 5).

Rock failure criteria

Mohr-Coulomb criteria were used to determine shear failure, and maximum tensile stress criteria to determine tensile failure.

Planned well MEM

After rigorous history matching and calibration, MEMs for the offset wells were generated. In order to estimate rock properties, mapping/ propagation of logs at planned trajectory was done using the curtain section process. The well offset was planned to be drilled with 52º tangent section at an azimuth of 119º giving a horizontal displacement of approximately 2,000 m. Formation tops were picked on the basis of offset well logs while expected depths for well tops was based on seismic horizon. To optimize the mud weight for drilling along the planned trajectory, wellbore stability analysis was conducted and results are shown in Figure 6. Results indicated narrow mud weight window along with lower mud loss limit. The recommended mud weight is given in Table 2.

Depth (m)	MW (ppg)
x630 - x300	9.0 - 9.6
x300 - x640	9.6 - 9.9
x640 - x800	9.9 -10.2
x800 - x446	10.2 - 10.6

Table 2. Recommended mud weight for the planned well.

Recommendations for drilling

Based on the results of the wellbore stability analysis, the following conclusions and recommendations were presented:

- Wellbore stability results indicate narrow mud weight window of ~ 1 ppg.
- ECD and borehole cleaning should be monitored closely for borehole cleaning and to avoid surge.
- LOT/XLOT should be conducted to calibrate the fracture gradient.
- Planned ERD well has a horizontal drift of 2,000 m which brings uncertainty about lateral variation in formation with varying sea water depth.
- Formation pressure measurements should be taken during drilling to reduce uncertainty.
- Real-time geomechanics was recommended due to narrow stable window.

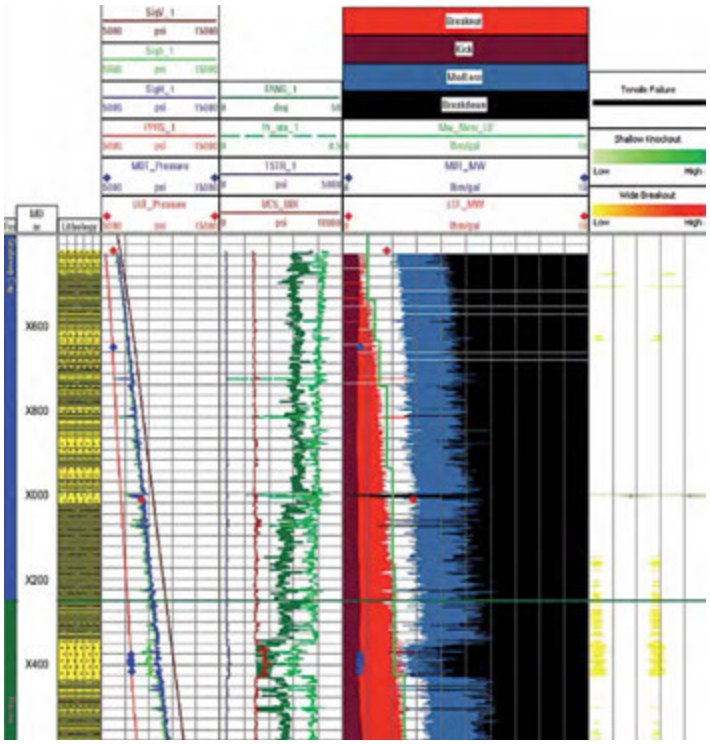

Figure 6: Predrill wellbore stability model for the offset well, prepared using curtain section. Planned well WBS model suggest narrow mud weight window due to wellbore trajectory.

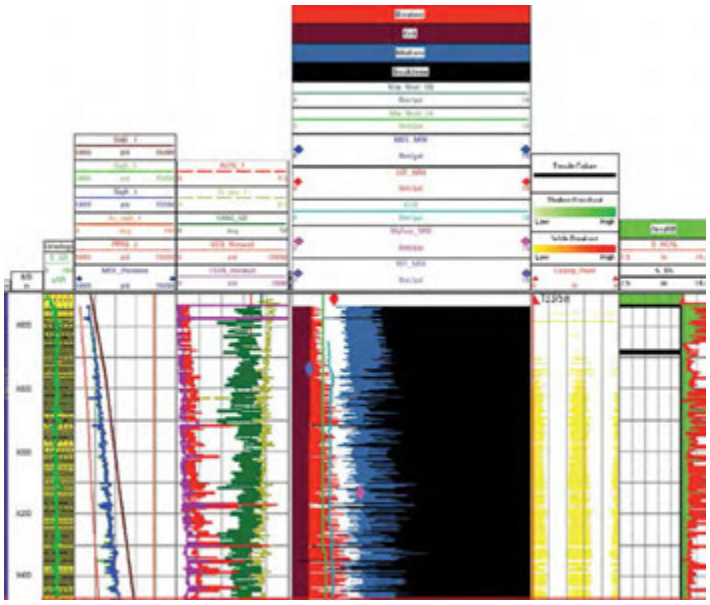

Figure 7: Higher caliper readings possibly due to breakouts as mud weight (even ECD) was lower than the breakout limits.

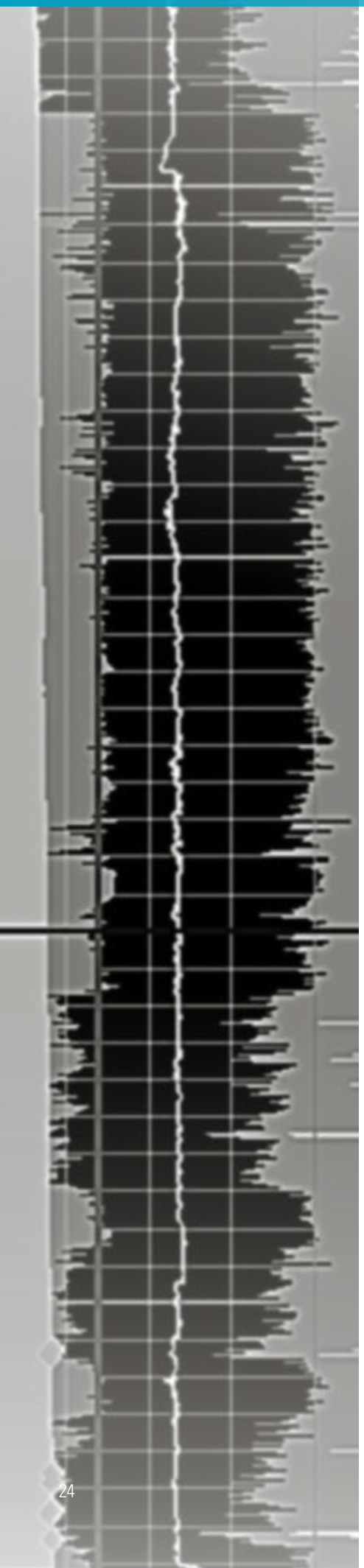

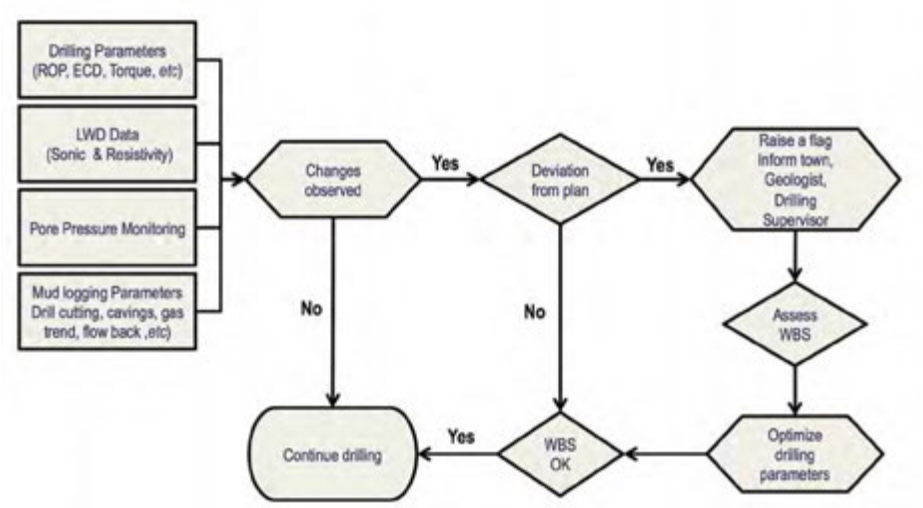

Figure 8. Flow chart showing process followed during real-time geomechanics and communication protocol.

Drilling phase

Considering the risks of stuck pipe during a side track in the 12.25-in section, basic LWD (ARC) tools were used to drill the section. Hence, the section was drilled without real-time geomechanics support. In the absence of real-time support of geomechanics, drilling complications could not be captured. Later on, post-drill wellbore stability analysis was carried out using wireline logs. A post-drill MEM for the section suggested the presence of breakout in the drilled interval (Figure 7).

Challenges

A comparison of a predrill WBS model (based on offset data) with a post-drill model (using wireline logs) suggested a good match. In the upcoming section, where a stable window was predicted to be quite narrow and would be further reduced by higher ECD—common in high-angle geometries. The predrill model was prepared for a 52° tangent. However, due to lost directional control, the angle was continuously increasing. Although a predrill model can serve to support overall well design, controlling wellbore stability during well construction often requires a more interactive approach between geomechanics and drilling operations to minimize wellbore degradation and understand the root causes of specific instability events.

Considering all operational risk, the real-time geomechanics engineer was mobilized to the rig to closely evaluate and communicate geomechanical recommendations on a daily basis (Figure 8).

8.5-in section

Real-time drilling geomechanics analysis was conducted for the 8½-in section to optimize the drilling process and reduce possible risks and complications. A 9.625-in casing shoe was drilled out with mud weight of 9.4 ppg and leak off was found at 10.50 ppg, which was lower than the expected value. But this value matched the mud loss curve predicted in predrill, suggesting good predrill wellbore modeling.

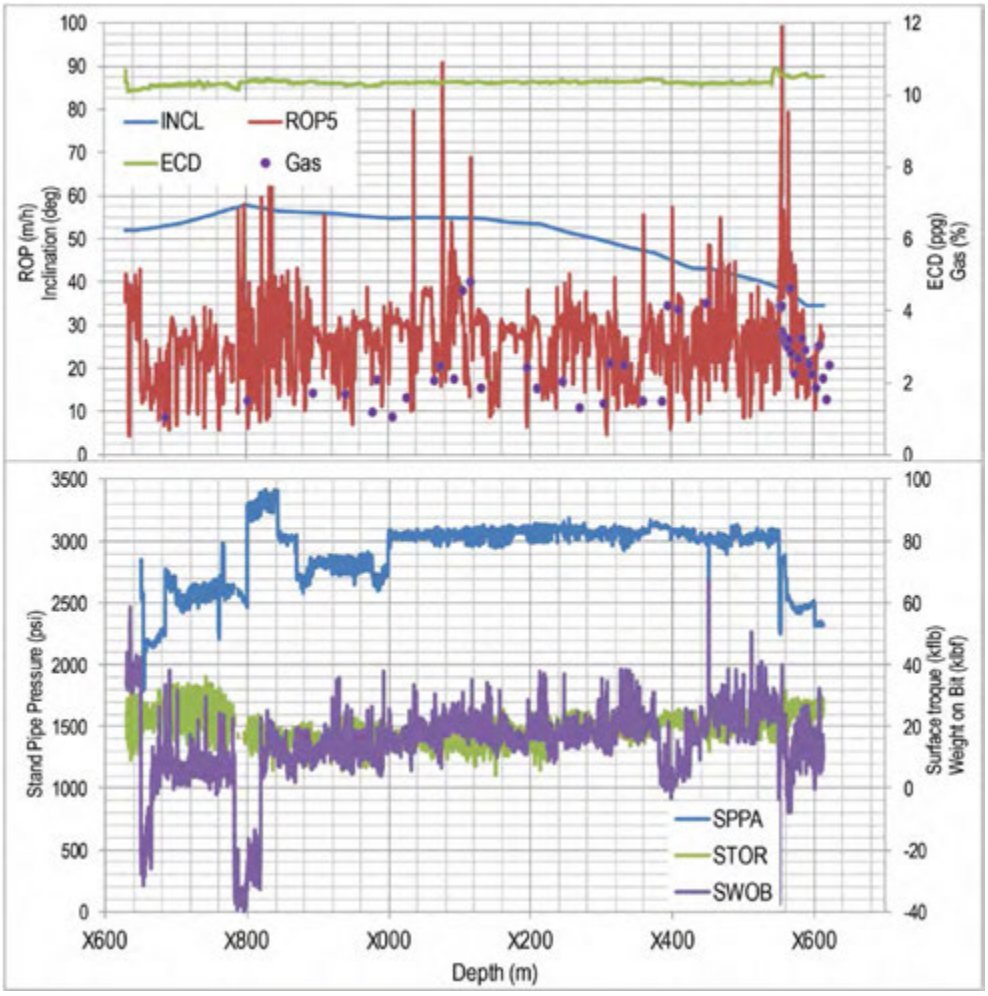

Figure 9: Drilling parameters ROP, ECD, Gas, SPP, STOR, WOB along with borehole inclination for the section. No anomalous signatures observed during drilling, suggesting wellbore instability.

The profile of breakout and mud loss obtained in the predrill analysis was used during monitoring. Considering geomechanical risk, hydraulics was run to simulate ECD generated with the mud weight of 9.4 ppg in the section. Simulation results predicted ~10.4 ppg, i.e., very close to the leak-off pressure at the shoe. A small deviation from the plan could have led to wellbore instability; moreover, encountering any weak zones in the open hole could also result in disaster.

After conducting the LOT, it was decided to drill ahead with the same mud weight (9.4 ppg). Inclination from the previous section was 52°, which kept on increasing for the next 5 stands (~200 m) until 58°.

Considering the loss in directional control, it was decided to pull out to change the bottomhole assembly and one stabilizer was removed to have better control. Drilling ahead with the new BHA showed much more directional control and borehole inclination started dropping (Figure 9).

Mud weight in and out, along with mud rheology, was closely monitored for any anomalous behavior such as changes in oil-water ratio, density reduction etc., which could have served as early indicators of borehole instability.

Mud weight going in and coming out of the borehole remained at 9.4 ppg throughout the section. ECD behavior in the section was constrained by the ROP. An increase in ROP resulted in higher ECD values, so it was recommended to keep ROP ~30m/h, to ensure good borehole cleaning.

Average background gas level remained between 1 to 2%, though maximum gas peak observed in the drilling interval was 4.82% at depth x209 m. Flow check was also conducted at this depth for influx from formation, which was reported negative. Before drilling ahead, background gas levels were further increased for an interval of 200 m, while drilling interbedded sand-shale sequence. No connection/ pump off gas was observed to suggest signatures of underbalance drilling.

Borehole cavings are the first and foremost indicator of wellbore deterioration, during and after drilling operations and the correct knowledge and interpretation of cavings can help optimize drilling. Shale shakers were regularly observed for cavings, but no cavings were observed (also evident from real-time density caliper log). Flowback was also monitored and fingerprinted at each connection/pump off by mud log unit, no anomalous flowback has been observed to indicate any influx from wellbore.

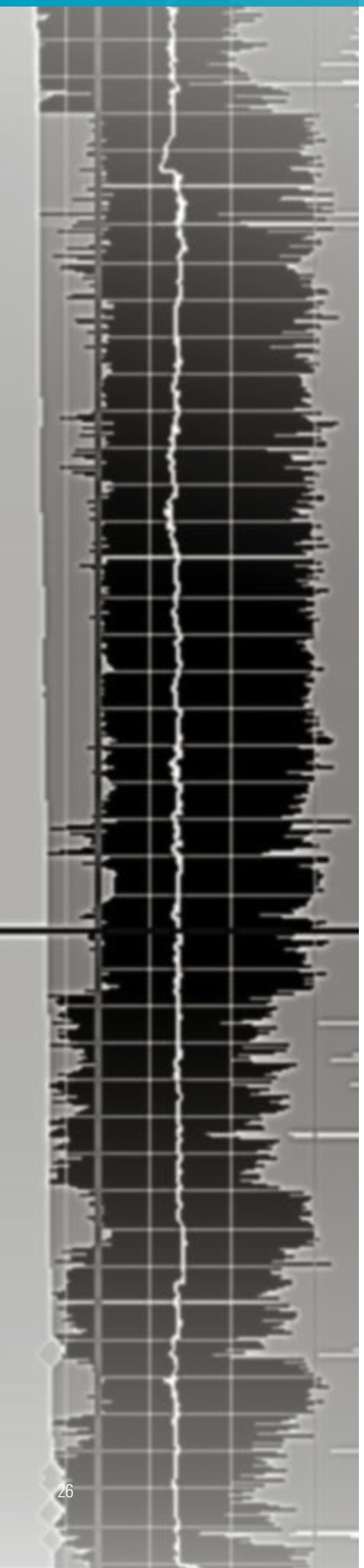

Other drilling parameters, torque/drag, standpipe pressure, weight on bit, ROP, etc., are closely observed for any deviation from the plan. No evidence pertaining to borehole instability was noticed during drilling.

LWD logs were mainly used to compute wellbore stability; updated mud-loss curve from look-ahead model was used to define maximum permissible ECD limits. Gamma ray and density-porosity curves were used to define the pure shale interval to pick the shale points for pore pressure computation. These shale points were also verified by lithocutting samples collected by the mud logging unit. Sonic compressional slowness and resistivity logs were used to compute pore pressure using Eaton's normal compaction trend method in real time (Eaton, 1972). Both the logs suggested normal compaction and the pore pressure in the drilled section varied from 8.6 to 9 ppg (nearly hydrostatic). Real-time density caliper analysis suggested minor washouts in a few sandy intervals, but the borehole remain gauged during drilling (Figure 10).

Post-drill discussion

Post-drill 1-D MEM and WBS analysis was also conducted using wireline logs recorded in the 8.5-in section and the model was calibrated with the LOT, MDT pressure points, and caliper log in the section. Except minor washouts in sandy intervals, the condition of the borehole was found to be in good condition (Figure 11).

Conclusions

Detailed geomechanics modeling and analysis of pore pressure was conducted to reduce possible drilling risks and complications during an ERD well in the KG basin, India. A review of the drilling report indicated that breakouts and tight holes were the major drilling-associated problems encountered in the offset wells. Drilling deepwater wells with narrow margins needs coordination of operational geosciences and well engineering teams.

Predrill planning holds a key position to envisage the possible risks during drilling, whereas real-time analysis provides current wellbore condition and remedial actions to avoid any NPT. Awareness and communication is another important aspect of successful execution of narrow margin wells.

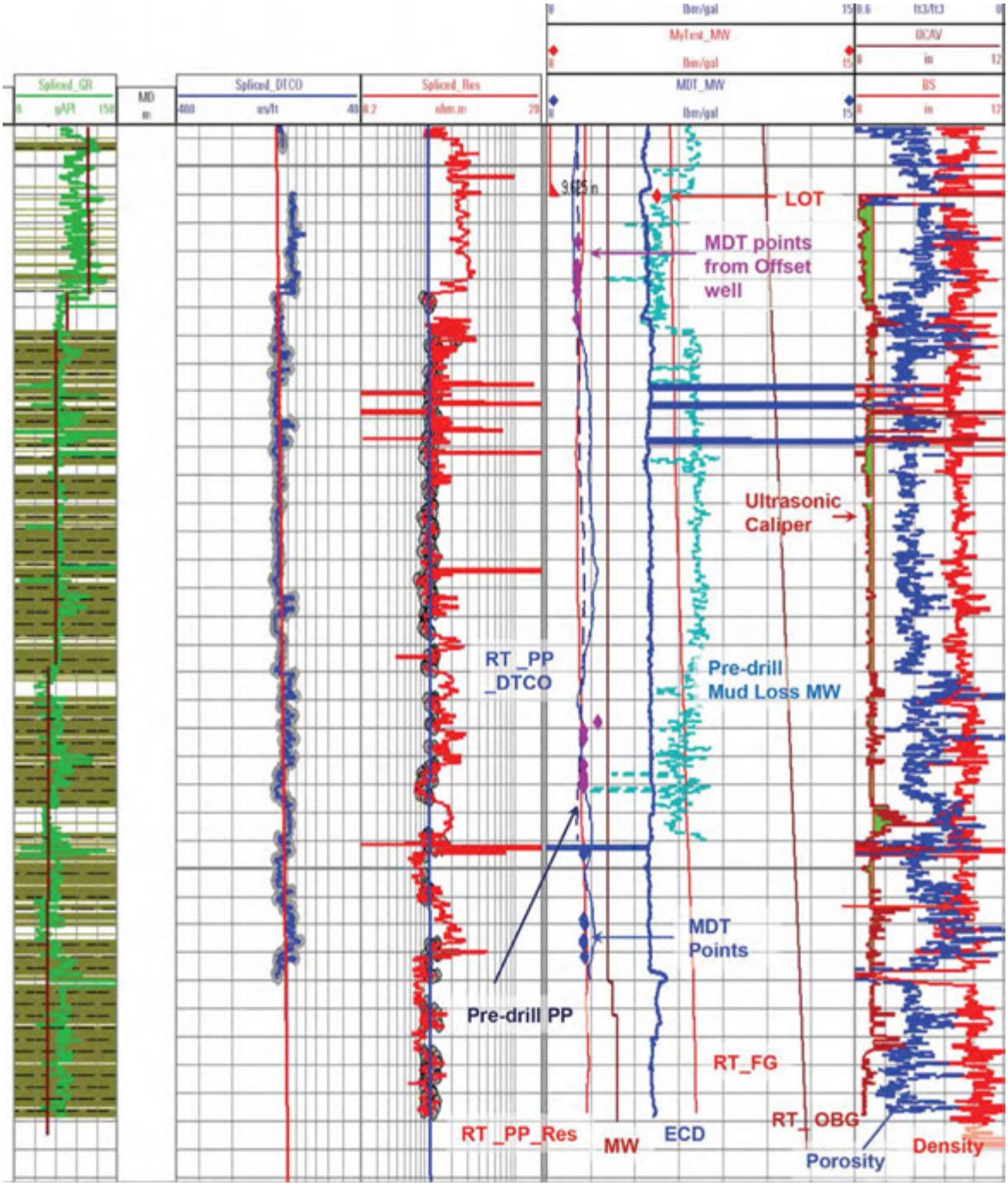

Figure 10: Real-time pore pressure model of 8.5-in section. Pore pressure was computed using sonic compressional slowness and resistivity data and ranged between 8.6–9.0 ppg in the section. MDT data acquired in the section also confirmed the pore pressure estimated in real time.

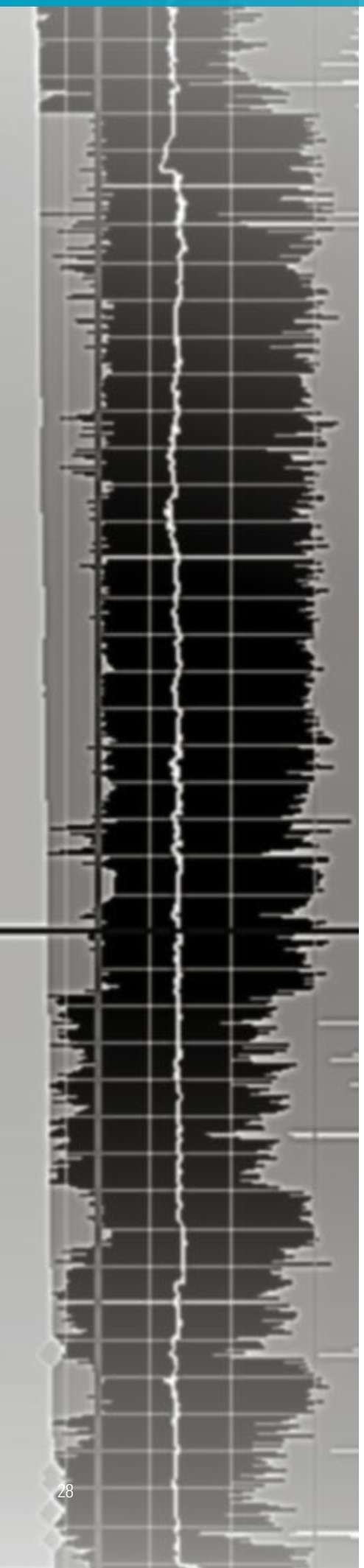

Acknowledgements

Authors are thankful to Schlumberger and ONGC management for permission to present this work. Authors are also thankful to the reviewers of this manuscript. The help provided by John Fuller in preparing this manuscript and his guidance is also gratefully acknowledged.

References

Bradford, I.D.R., Aldred, W.A., Cook, J.M., Elewaut, E.F.M., Fuller, J.A., Kristiansen, T.G., and Walsgrove, T.R. [2000] When Rock Mechanics Met Drilling: Effective Implementation of Real-Time Wellbore Stability Control, IADC/SPE 59121.

Eaton, B. A., [1972] The Effect of Overburden Stress on Geopressure Prediction from Well Logs, Journal of Petroleum Technology.

Plumb, R.A, Edwards, S., Pidcock, G. and Lee D. [2000] The Mechanical Earth Model Concept and its Application to High-Risk Well Construction Projects, IADC/SPE 59218.

Plumb, R.A, Hooyman, P., Veeningen, D., Dutta, N., Ritchie, G. and Bennaceur, K. [2004] A New Geomechanics Process Reduces Operational Risk from Exploration to Production, ARMA/NARMS 04–616 Gulf Rocks 2004, the 6th North America Rock Mechanics Symposium (NARMS), Houston, Texas.

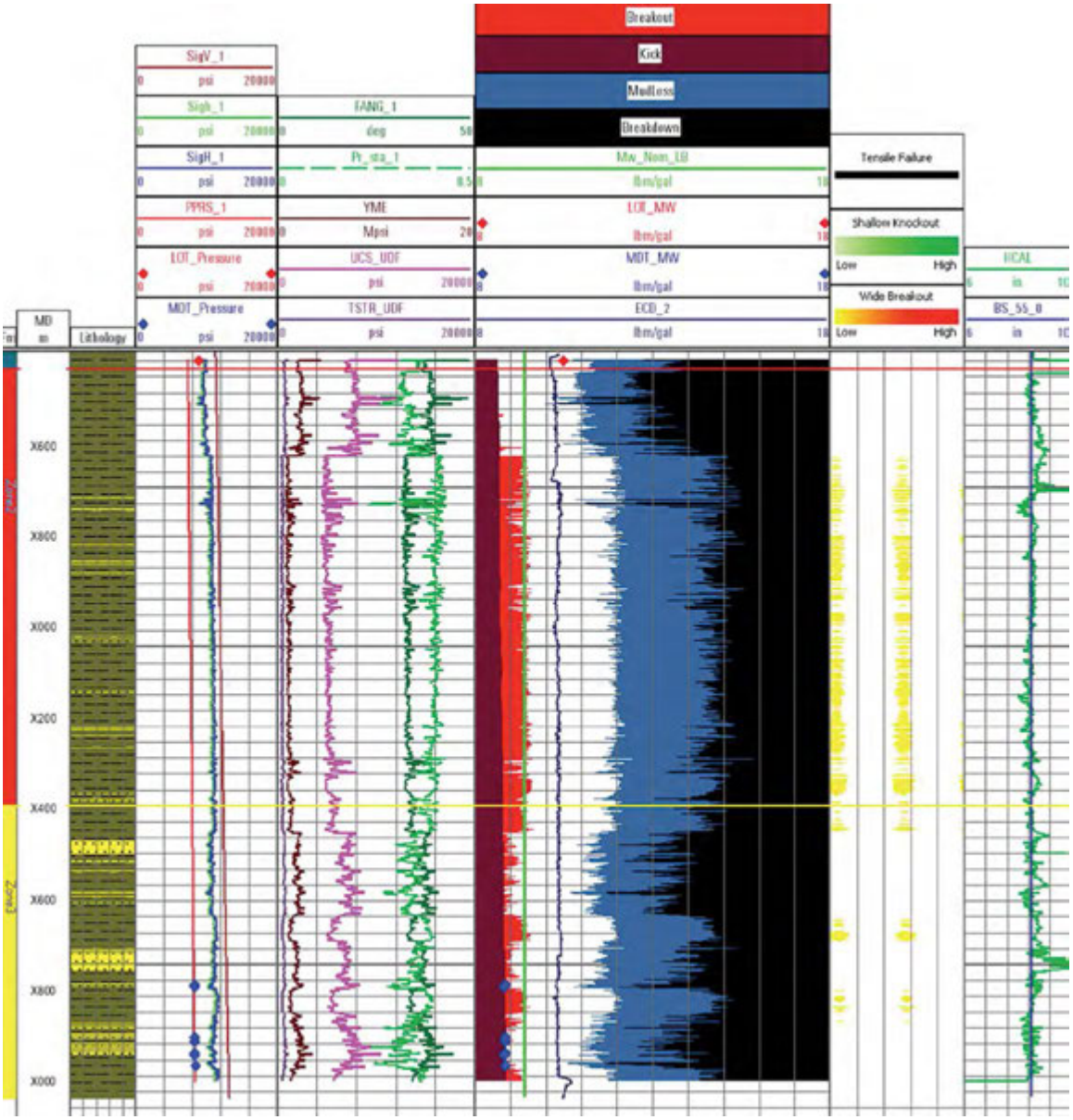

Figure 11: Post-drill wellbore stability model of 8.5-in section. Wireline caliper suggests good wellbore condition except minor washout in sandy intervals.

Find out more about Interpretation Services for Geophysics

Using Borehole Geophysics Measurements to Assist Drilling:

A case study from presalt Brazil.

This case study aimed to assist drilling decisions by obtaining a more accurate prediction of base of salt depth. Setting the 9 ⅝-in casing point was key from a drilling perspective.

Introduction

The thick and heterogeneous salt layers found offshore Brazil present unique challenges for drilling presalt targets. Some of the well construction difficulties include salt creeping, possible casing collapse, leaching, and difficulties in cementing. Exiting the salt layer with inadequate mud weight is also a point of concern. In Brazilian presalt scenarios, the most common salts present are halite, carnalite, tachyhydrite, and anhydrite and they often appear as thin layers below seismic resolution. Surface seismic provides key information about the salt geometry but it is hampered by limited vertical resolution and by insufficient depth accuracy. Borehole seismic methods can improve both of these limitations by recording a wider frequency bandwidth and by measuring more accurate interval velocities.

The surface seismic uncertainty in salt thickness prediction, the variability of the salt composition seen in offset wells, and some past drilling issues, prompted BP Brazil to record a comprehensive set of borehole seismic measurements in one exploration well drilled offshore Campos basin. A combination of rig source look-ahead VSPs run on wireline and LWD seismic while drilling (SWD) combined with LWD sonic data, aimed to assist drilling decisions by obtaining a more accurate prediction for the base of salt (BoS) depth. Setting the 9 ⅝-in casing point at the BoS was key from a drilling perspective and the borehole seismic objectives included the following:

(i) To place all salt behind casing to prevent any tight hole issues after mud weight reduction.

(ii) To penetrate basal anhydrite.

(iii) Not to drill into the presalt Upper Sag formation (e.g., to prevent losses by exposing the presalt target with heavy mud in the 12 ¼-in hole section).

With the 9 ⅝-in casing properly set, the 8½-in hole reservoir section could then be drilled safely with a smaller mud weight. Otherwise, drilling the 12¼-in hole into the reservoir could jeopardize the evaluation program and increase the risk of mud losses. The drilling program included a full suite of borehole geophysical measurements to accurately predict the BoS depth and to assist in the drilling optimization (controlled drilling, cuttings identification, and ROP change). Without the borehole seismic look-ahead data, the BoS seismic event would be very difficult to correlate with the well data, at least with the level of confidence required.

Method

When the presalt exploration well had tagged top of salt (ToS), which was mainly composed of anhydrite, the base of salt depth prediction was updated based on surface seismic data (both prestack depth and prestack time-migrated volumes available). However, the depth uncertainty at the BoS was still high, as demonstrated later by the drilling results and by the borehole measurements. Based on the results from other offset wells, the BoS event was expected to correspond to an increase in acoustic impedance (going from halite to possible thin basal anhydrite and/or to carbonates). To reduce the depth uncertainty at that stage, a look-ahead VSP was recorded in 12 hours using a four-level wireline VSP tool equipped with accelerometer sensors, a six-airgun source array (1,200 in^3) in a dual delta cluster configuration and an automatic in-sea gun controller. The latter was capable of tuning all guns with 0.5 ms accuracy and of recording for every shot: high-fidelity, near-field source signatures, the firing pressure and the gun depth (Figure 1). For this project, recording wideband seismic data at more than 6,000 m depth was of paramount importance and an effort was made to use adequate sensors and sources. The high-resolution zero-phase VSP corridor stack provided an accurate time thickness for the salt. The two-way time of the BoS reflector was further refined by acoustic impedance inversion (Sacchi and Ulrych, 1996).

The use and interpretation of wireline lookahead VSP, combined with LWD seismic while drilling and LWD sonic log, for base of salt prediction, in deep water, Campos basin, Brazil.

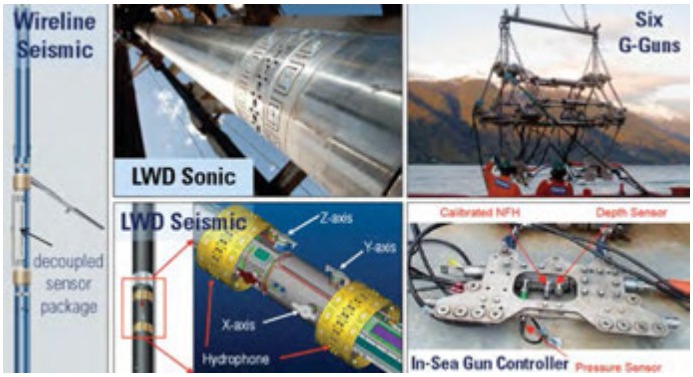

Figure 1: Enabling borehole geophysics technology. Some of the key equipment used in this project included the multi-level versatile wireline seismic tool fitted with 3-C high-fidelity accelerometer (left), the LWD sonic and the SWD seismic tools (middle), the six-airgun array of 1,200 in^3, and the insea automatic gun controller which has a gun tuning accuracy of 0.5 ms (right).

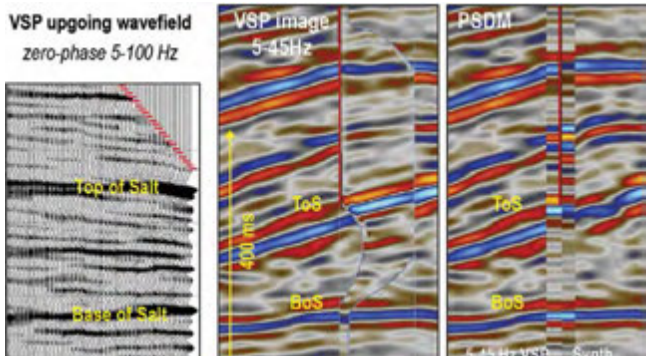

Figure 2: Look-ahead VSP 5–100 Hz upgoing waves (left), 5–45 Hz VSP CDP image (middle) and 5–45 Hz corridor stack (right). Drilling results and post-mortem synthetics (right panel) confirmed look-ahead VSP accuracy and that the surface seismic did underestimate the salt thickness.

As drilling progressed through salt, LWD sonic, and SWD seismic tools transmitted uphole time-depth pairs, waveforms, and sonic DT values without any drilling delays. The SWD velocity data were processed with the wireline VSP data in nearly real time to further reduce the uncertainty in the BoS depth prognosis. Average salt velocities from extensive salt stratigraphy analyses of wells drilled offshore the Campos basin were also used to constrain the VSP predictions.

Results

The look-ahead VSP had a bandwidth at the target depth (>6 km) of 5–100 Hz, more than doubling the surface seismic bandwidth. It clearly showed the BoS seismic reflector and indicated that the salt thickness was larger (in vertical travel time and in depth) than that seen in the surface seismic data. Although based on limited data (single rig-source and dips input from the seismic model) the VSP CDP image helped tie and visualize data ahead of the bit to correlate with surface seismic. The latter observation was confirmed post-mortem by the synthetic seismograms (Figure 2). VSP acoustic impedance inversion further helped pinpoint the two-way-time of the BoS event (Figure 3). At this well location, the VSP wavefields are quite complex due to top salt and intrasalt structural dips and resulting multiple scattered energy. The problem deviates then considerably from the 1D acoustic impedance assumption and post-mortem analyses were performed in order to evaluate the sensitivity of the results (Figure 3). Furthermore, as seen in Figure 4 the lack of low frequencies below 5 Hz affects the look-ahead acoustic impedance inversion results.

The LWD sonic shows some intra-salt variations dominated by halite (Figure 3). The real time SWD velocity trend is following the LWD sonic well. In this vertical well the transit times considered from the SWD hydrophone are more accurate than from the SWD geophone. The sonic drift (VSP time minus integrated sonic time) has a negative slope above ToS and it is flat underneath (Figure 5). This is likely due to the structural dips above ToS (Goetz et Dupal, 1979).

Measuring the sonic drift was paramount as this could add error to the depth estimations. Inside salt, the sonic drift slope is nearly zero, meaning that no sonic correction is required throughout that zone. This also means that the intra-salt reflections seen are likely due to density contrasts.

The drilling results and the advanced borehole geophysical measurements acquired in this presalt exploration well confirmed that the initial BoS depth prognosis was about 75 m too shallow. The initial estimate was based on surface seismic data after tagging ToS, once this had been drilled. Both prestack depth and prestack time surface seismic images equally underestimated the salt thickness. Naturally, the predrill prognoses for the BoS depth had an even larger uncertainty. The intermediate wireline look-ahead VSP, confirmed unequivocally that the salt was thicker than seen in surface seismic (Figure 2). This survey reduced the uncertainty from about 75 m down to less than 25 m. The integration of the wireline VSP data with the LWD seismic while drilling and LWD sonic measurements, further reduced the depth uncertainty to less than 15 m.

Conclusions

By integrating all borehole geophysics measurements recorded in this exploration well BP was able to set the 9 ⅝-in casing successfully inside salt within less than 15 m from the actual BoS depth. The greater certainty on the BoS depth removed the need for an additional casing string, and resulted in a simpler and more robust well construction. With only the initial prognosis of BoS depth the 9 ⅝-in casing would have been set 75 m too shallow and an additional casing string may have been needed. The correct decision taken for the casing depth, supported by the look-ahead VSP and LWD sonic measurements provided more options to drill the presalt section and to be able to reach the total depth planned for the exploration well.

This project enabled assessment of the real benefits of recording each individual measurement (look-ahead wireline VSP, seismic-while-drilling and LWD sonic data). This helped to build a strategy on how to use and integrate RT information in order to come up with robust results and a clearer understanding of drilling depth uncertainties in subsequent projects. Finally, the good communication between BP and Schlumberger was critical for achieving a seamless integration in this complex and iterative project.

Acknowledgments

We would like to thank the Exploration team for the Campos basin at BP for the authorization to present this work and also BP and Schlumberger Brazil for the excellent job execution and collaboration throughout the data acquisition, processing, and integration; in particular, Doug Haun, Robert Bodek, Alistair Taylor, Paul Hoenmans, and Brian Hornby (BP), Helmut Gmach, Ryan Chapman and Ekaterina Sazonova (Schlumberger).

References

Goetz, J. F., Dupal, L., and Bowler, J. [1979] An Investigation into Discrepancies Between Sonic Log and Seismic Check-Shot Velocities. APEAJ, 19, part 1, 131–141.

Sacchi, M., and Ulrych, T. [1996] Bayesian Inversion of Acoustic Impedance: 1996 Annual Report of Consortium for the Development of Specialized Seismic Techniques, UBC, Canada, 152–166.

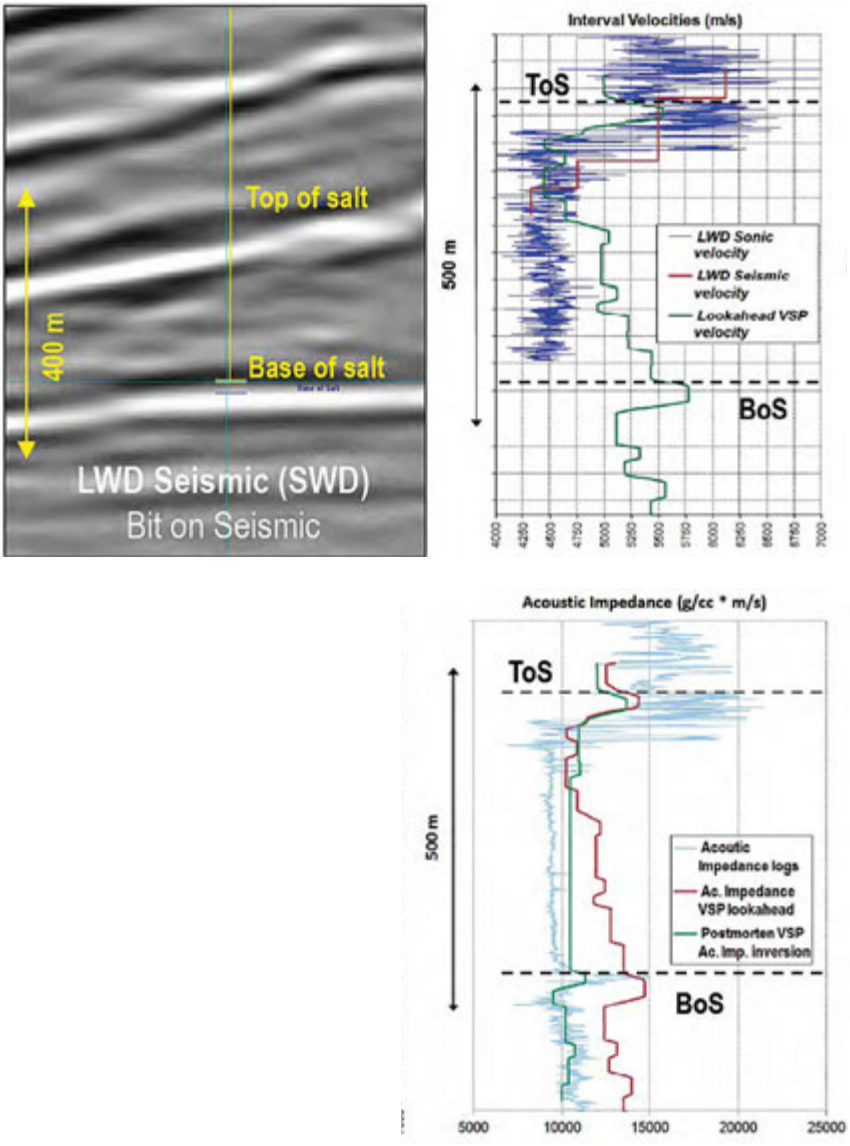

Figure 3: SWD bit on seismic in real time (top left), velocities from SWD in red, from LWD sonic in blue, and from wireline look-ahead VSP inversion in green (top right). On the bottom right, the acoustic impedance logs in blue are compared to look-ahead VSP inversion and to the final VSP inversion results.

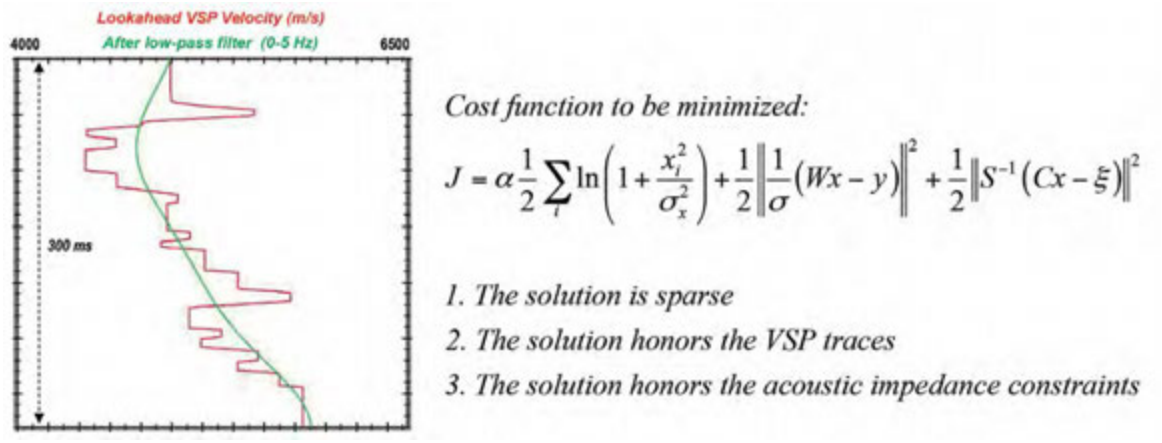

Figure 4: Low-pass filter (5 Hz) shows imprint of low frequency trend on the wireline look-ahead VSP. Most of the velocity increase comes from the low frequency velocity trend.

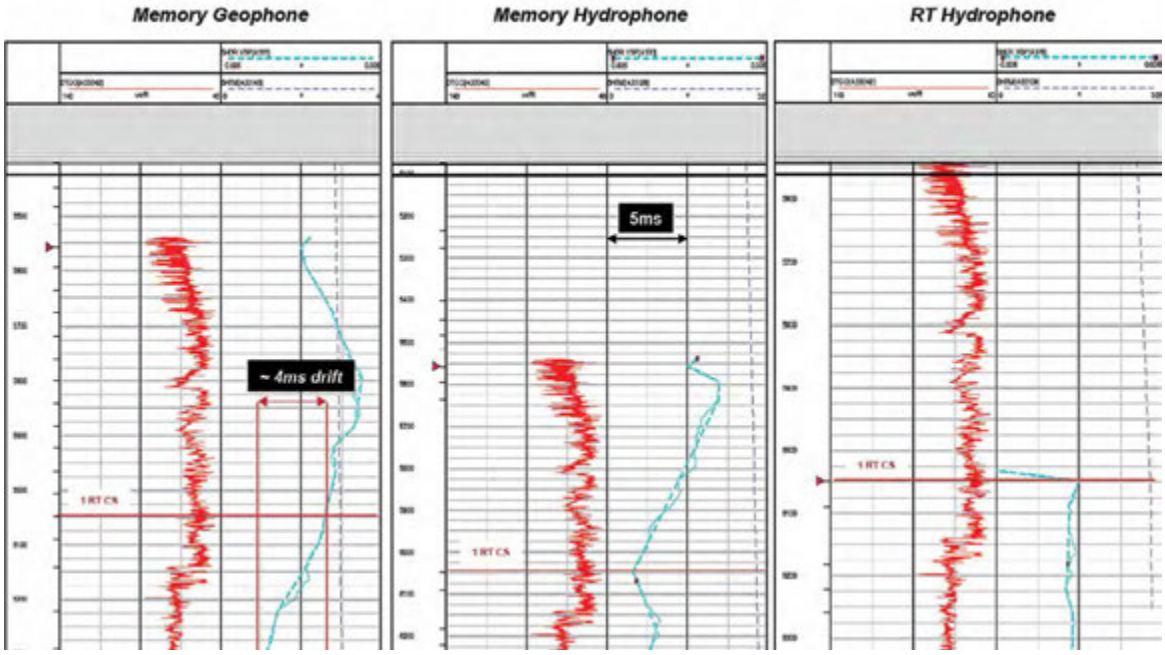

Figure 5: LWD sonic drift. In red, the LWD sonic, and, in blue, the sonic drifts computed using the SWD data: memory geophone (left), memory hydrophone (middle), and real-time hydrophone (right).

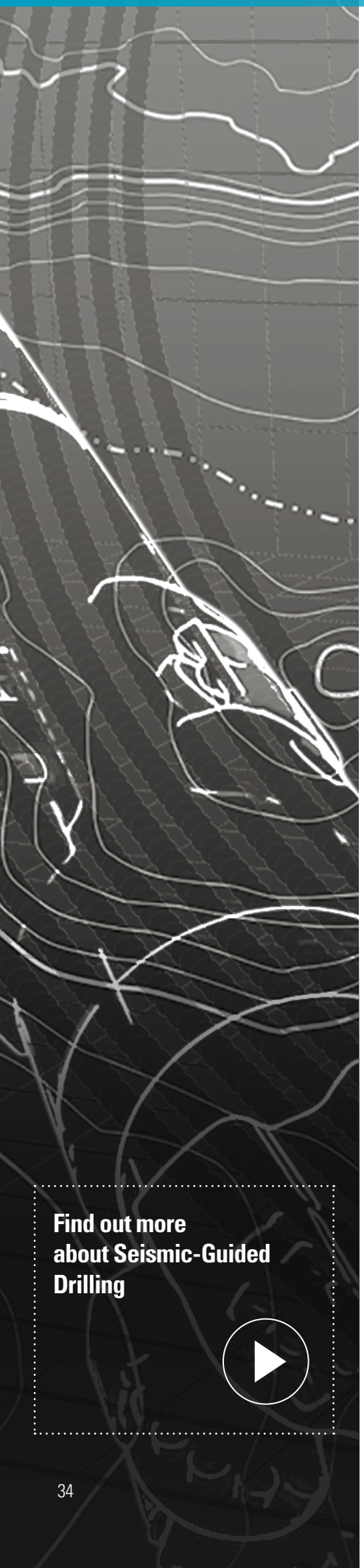

Find out more about Seismic-Guided Drilling

Seismic-Guided Drilling:

Near real-time 3D updating of subsurface images and pore pressure model.

Seismic-guided drilling (SGD) is a workflow that uses drilling information from a well being drilled and existing surface seismic data plus offset well information, to recalibrate and update the existing 3D earth model, including the seismic image, pore pressure, fracture gradient, and geological hazards in order to reduce drilling uncertainty and mitigate drilling risk ahead of the bit.

The modern practices in drilling heavily rely on the predrill earth models. Often, the predrill models are not precise due to the inherent non-uniqueness in our remote sensing techniques. While LWD, seismic while drilling (SWD), and wireline provide useful information along the borehole, they offer little understanding about the rock property ahead of the bit. SGD is a technology that constantly improves the 3D earth model ahead of the bit through the integration of current well measurements with existing surface seismic data, with a turnaround time of 24 hours. It not only corrects the model error behind the bit but also improves prediction ahead of the bit.

The lack of adequate technologies, measurements, and turnaround time limitations has made this type of optimum utilization/integration of seismic data and well data impractical until now. Recent developments in model building, rapid and accurate imaging technologies, and the availability of new well measurements, aided with modern engineering and computation, have made this optimum combination a reality. SGD has been used in several high-profile deepwater HPHT wells worldwide with considerable successes. The technology is especially valuable in areas of low exploration activity or high geological complexity.

The paper focuses on illustrating the concept of SGD technology and presenting a field example in the Gulf of Mexico, USA.

Introduction

An accurate 3D earth model, in terms of spatial positioning of geological structure, fault, and reservoir rock properties is the key for success in petroleum exploration and exploitation drilling. Particularly formation pore pressure profile, more accurately, the drilling window profile (which is the corridor between pore pressure and fracture gradient versus drilling depth) determines the drillability of a proposed target.

Seismic information has been extensively used for earth-model building—including imaging and pore pressure estimation—in petroleum basins worldwide. These tasks usually take months, even years, to accomplish because of geological complexity and demand for large-scale computation. Despite the effort, the earth model, including formation pressure and other beyond-imaging products, is still error-prone because of the lack of resolution, high noise level, and the intrinsic nature of non-uniqueness. The error not only directly affects the success rate of exploration, but also poses engineering hazards throughout drilling.

Often the "ground truth" measurements from drilling such as LWD, seismic vision while drilling (SVWD), vertical seismic profile (VSP), modular formation dynamics testing (MDT), leakoff test (LOT), etc., show that predrill prediction is not accurate enough. These real-time measurements are crucial information for recalibrating and updating the predrill earth model in order to improve predictions in the deep section. In the past, the recalibration is usually done post-drill due to the time and effort needed. For this reason, the recalibration with the latest drilling information does not impact the actual drilling of the well.

To maximize the information usage and to optimize the drilling,an SGD workflow is devised. SGD builds an earth model, including imaging, formation pore pressure, and other beyond-imaging products. It updates the earth model multiple times at designated depths during drilling. The target SGD depths are of either geological or engineering importance, such as

Seismic-guided drilling is used to successfully modify well trajectory, casing points, and mud-weights in real time in the Gulf of Mexico.

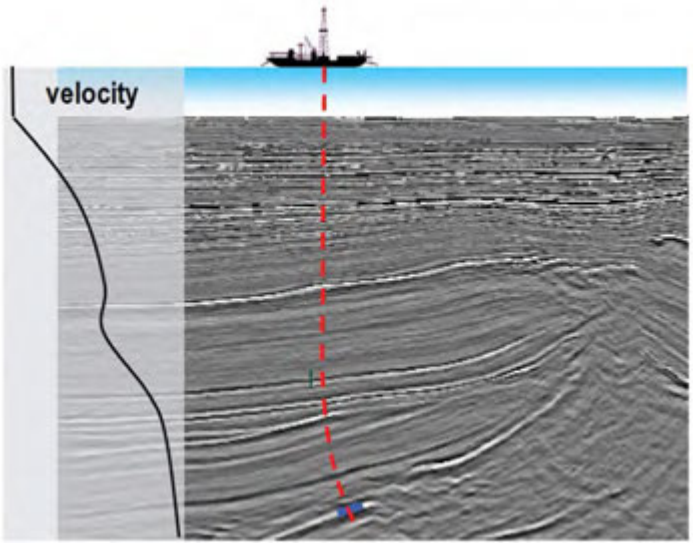

Figure 1: Predrill planning of a well with the new process. The local seismic data are reprocessed for the best local high-resolution predrill image, and pore pressure and fracture gradient estimate. Benefits are improved predrill planning of well trajectory, casing points, and mud weights.

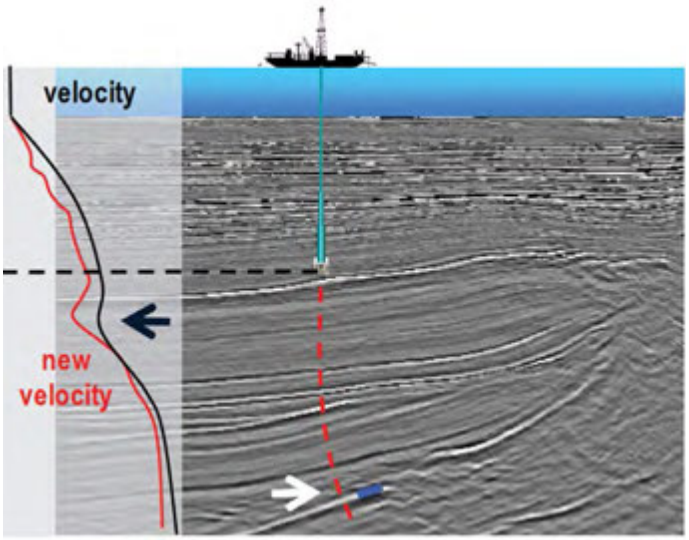

Figure 2: Seismic data are completely reprocessed by using new data as constraints. Structural and velocity data, and, therefore, pore pressure and fracture gradient are updated and uncertainty ahead of the bit is reduced. Note that the depth and lateral position of the target (blue box) has moved.

pressure ramps, fault locations, casing depths, etc.This paper focuses on illustrating the SGD workflow and presenting a field example of the Gulf of Mexico.

Seismic-guided drilling

A typical SGD study covers an area of ~10 x 10 km around a proposed well location. It usually includes a baseline study in predrill to construct the initial earth model and several updates to the earth model while drilling.

In baseline, the best predrill earth model is generated through the application of modern seismic imaging and inversion and offset well calibration (velocity, pore pressure, lithology). The process is constrained by the first principle of rock physics (Dutta et al., 2012). This is done by taking only a small volume around the well location and producing an image only in this drilling volume of investigation using advanced, typically computationally intensive, techniques that may not be practical for large datasets. Furthermore, localization of the process allows the creation of a velocity model representative of the local geology.

Predrill analysis of a well in SGD is made using the seismic image and estimated rock properties important for drilling, such as pore pressure, fracture gradient, and other geomechanical properties derived from reprocessed baseline volumes. Figure 1 shows an example SGD baseline seismic image, and a velocity model, that normally would have come from the processing of a large exploration dataset. A well plan is made including trajectory, casing locations, mud program, etc. The better this initial predrill model is, the better the drilling and completion plan can be.

As the well is being drilled, new information becomes available from the LWD logs, checkshots, MDT, LOT, mud weights, cuttings, drilling events, etc. These could come from LWD or intermediate wireline measurements. The new information represents the "true" property of the earth in the drilled interval.

At the depth indicated by the black-dash line shown in Figure 2, an SGD update is triggered. Seismic data are completely reprocessed by using this local information thus far as constraints (recalibration). Checkshot-constrained local tomographic inversion is used to get new velocities (Bakulin et al., 2010). This is followed by a full-depth migration. An updated image with updated velocity profile along the wellbore (red curve) is shown in Figure 2. Note that the drilling target (blue box) has now moved in both a vertical and lateral position.

In addition, well logs are used to update the local rock model used in pore pressure prediction, and the pore pressure and fracture gradient are updated with the enhanced rock model and velocity information in near real time. This provides key information in a timely fashion to modify the drilling program such as casing plan and mud program ahead of the bit (~24 hours turnaround time). The work cannot be accomplished by any other workflow that only uses well data for model updates.

As a result of the update, the drilling trajectory (blue dash-line), casing design, and mud program are adjusted in order to successfully intersect the target, as shown in Figure 3. The target would have been missed without the aid of SGD implementation on this well.

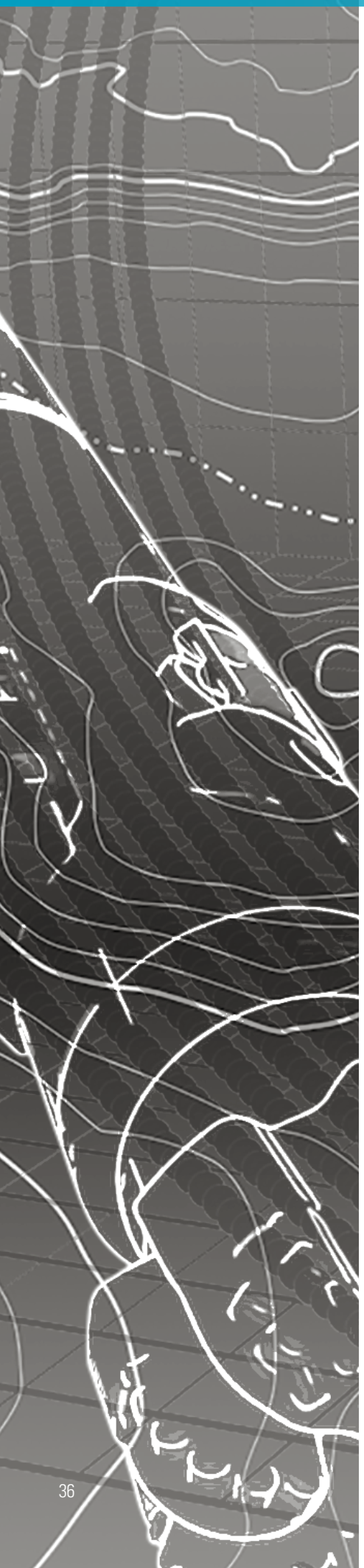

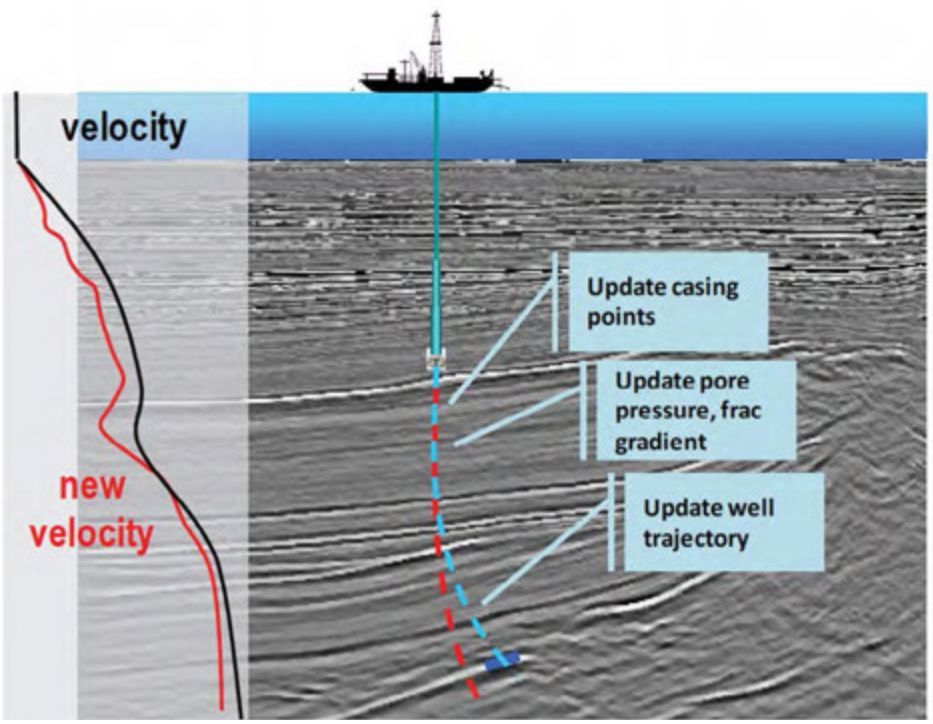

Figure 3: Well trajectory, casing points, and mud weights are modified based on the new image and predictions ahead of the bit. Benefit is reduced risk and/or elimination of unnecessary casings.

In real SGD applications, model updates usually occur multiple times at designated depths which are of either exploration or engineering importance. Sometimes, SGD updates are triggered when significant errors in predrill models are detected from the LWD measurements or other drilling information.

SGD field example

The SGD workflow was tested in the drilling of Well C in the Gulf of Mexico as shown in Figure 4.

The primary challenge was to place a 13 ⅝-in casing below a secondary fault at the interval covered within the blue circle shown. This was necessary for the hole size requirements in the final well completion.

Locating both primary and secondary faults accurately was deemed critical for drilling-hazard mitigation purposes. Data from one offset well, Well B (see Figure 4) were used to build a local anisotropic model extending into the new well location. However, Well B data were limited to the deeper sections and could not be used to build a reliable predrill model in the shallower section in the drilling volume of interest. Large uncertainties were expected in the positioning of pressure-changing faults on existing seismic data. It was important to improve the velocity model and reimage while drilling using shallow information from Well C itself to reduce the positional uncertainty of the fault locations.

LWD, checkshot, and wireline data were acquired all the way up to the mudline to complement the offset well for a good velocity model. Anisotropic velocity models were created in several stages by seismic tomography where the vertical velocities were constrained by well data. The volume for velocity models included the offset well to ensure a proper tie to Well B, in addition to the well being drilled.

Multiple updates were triggered throughout the drilling. For each updated velocity model, the surface seismic data were reimaged while drilling, enhancing fault location accuracy in time to impact drilling and casing decisions. The desired casing location was accurately predicted within +/- 10 ft (right-hand panel in Figure 5), compared to ~750 ft error existed in the legacy data (shown in Figure 5). The final SGD update is made at ~1,500 ft above the planned casing depth.

Comparison of structure maps for the key horizon between legacy and the latest update is shown in Figure 6. Faults definition and positioning, and structure accuracy are much enhanced in the latest update. The SGD update not only helps the well placement, but also reduces uncertainty in planning subsequent development wells (including side tracks).

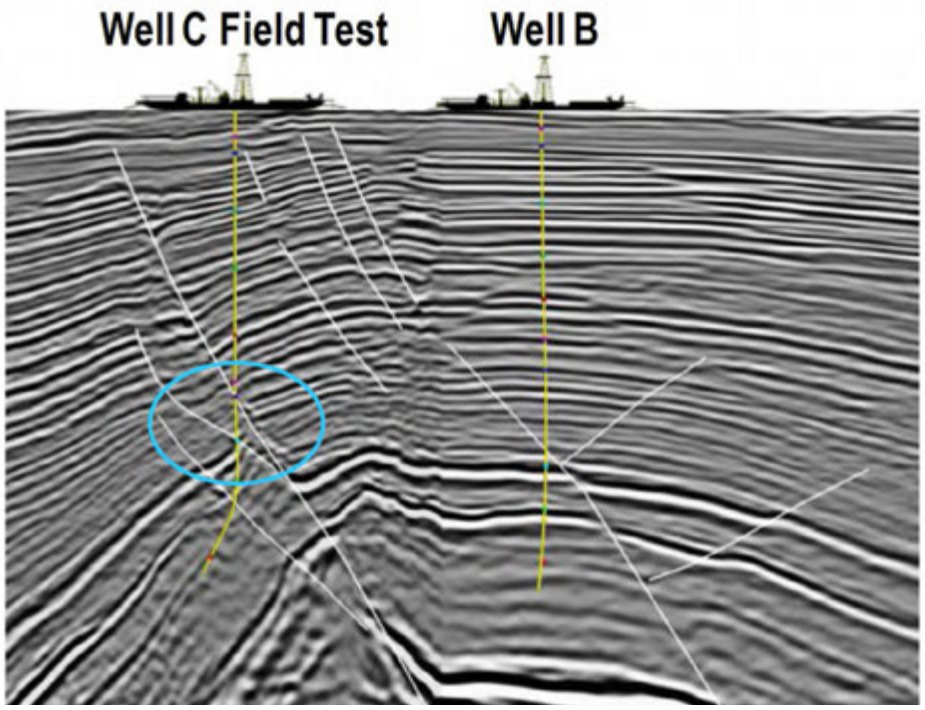

Figure 4: In a Gulf of Mexico well (Well C), a primary challenge was to place the 13 ⅝-in casing below a secondary fault due to hole-size requirements in the final well completion. Locating both primary and secondary faults accurately was critical. Large uncertainties were expected in the positioning of events using the existing seismic image. While-drilling data from Well C was used to improve the velocity model and reimage to reduce the positional uncertainty of the fault locations.

Figure 7 shows the faults enhancement of the final update as against the legacy images.

Substantial fault shifts are observed between the two-stage images. Accurate fault positioning in the SGD-updated image is crucial for the correct setup of the 13 ⅝-in casing for the test well, which is the key objective of the SGD test project.

The field test shows that SGD is a powerful workflow to recalibrate and enhance the earth model in real time for drilling decisions, by incorporating new information from the well being drilled. It utilizes the latest imaging technology and produces model updates in a very short time. Well C would be extremely challenging to drill without the aid of the SGD implementation.

Conclusions

Successful drilling, planning, and execution can greatly benefit from an accurate high-resolution earth model obtained from seismic data integrated with real-time well information. The workflow is called seismic-guided drilling (SGD). SGD is the only workflow that can update the subsurface geophysical and geological models and provide in-time corrections to predrill mud weights, casing depth, fracture gradients, and other geological hazard predictions. The workflow enables the application, for the first time, of traditional geological and geophysical analysis in the context of active well drilling.

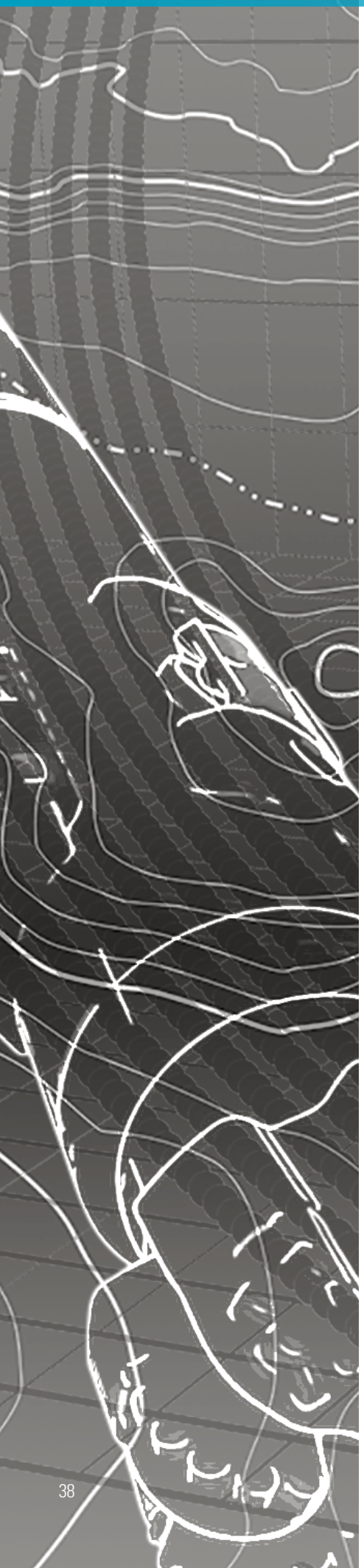

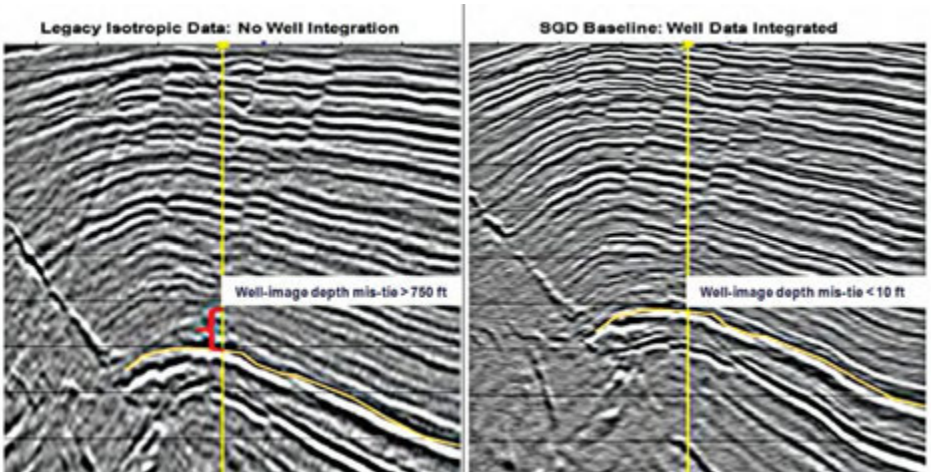

Figure 5: The left panel shows the legacy image that existed prior to the project. An anisotropic velocity model was built using the offset well (Well B) data and seismic data were depth migrated. The right panel shows the result giving the best possible predrill image at the baseline stage. There is a significant (>750 ft) depth shift in the new image compared with the legacy image. Drilling showed that the new image for this horizon was within 10 ft of the prediction.

References

Bakulin, A., Woodward, M., Nichols, D., Osypov, K., and Zdraveva. O., 2010. Building Tilted Transversely Isotropic Depth Models Using Localized Anisotropic Tomography with Well Information. Geophysics, 75, D27–D36.

Dutta, N.C., Yang, S., and Dai, J., 2012. Advances in Depth Imaging Technology: Rock Physics Guided Migration of Seismic Data in 3D. Proceedings of Indonesian Petroleum Society, 36th Annual Conference, May 2012.

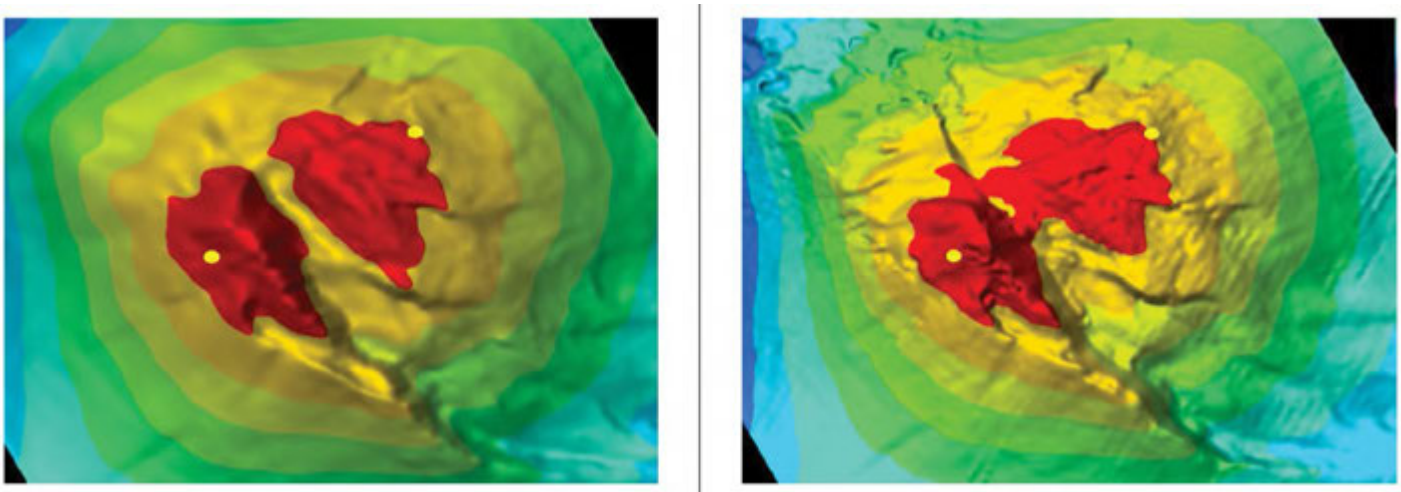

Figure 6: The same comparison as in Figure 5 in plan view. The left panel is the legacy image that existed prior to the project. The right panel shows the new image. The updated image shows a better description of structure and faults because of the utilization of all available data and better focusing provided by the new anisotropic local velocity model. The updated image has higher-frequency content than the legacy image due to parameterization of legacy processing.

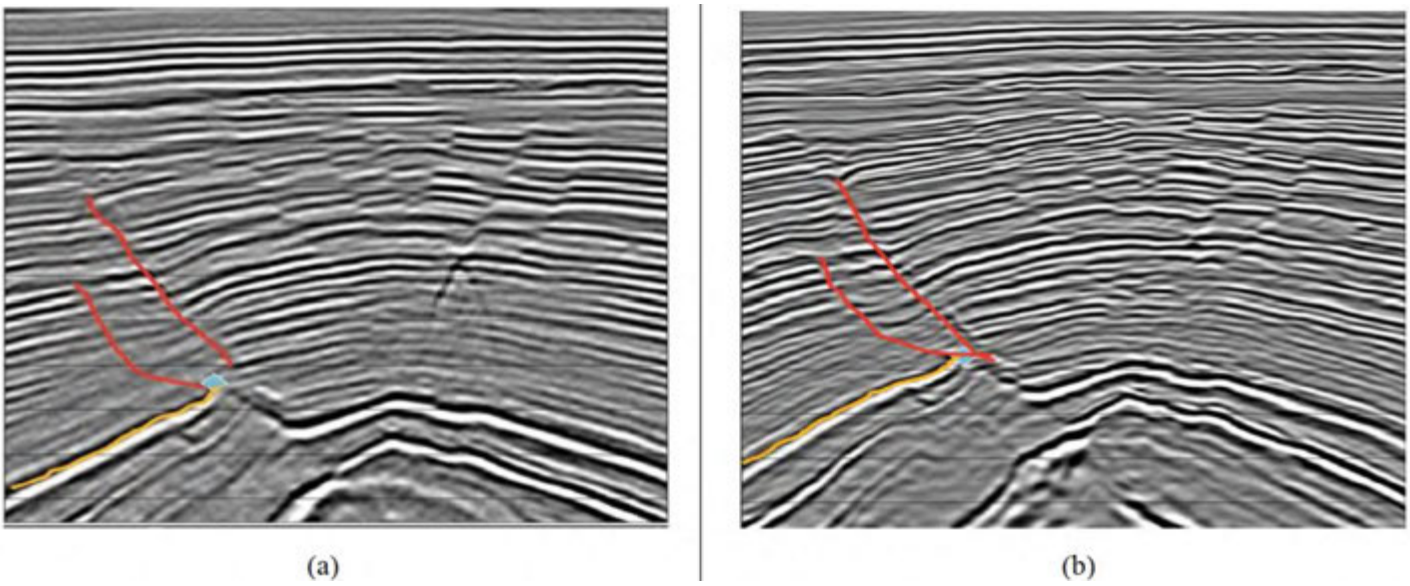

Figure 7: The left panel (a) is the legacy image that existed prior to the project. The right panel (b) is the seismic image after the final update. Both have fault interpretations displayed. There was a significant shift in the spatial locations of the faults targeted for the casing point. The lower fault is believed to be sealing.

Find out more about the RHINO XC reamer

Solving Deepwater GoM Pore Pressure Puzzle:

Multiple activation reamer eliminates trip prior to running coring bottomhole assembly.

The nature of pore pressure profile on deepwater Gulf of Mexico wells dictates the need for hole enlargement while drilling (HEWD) on several intervals. HEWD is a well-established practice in deepwater GoM and allows casing programs with smaller ID clearance between consecutive casing strings.

Abstract

Although the reservoir section is typically drilled as a single diameter, HEWD is required for many of the larger upper hole sections. However, in some cases, drilling conditions require the operator to deviate the casing program from plan. On a recent deepwater Gulf of Mexico Lower Tertiary well, pore pressure anomalies, high mud weight, and associated equivalent circulating density (ECD) required the operator to raise the formation integrity test (FIT) to the maximum limit while drilling the 14 ½-in x 16 ½-in section. To solve the problem it required the premature setting of a 14-in casing string.

The subsequent 12 ¼-in section was initially planned as a single diameter drilling interval.

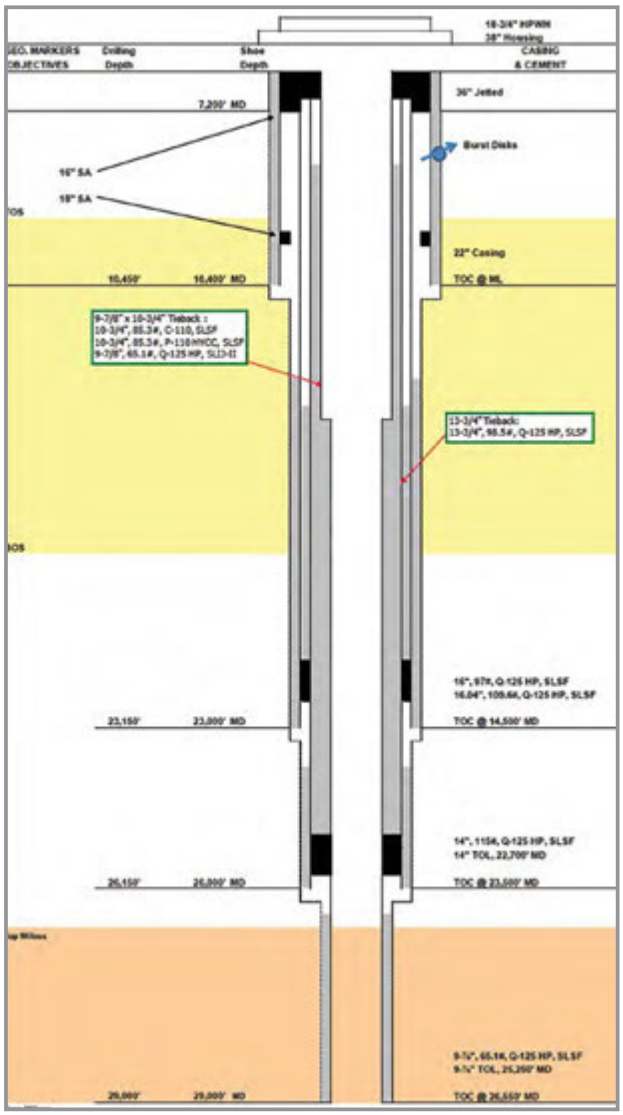

Figure 1: Casing plan for GoM lower tertiary field.

Use of ream-on-demand technology reduces pore pressure uncertainties and significantly increases operational efficiency while drilling a development well in the Gulf of Mexico.

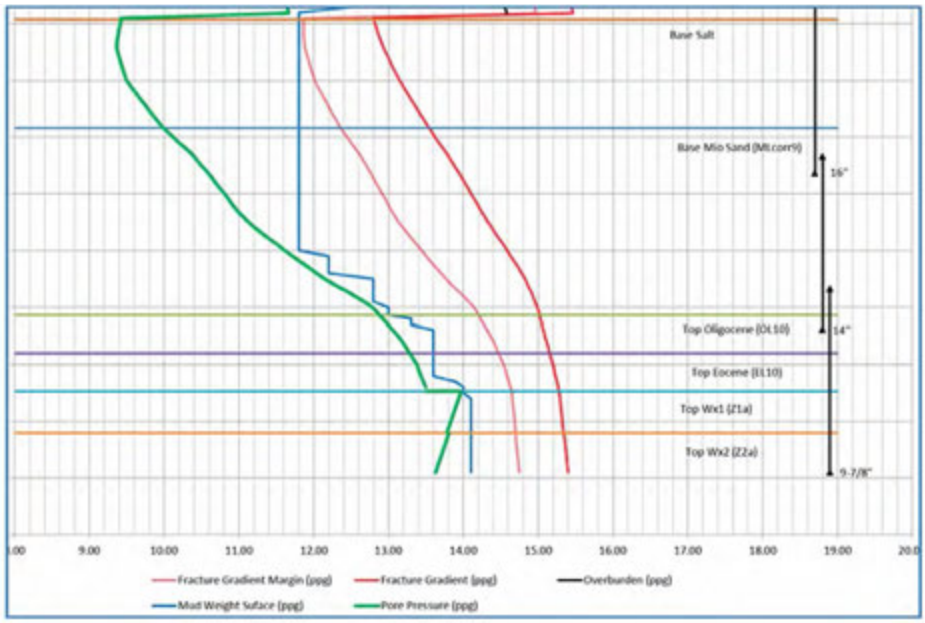

Figure 2: Predicated pore pressure and fracture gradient trend in GoM Lower Tertiary field.

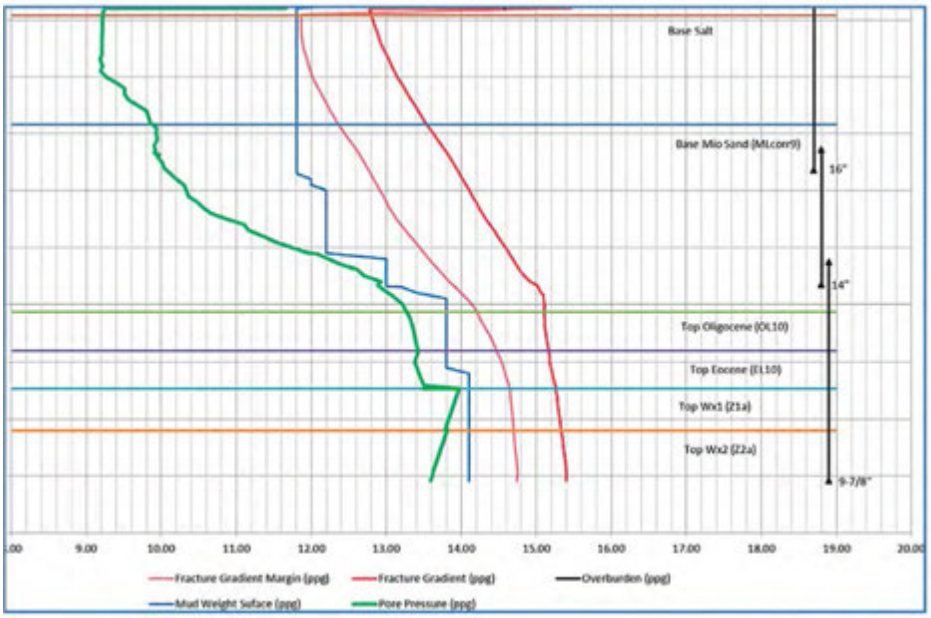

Figure 3: Actual pore pressure and fracture gradient trend in GoM Lower Tertiary field.

However, to account for pore pressure variations experienced on the previous section and to avoid narrowing of the producing casing size, the plan was modified to incorporate a contingency liner. The 12 ¼-in section would have to be enlarged to 13 ½-in in case a contingency 11 ⅞-in liner was needed. Adding to operational complexity, the original drilling program included a plan to core the 12 ¼-in section. To stabilize the coring BHA would necessitate a minimum of 250 ft of 12 ¼-in rathole. To achieve all 12 ¼-in objectives, an extra unplanned trip would be required.

To solve application intricacies, the operator elected to use a new-type ream-on-demand (RoD) system in the 12 ¼-in section and eliminate multiple trips to change out BHAs. RoD technology is equipped with an innovative hydraulic mechanism that can be opened and closed multiple times as required while drilling.

After risk assessment and pre-job planning, the 12 ¼-in section was successfully underreamed to a 13 ½-in diameter with the RoD tool. The pressure regime was carefully monitored and it was determined the 11 ⅞-in contingency liner was not required.

The reamer was then closed at the top of the coring section and a 12 ¼-in borehole was drilled an additional 250 ft, offering the required stabilization for the subsequent coring run.

Utilization of the RoD technology eliminated a round trip prior to using the coring BHA and significantly increased operational efficiency while enhancing project economics.

Introduction

Typical top-hole design for the well includes 36-in conductor casing and 22-in structural casing (Figure 1). Pushing the well design limit to use the full hoisting capability of the sixth-generation drillship, the well design features one of the longest and heaviest 16.04 × 16-in liners installed in a Gulf of Mexico (GoM) deepwater well. A 13 ¾-in drilling tieback has to be installed before drilling a 12 ¼-in hole into the reservoir section to satisfy the worst-case discharge casing design.

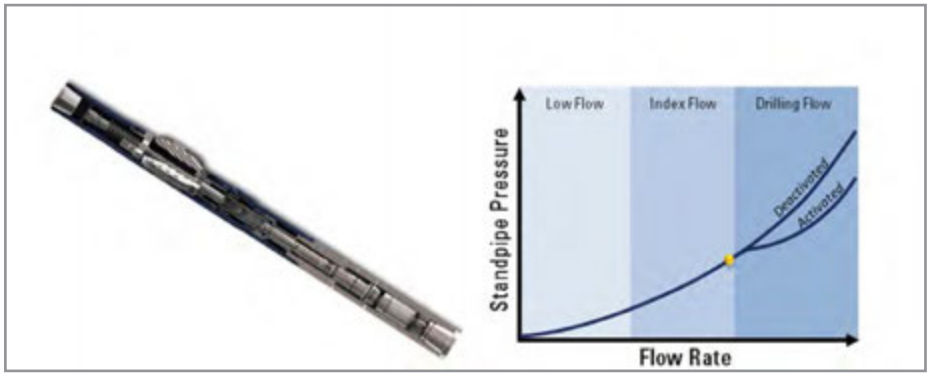

Figure 4: Schematic of ream-on-demand system (left). Index flow rate and drilling flow rate for tool (right).

The 10 ¾-in x 9 ⅞-in production tieback is also incorporated as part of the well design to accommodate current and future completions design.

Geological overview and well plan

The well was proposed to drill directionally from a drill center to a total depth exceeding 29,000 ft MD with a maximum angle of 24°. Sections to be drilled through in this well include a thicker faulted carapace section above salt compared to offset wells; a thick salt section and subsalt Pliocene, Miocene, Oligocene, and Paleocene age siliciclastics with marls and some carbonates.

The drilling and casing plan for the development well consisted of the following intervals:

- 26-in hole section (22-in casing): The 26-in section would be drilled riserless and 22-in casing was set in salt.
- 18 ⅛-in x 21-in hole section (16-in casing): This interval was designed to drill a largely homogeneous, clean salt body with a potential of tar and/or salt inclusions. The directional plan in this interval called for build-up to 24° and then to hold this inclination until the well reached TD.
- 14 ½-in x 16 ½-in hole section (14-in liner): This hole section would drill through Early Miocene formations and reach section TD in the top of the Oligocene. This section contained a tar hazard due to a fault intersecting the borehole. A poor leakoff test (LOT) occurred at one of the offset wells in this hole section at the 16-in casing shoe. Additionally, there was a potential for weak formation issues and lost return zones in this hole section.
- 12 ¼-in openhole and coring: This hole section contained the primary objective interval and was expected to penetrate interbedded sandstones and shales. A fault was identified as a potential tar source. Additionally, there could be lost return zones above the Wilcox formation.

BHA
12 ¼-in PDC bit
RSS
12 ⅛-in real-time stabilizer
Resistivity tool
MWD
Crossover sub
Filter sub
12 ⅛-in IB stabilizer
12 ¼-in x 13 ½-in ream-on-demand tool
1 x 8 ¼-in collar
12 ⅛-in IB spiral string stabilizer
Circulating sub
6 x 8 ¼-in drill collar
Crossover sub
6 ⅝-in spiral HWDP
Hydraulic jar
6 ⅝-in spiral HWDP

Figure 5: BHA with ream-on-demand tool.

Pore pressure uncertainties and contingency plans

Data from offset wells in the same field were used to predict pore pressure uncertainties and prepare contingency plans.

It was predicted that the pore pressure gradient would increase in the 14 ½-in x 16 ½-in hole section below the proposed 16-in casing and pressure would increase steadily to around 13 ppg at the top of the Oligocene (Figure 2).

This pressure ramp was seen on one of the offset wells and resulted in high background gas which required heavier mud weight that resulted in setting the casing shallower than expected.

This pressure ramp was controlled in a different offset well with equivalent circulating density (ECD) and a proper mud-weight increase program.

The small flow at the TD of the 14 ½-in x 16 ½-in hole section suggested that the well was drilled close to balance towards section TD. The flow was controlled with an increase of 0.3 ppg MW to the drilled MW from 13.1 ppg to 13.4 ppg. A maximum pore pressure of 13.05 ppg was anticipated for this hole section.

Figure 6: RoD tool activation sequence.

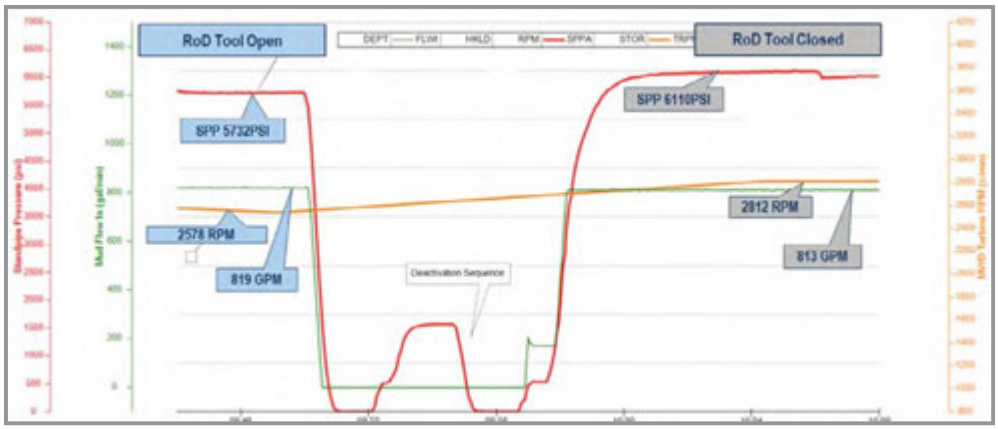

Figure 7: RoD tool deactivation sequence.

Based on these uncertainties, the contingency plan for the development well was as follows:

- If pore pressure while drilling the 14 ½-in x 16 ½-in section exceeds the formation integrity test (FIT) of the 16-in casing shoe pressure, set the 14-in casing shallower than planned.
- Drill the next section 12 ¼-in x 13 ½-in instead of 12¼-in section to accommodate 11 ⅞-in liner.
- Continue farther with 10 ⅝-in x 12 ¼-in section to TD to run 9 ⅞-in liner.

Drilling events

Drilling commenced on the well and the 16-in casing was set without any notable drilling events. The pore pressure increased at a steeper slope than the prognosis while drilling the 14 ½-in x 16 ½-in section, approaching the high side of the model (Figure 3).

As drilling proceeded, a gain was observed in the active system while drilling and a flow check was performed. A total of 6 bbl influx was detected and the well was shut in.

The well was killed with 13 ppg kill weight mud (KWM). Drilling continued for approximately 200 ft after the influx event depth before the mud weight was raised to 13.4 ppg and the ECD value observed was 13.74 ppg. With the ECD close to the FIT of 13.97 ppg EMW, the decision was made to call the section TD approximately 700 ft shallower than the planned casing shoe depth. Since the 14-in casing was prematurely set, it was extremely important to perform a detailed risk assessment and properly plan for the next section.

The 12 ¼-in section was initially planned as a single-diameter drilling interval. However, to account for pore pressure variations experienced on the previous section and to avoid narrowing of the producing casing size, the plan was modified to incorporate a contingency liner. The 12 ¼-in section would have to be enlarged to 13 ½-in in case a contingency 11 ⅞-in liner was required. Adding to operational complexity, the original drilling program included a plan to core the 12¼-in section.

Stabilizing the coring BHA would necessitate a minimum of 250 ft of 12 ¼-in the rat-hole. In effect, two separate hole sizes would be required to achieve all the objectives of the 12 ¼-in interval.

Planning and execution

Ream-on-demand system

The service company has developed a ream-on-demand (RoD) system (Figure 4) that provides operators with the flexibility to activate and deactivate the reamer on demand. The innovative hydraulically-actuated mechanism minimizes the time required to change the status of the reamer and does not require pumpdown activation devices.

The tool is activated and deactivated by staging the mud pumps on and off with a predetermined flow rate. Additional details of the tool and its applications can be found in the listed references.

The operator's requirements for the 12 ¼-in interval were identified as a suitable application for the deployment of the RoD system.

Since the RoD system had been recently introduced as a commercial offering, a joint risk assessment of the tool's design and features was conducted by the operator and service company personnel. The service company initiated pre-section planning after the initial approval from the operator.

BHA design

The BHA was planned based on the formation evaluation requirements of the 12 ¼-in interval (Figure 5). The RoD tool was deployed in the conventional position of reamers in HEWD BHAs. Tools were shipped out to the rig-site and the BHA was assembled. The RoD tool also features a unique surface test feature that allows the operator and service company to verify the tool functionality and calibrate the hydraulics analysis prior to tripping in hole. The surface calibration test was successfully conducted. Flow rate and standpipe pressure measurements indicated that the hydraulics matched closely with pre-job planning estimates.

Activation of RoD tool

The reamer was activated below the 14-in casing shoe by following the pre-established indexing procedure (Figure 6). Bypass of drilling mud from the reamer to the annulus created a 300 psi drop in the standpipe pressure. The flow bypass also caused a 351 RPM drop in MWD turbine RPM. Finally, the deployed cutter blocks were used to pull upwards against the casing shoe and 10,000 lbs overpull was observed. These three indications confirmed that the reamer had been activated as planned. The total time for activation was approximately 18 minutes, of which approximately 8 minutes were required for indexing the RoD tool from the closed to open position.

Drilling/reaming

HEWD commenced after the RoD tool was activated. A total of 1,600 ft was simultaneously drilled and reamed from the 14-in liner shoe to the top of the reservoir section. At that point, the 11 ⅞-in was no longer deemed necessary and the forward plan was to close the RoD tool and drill ahead to the coring point.

Deactivation of RoD tool

The reamer was deactivated at the chosen depth by following the pre-established indexing procedure (Figure 7). The deactivation of the RoD tool resulted in an increase in standpipe pressure of 378 psi and MWD turbine revolutions increased by 234 rpm. The total time for the activation was approximately 15 minutes.

Drill ahead with bit

An additional 538 ft were drilled with the reamer in the closed position until the bit reached the coring point. Changes in surface torque with the RoD tool in the open versus closed position provided additional confirmation of reamer deactivation. Gamma ray and resistivity measurements were used to identify coring point markers.

The flow rate and standpipe pressures were continuously monitored during these operations to ensure the RoD tool remained in the deactivated state. The BHA was pulled out of the hole after circulating bottoms up. The flow rate and standpipe pressure were continuously monitored during these operations to ensure the RoD tool remained in the deactivated state.

Details of the coring and wireline operations are considered outside the scope of this paper. However, it should be noted that the coring BHA run was uneventful and the operator was able to successfully recover 240 ft of core. The subsequent wireline operations included a caliper log which confirmed the RoD tool had successfully enlarged the hole to 13 ½-in up to the depth where it was deactivated (Figure 8).

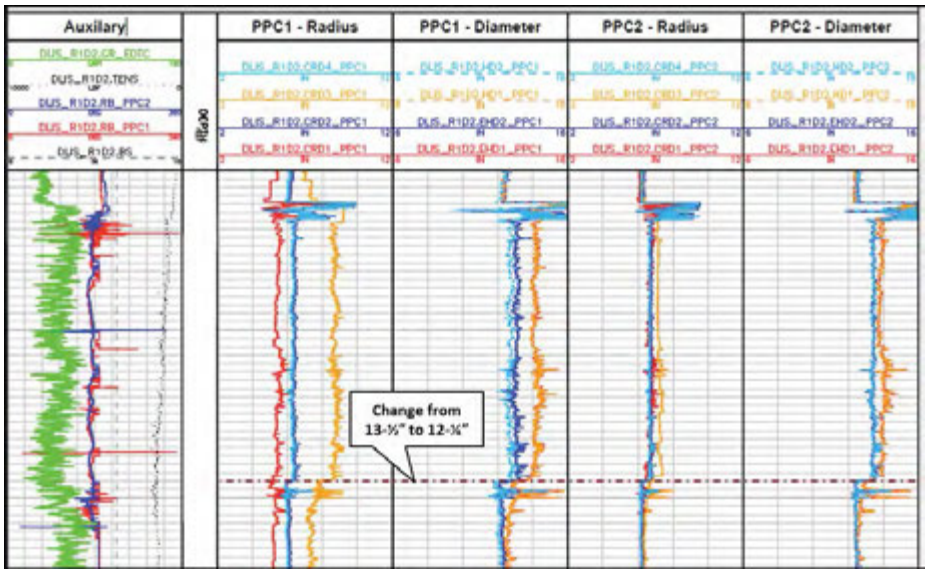

Figure 8: Wireline caliper log showing transition from 13½-in to 12¼-in hole size at reamer deactivation depth.

Conclusions

Pore pressure uncertainties while drilling can add significant cost due to the possibility of requiring contingency casing sizes. When coupled with the need to maintain the hole size in the reservoir section as planned, PP uncertainties could add multiple BHA runs to the drilling program which ultimately result in significant cost additions to the project. Until recently, the low-risk option for operators has been to run HEWD BHAs to evaluate the need for the contingency casing and add an additional trip to remove the reamer from the BHA if the contingency was deemed unnecessary. The RoD tool now offers operators the flexibility to activate and deactivate the reamer as needed while evaluating PP trends in the well.

The RoD tool was successfully deployed to overcome the potential additional time and complexity of navigating through the pore pressure issues on this development well. Significant time and cost savings were realized by eliminating a BHA trip from over 25,000 ft MD.

Additional time and cost savings were achieved by eliminating the need to pump down devices.

Acknowledgements

The authors would like to thank the management at Chevron North America E&P and Schlumberger for their permission to publish the well data and engineering concepts outlined in this paper. The authors would like to thank Craig Fleming, Schlumberger, and Aaron Conte, Chevron, for their technical writing and editorial contributions.

Nomenclature

HEWD = Hole Enlargement While Drilling
BHA = Bottom Hole Assembly
TD = Total Depth
MD = Measured Depth
MWD = Measuring While Drilling
LWD = Logging While Drilling
RSS = Rotary Steerable System
PP = Pore Pressure
FG = Fracture Gradient
MW = Mud Weight
FIT = Formation Integrity Test
LOT = Leakoff Test
ECD = Equivalent Circulating Density
KWM= Kill Weight Mud

References

1.Torvestad, B.T., Ray, T., Hu, J., Gjertsen, O.J., Muir, M.: "Development of a New Advanced Multiple Activation System for Concentric Underreamers," Paper SPE 151337 presented at the SPE/IADC Drilling Conference & Exhibition, March 6–8, 2012, San Diego, California, USA.

2. Torvestad, B.T, Bjoerneli, H.M, Toerge, K., Andreassen, L., Haavardstein, S., Blikra, H.: "Industry's First Hydro-Mechanical Surface Controlled System for Multiple Reamer Activation/Deactivation Increases Drilling Efficiency," Paper SPE 163537 presented at the 2013 SPE/IADC Drilling Conference and Exhibition, March 5–7, 2013, Amsterdam, The Netherlands.

3. Lirette, N., Aubin, M., Davis, J., Duvvuru, H., Nagaraj, M.: "Ream-on-Demand System Eliminates Dedicated Trip to Enlarge Rathole in Deepwater Gulf of Mexico," Paper SPE 166127 presented at the 2013 SPE Annual Technical Conference and Exhibition, September 30–October 2, 2013, New Orleans, Louisiana.

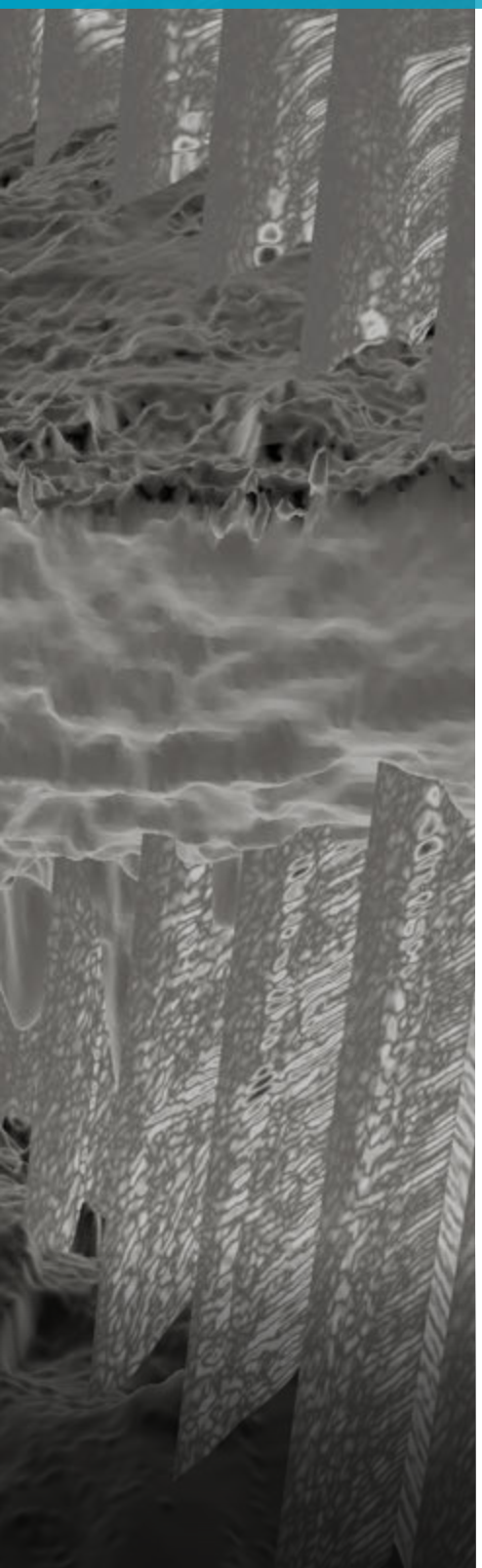

Find out more about Seismic-Guided Drilling

Drilling a Deepwater Well

in a subsalt structure in Mexico.

In the Gulf of Mexico, large oil and gas reservoirs are associated with subsalt structures and are very attractive for potential hydrocarbon reservoirs. In 2009, Pemex pursued drilling a prospective location identified with 3D seismic located in a subsalt structure in the Tertiary formations. The Kabilil-1 well was located in 740 m water depth and the plan was to drill to the Lower Miocene and Upper Oligocene alluvial sediments. The well was drilled with the Ocean Voyager (third generation) in 94 days and reached a TD of 5,350 m.

Although subsalt drilling is a challenge in itself, it is not uncommon for operators in the deepwater Gulf of Mexico (GoM). The Pemex Kabilil-1 well was a deepwater subsalt first for Pemex in this challenging environment. The decision was taken to avoid the drilling risk through the salt and the trajectory was planned to go around the salt flank. This alternate strategy also posed challenges such as drilling through the sheared zone (rubble zone) that is commonly found underneath salt tongues or adjacent to salt diapirs where there is always a risk of getting stuck. In the well preparation phase, a finite-element numerical model was employed along with a 3D-MEM simulator (Stonefish geomechanics software and VISAGE* finite-element geomechanics simulator) to predict the effects of the initial in-situ stresses and induced increases in stress as a result of the salt intrusion. The induced stresses increase near the salt intrusion and result in subsalt overpressure, pressure reversion formations, and wellbore stability problems.

The predrill model was updated in real time using the Stonefish-RT geomechanics real-time software that has the ability to assimilate logging-while-drilling sensor data (sonicVISION* sonic while drilling service, arcVISION* array resistivity compensated service, seismicVISION* seismic while drilling service) to allow calibration of the pore pressure and breakdown pressure against predrill model. According to the predrill geological well prognosis, the salt proximity to the well was within 200 m of the well trajectory, but reliable calibration was needed to verify top of salt and salt flank proximity in real time. In an effort to reduce the geological uncertainties, the seismicVISION service was employed to look ahead of the bit to determine the salt distance to well in real time. This service was acquired for the first time in Mexico deepwater basins and was employed to mitigate the drilling risk associated with drilling near salt domes.

It was necessary to set the intermediate casing strings at the appropriate depth to improve the drilling performance of the subsequent well sections (maximize drilling window), segregate the overpressure intervals induced by the salt intrusion, and separate the incompatible formations divided by regional unconformities. During the drilling phase, a drilling optimization service and real-time geomechanics surveillance was performed using onsite drilling optimization engineers on the offshore rig along with geomechanics/geological support at the operator's office. The operation also employed real-time data transmission, advanced PDC drill bits, rotary steerable systems, LWD SCOPE family tools, SVWD service, APWD-annular pressure while drilling, and hydraulic reamers for hole enlargement.

Introduction

In the Gulf of Mexico, successful deepwater exploration and development has been ongoing for almost 20 years, but the experience and knowledge lies predominantly with those involved in deepwater GoM USA, Brazil, and West Africa projects or commonly known as the Golden Triangle. PEMEX (Petróleos Mexicanos) a National Company is embarking on a campaign to explore the high potential deepwater GoM Mexican waters to offset declining production and improve Mexican reserves. The exploratory wells drilled have faced many of the known deepwater problems and the learning curve has been steep and expensive. Leveraging deepwater knowledge and experience is vitally important in reducing technical and financial risk with these costly projects.

According to international classifications, a well is considered deep water when the water depth is greater than 500 m (1,640 ft). In Mexico, these deepwater well types were commenced in 2006 and continue to be drilled in the Mexican Gulf of Mexico employing sixth-generation semisubmersible rigs.

A risk assessment was performed with subsalt/through salt drilling scenarios. Multiple casing strings were implemented in the design to be able to isolate problematic areas and also manage the narrow mud

The application of new technologies, effective predrill modeling, workflows and real-time monitoring have resulted in exceptional drilling performance for Pemex in this challenging environment.

weight drilling window between pore pressure and fracture pressure.

In summary, the Pemex Kabilil-1 well results demonstrated the ability to drill a challenging subsalt well that faced many potential drilling problems. The application of new technologies, effective predrill modeling, and real-time monitoring resulted in exceptional drilling performance.

Geological setting and structure

The Kabilil-1 well is located in the Mexican portion of GoM approximately 105.5 km northeast of Coatzacoalcos, Veracruz, and 253 km northwest of Ciudad del Carmen, Campeche. The water depth is 739 m. (Figure 1). The key structural features in the well location are a salt dome with an overhang feature that is covered by a large regional unconformity as shown in the geological section. The well was located in a structural trap on the east flank of a large anticline deformed by the effect of salt intrusion created during the salt tectonic activity in the Late Miocene and Lower Pliocene.

The target reservoir consists of turbidites, commonly arranged in thickening-upward packages, and amalgamated turbidites in channels that commonly have an initial lateral accretion phase with interbedded sandstone and mudstone deposits, and a subsequent vertical aggradation phase.

Geomechanics modeling

The salt diapir and the mechanics of the deformation of sediments adjacent to salt are complex. Models created in the predrilling design were applied to assist with the well planning and to ascertain the best strategy to reach the subsalt target. The initial 1D mechanical earth model (MEM) was determined insufficient to model the predicted geology, the ability to examine the influence of the salt intrusion, and ability to characterize the induced pressure and earth stresses. The better approach was to create a 3D MEM with a 3D finite element geomechanical simulator for a stress-strain analysis on a 5 x 5 km^2 cube including sedimentary layers and salt bodies (Figure 2). The geomechanical simulations were performed using the VISAGE software and the finite element models were meshed directly from geologic structure maps in Petrel* E&P software platform. A complete description of the geomechanical modeling developed for Kabilil-1 well was published by Aguilera et al, 2011. The 3D MEM approach consisted of using multiple 1D MEMs from offset wells, property propagations using 3D seismic data (velocities and structural), 3D finite element MEM modeling, and wellbore stability analysis along the proposed well path that considered the stresses and pore pressures obtained from the 3D MEM. (Figure 4).

According to Aguilera et al (2011), the stress-strain analysis revealed a significant variation in stress orientation and stress magnitude around the salt bodies. Results indicated that vertical and horizontal stresses were not the principal stresses initially assumed from the 1D modeling. A stress profile created along the planned well trajectory shows a clear increase in horizontal compressive stresses as a result of salt perturbations. It also shows a distinct increase in shear stresses at 1,500 to 2,100 m (TVD) where maximum shear was noted. This depth range coincides with a decrease of vertical effective stress and was interpreted as a high deformation zone with a fault at 2,100 m. The stable mud-weight window from the 3D analysis expressed a distinctly different behavior compared to the 1D model. The 3D model results displayed a higher breakout pressure prediction where the proposed trajectory was close to the salt bodies signifying that the salt body influenced stress in the surrounding sediments more than 1.5 km from the salt domes.

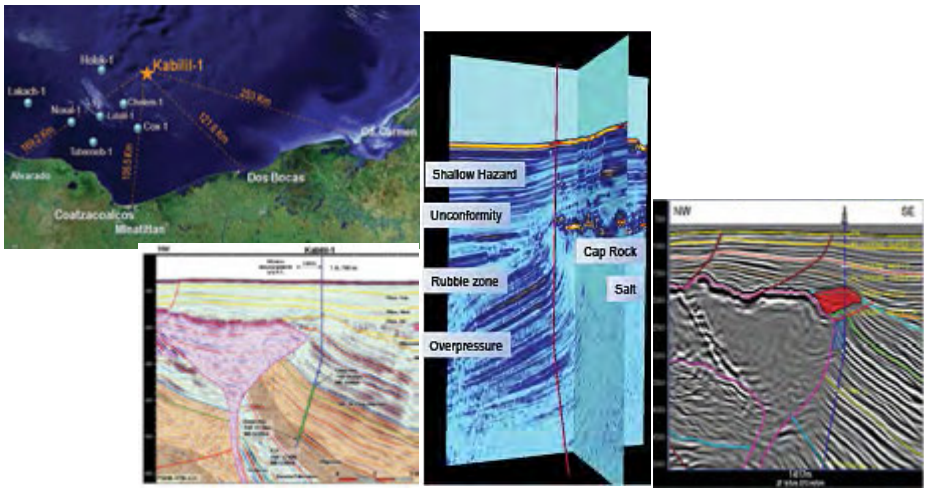

Figure 1: Kabilil-1 well location map—geological settings.

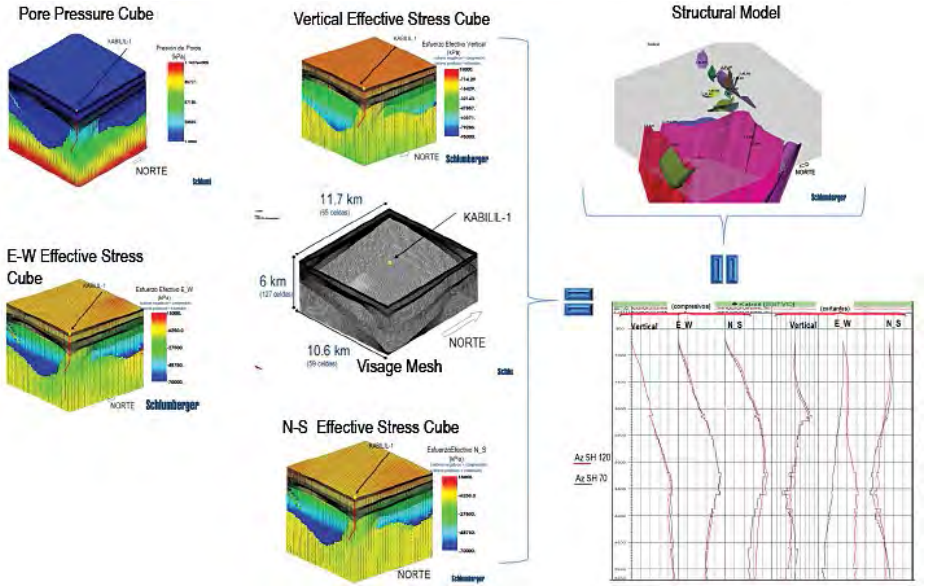

Figure 2: Application of a finite-element numerical model, the VISAGE simulator predicts the effects of initial in-situ stresses and increasing induced stresses as a result of the salt intrusion.

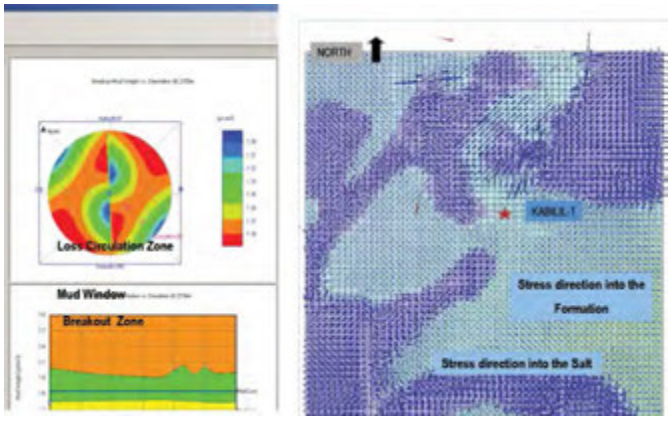

Figure 3: In this graphic, the strong variation of the stress direction can be appreciated from the effect of the surrounding salt bodies. This variation makes it challenging to model the drilling operative mud window considering the additional effects of changing well trajectory (azimuth and inclination).

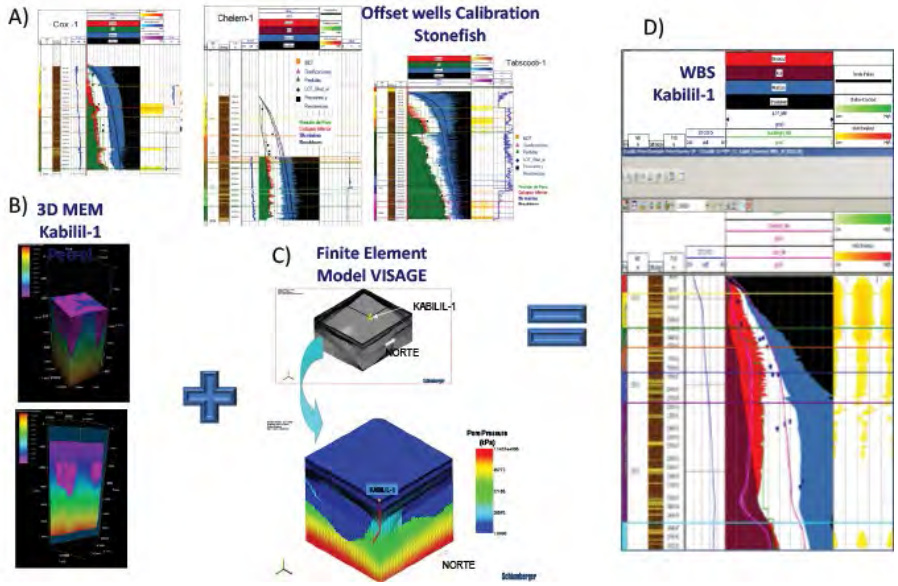

Figure 4: Geomechanics modeling workflow. A) 1D wellbore stability analysis performed over three offset wells. B) Modeling of the pore pressure in a 3D space. C) 3D finite element modelling. D) Wellbore stability analysis along the proposed well trajectory.

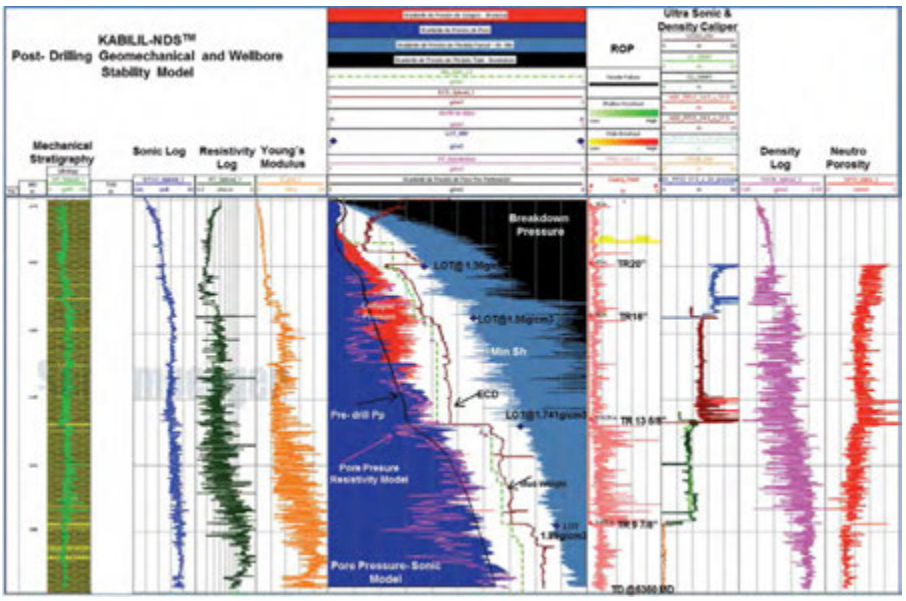

Figure 5: Post drilling geomechanical and wellbore stability model, Kabilil-1.

The mud-weight window obtained from the 3D analysis and sensitivity analysis was prepared considering the in-situ stresses and those generated by the salt intrusion resulting in a defined drilling optimization plan with adequate mud weights for safe drilling. (Figure 3 and Figure 5).

Drilling optimization and real-time surveillance

A fit-for-purpose drilling optimization service was introduced and executed for the drilling of the first deepwater subsalt well in Mexico, Kabilil-1.
The service "No Drilling Surprises" (NDS) comprised drilling optimization and real-time geomechanics workflows implemented during the drilling of the well.

The NDS workflow is founded in a risk-management workflow that consists of creating models for geomechanics, geology, geophysics and drilling parameters (hydraulics and torque and drag), and calibration of the same models by using drilling events gathered from offset well analysis (predrill phase) and in real time during the well execution (Execution Phase). Real-time calibration of these models and controlled adjustments to the drilling program during well execution is one of the most critical tasks to ensure positive results with the NDS scheme, but this requires an attitude and alignment from the team for the shared objective of continually improving the drilling practices when drilling the conventional well. A key component is establishing a clear and agreed communication protocol between the multidisciplinary operator and service company team members that include the operating and office based project organization. The severity and potential risk of drilling events are classified and rated by importance with a color coded system. Examples include low ROP, hole cavings, well influxes, unexpected lithology changes, mud losses, BHA vibrations, etc. These events are communicated from the drilling optimization engineers and real-time geomechanics to specific identified team members involved with the decisions based on order of importance and priority. (Figure 6).

This ensures that decisions are taken by the right technical expertise/hierarchy and the adjustments to the drilling program are properly communicated to the rig.

For the Kabilil-1 well, the communication protocol included team members of different disciplines within the operator and service company organization (drilling engineering, geosciences, drilling operations and rig crew). This protocol resulted in an additional benefit by alleviating the additional complexity that team members were not colocated and in different cities.

Good communication and decision-making required a structured methodology.

Predrill planning phase

The NDS workflow applied on the Kabilil-1 well supported PEMEX multidisciplinary workflows, known as visualization conceptualization development (VCD-SE) or front-end loading (FEL) to identify the most critical risks and important considerations during the predrill planning phase by building 3D and 1D MEM with input data from the offset wells Lakach-1, Lakach-2DL, Holok-1, and Labay-1.

After the completion and validation of the MEM, it was determined that drilling close to the salt body resulted in higher than expected collapse pressures at the end of the riser-less section with potential considerable risks to the well construction. Additionally, the model highlighted several potential drilling hazards that required mitigation:

1. Potential well collapse in the 20-in riserless section required optimizing the drilling fluid. If only sea water was used for drilling fluid, there was potential well collapse in the 20-in riserless section and it impeded the ability to set the casing deeper thus achieving a higher fracture gradient for the deeper hole sections.

2. The shear stresses from the salt body influence resulted in narrower mud weight windows for the 20-in and 16-in openhole sections.

3. Potential for well losses due to natural fractured formations were also expected in this interval due to the presence of a reverse fault identified in the 3D geomechanical model.

4. The potential of inadvertently drilling into the salt flank would add complexity to the drilling of the well. It was recognized that the surface seismic model contained uncertainty in the precise location of the salt flank and the planned well trajectory required precise navigation around the salt body.

Preventative measures were incorporated into the predrill well design stage to mitigate the most important hazards. They include

1. The application of the Pump and Dump technique in the riser-less section using a weighted drilling fluid that would minimize the risk of well collapse and also achieve a deeper setting depth for the 20-in casing. This method utilizes a combination of sea water and weighted bentonitic mud as drilling fluid with returns to the seafloor for the entire section.

The method uses mixing devices where the fluid density can be adjusted "on the fly" and results in a homogenous blend with less rig time. The Pump and Dump method has been performed successfully in many deepwater wells, but a principal challenge is the logistics because of the requirement for a large amount of mud storage capacity that is either provided from larger floater rigs or supplemented with supply boat vessels. (P.R Roller, 2001).

2. Steps to optimize well geometry design by using unconventional intermediate casing ODs (16 in and 13 ⅝ in) to allow two additional contingency casing strings (11 ¾ in and 5 ½ in) for the interval with the narrower drilling windows (Figure 7). A detailed decision tree chart was prepared to define whether or not to use the contingency casing strings by analyzing all possible scenarios for wellbore instability at critical depths and formation tops. This well geometry required special under-reaming BHA designs to perform simultaneous hole opening without the need for extra pilot drilling dedicated runs. The stabilization of the BHA was optimized using drilling simulators to minimize drilling vibrations that might adversely affect the LWD tools measurements that are required for petro-physical evaluation and seismic calibration.

3. It was necessary to reduce the depth uncertainties and position the well trajectory around the salt flank and prevent inadvertent drilling into the salt body. The well depth to seismic velocity calibration was performed in real time using a seismic-while-drilling technology for a "bit on seismic" and "look-ahead check shot/VSP" that allowed real-time calibration of the seismic model. The look-ahead capabilities would allow pertinent and early adjustments to the well trajectory to avoid drilling into the salt dome and compromising the final well target. The initial original well trajectory was designed to intersect the zone of interest (pay zone) under the salt, but did not account for the uncertainty of the salt flank extension.

4. Minimize mud losses due to drilling-induced fractures or during the well cementing operations. It was important to maintain a constant equivalent circulating density (ECD) when drilling through the drilling zones with narrow mud weight widows. The solution was to use a flat rheology synthetic oil-based mud system to avoid any pressure surges or spikes that would lead to inadvertent fracturing and mud losses. As an additional preventive measure, lost circulation material was added into the mud system according to a pre-planned decision tree matrix that specified the LCM type and volume under different fluid loss scenarios. For the cementing operations, a foam cement system was chosen as the best option to minimize the ECDs and optimize the cement placement with the objective of reaching full returns during the cementing operations.

5. Formalizing a well-communicated plan would be required to define the potential specific drilling hazards, properly detect upcoming hazards, and identify/implement the mitigation measures. For this purpose, a DrillMAP* drilling and engineering operations plan was created and agreed with each of the drilling project members where the plan was graphically displayed by hole section and an agreed course of action was detailed for each of the well risks.

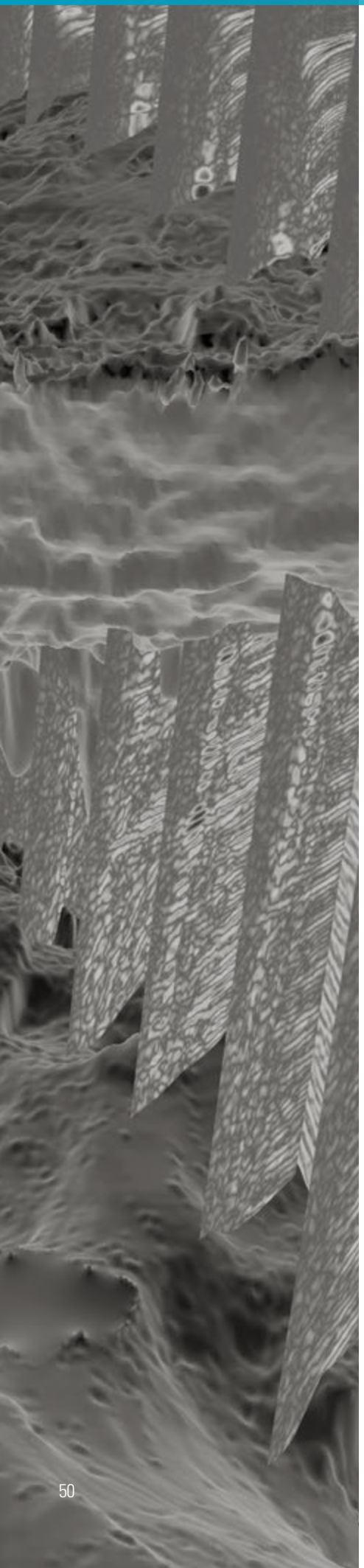

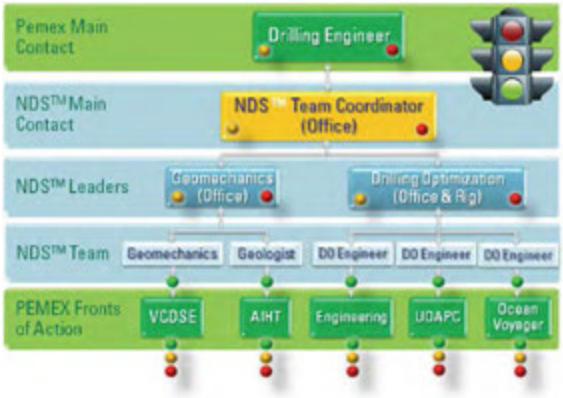

Figure 6: Communication protocol for NDS workflow in Kabilil-1. Five Pemex groups were involved in the well execution.

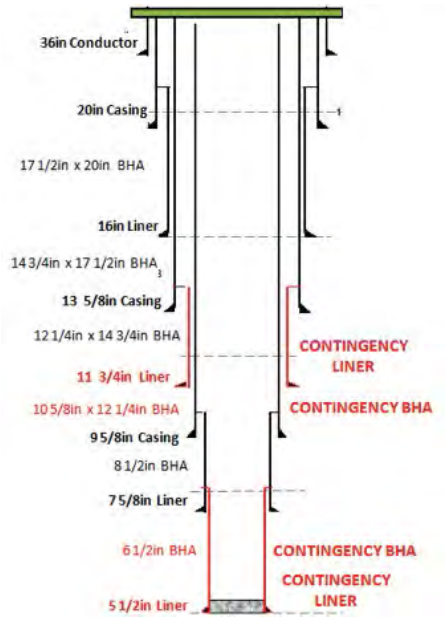

Figure 7: Advanced well geometry design in Kabilil-1 with contingency casings.

Execution-drilling phase

Drilling optimization engineers (offshore) and the geomechanics engineer (onshore) worked together to update the prediction models. They provided support for the real-time drilling geomechanics, and ensured that the measures detailed in the DrillMAP plan were followed.

At the offshore rig site, the responsibility of the drilling optimization engineer was to quality control (QC) and manage the full data flow for the NDS process. Various drilling models (mud hydraulics, torque and drag, and pore pressure) were updated and calibrated using real-time measurements provided by both surface sensors and downhole tools. All of the information was integrated using drilling optimization software that facilitated the data gathering, visualization, and measurement correlation to allow for quick analysis for optimized drilling performance.

Drilling overview
Riserless section—jetting 36-in and 20-in casing

The decision to jet the 36-in conductor casing was based on the shallow-hazard study that showed soft formation 100 m below the sea bed. The drilling ahead tool (DAT) was placed in the 28-in BHA inside the conductor casing to allow drilling ahead of the next section without the need to pull out of the hole to change the BHA.

The drilling plan accounted for industry-recommended practices to minimize conductor deviations from vertical and ensuring that the casing was jetted to programmed depth. (T.J. Akers, 2008). The following summary lists some of these:

1. 36-in X-56 552.7-lb/ft conductor was used to provide enough bending resistance to support the BOP stack.

2. The BHA weight below the drilling-ahead tool (DAT) was kept below 2/3 the weight of the conductor to keep the neutral point below the running tool.

3. Use of a mud motor to help removal of soils with bit rotation, ensure verticality control for the following section and improve ROP with higher mechanical power.

4. Bit space-out of 6 in below the conductor shoe.

5. Reciprocation of every joint.

6. The casing was allowed 3 hours of soaking time prior to releasing the DAT tool to drill ahead.

7. Seawater was used to drill this section with bentonite mud pills of 1.06g/cc.

There were no associated problems and the 30-in conductor was set to the planned depth with a maximum deviation of 1° of inclination.

The 28-in hole was drilled with a conventional steerable motor assembly with a BHA configuration listed in the Table 1. In this section the "pump and dump" technique was used to prevent wellbore stability problems due to high collapse gradient. For this operation, treated seawater was used with the addition of sodium carbonate to improve the bentonite performance. Weighted bentonitic mud (1.7g/cc) was prepared and stored beforehand to avoid any operation interruptions.

The section was drilled to the total programmed depth without any sign of borehole instability or hole cleaning problems. The success of this operation credits the mud rheology employed and the practice of pumping viscous pills of 15 m^3 every stand with high flow rates of (950 gpm) while drilling this section. The heavy pill of 1.38 g/cc was left in the openhole and the BHA was tripped out successfully.

17 ½-in x 20-in hole section—16-in casing

A rotary steerable BHA with a hydraulic hole opener was used to drill the 17 ½-in x 20-in section. Prior to reaching the expected shoe depth, the seawater was substituted with 1.21 g/cc spud mud to drill this interval. After drilling out of the cement/casing float collar and new formation, a leak off test (LOT) was conducted using the annular pressure while drilling tool (APWD) to accurately measure downhole pressures and for accurate LOT determination. The APWD tool measurement and extrapolated interpretation resulted in an equivalent mud weight of EMW of 1.36 gr/cm^3 and breakdown EMW of 1.38 gr/cm^3. An 80 to 20 oil to water ratio was used to approximate the well condition due to the influx of water while drilling necessitating the increasing of the mud weight to 1.33 g/cc. In this section, the drilling optimization engineers closely monitored the ECD, the drilling parameters, and ensured that the hydraulics were adequate for good hole cleaning.

The mud weight required to prevent water influxes was approximating the value of the leak-off pressure test and any pressure surges needed to be avoided from fracturing the formation. The flat rheology mud was critical during this section with a maximum ECD of 1.36 g/cc, just three points above the mud weight.

The total depth of the section was reached in 36 hours. Some tight spots were encountered that were reamed out during the short trips. After the acquisition of wireline logs, a wiper trip was made with a new BHA configuration for enlarging the rat hole from 17 ½ to 20 in. Due to adverse weather conditions, the drilling operations were suspended leaving the drilled hole section in a static condition for several days. When operations resumed, another wiper trip was performed and the 16-in casing was subsequently run and cemented to a planned depth with partial losses of 8.5 m^3.

14 ½-in x 17 ½-in hole section—13 ⅝-in casing

A rotary steerable BHA with a hydraulic hole opener was used to drill the 14 ½-in x 17 ½-in section. For the LOT, an additional 10 m of new formation was drilled. The initial slope change and fracture initiation pressures during the LOT were not observed. The fracture propagation and the initial shut-in pressure were also not observed. The maximum EMW before shutting down the pumps was estimated at 1.64 g/cc and 1.56 g/cc for the minimum stress Sh.

Drilling resumed and the O/W ratio continued to be monitored. Influx of water was determined and corresponding contingency measures of increasing the mud weight resulted with the mud weight gradually increasing from 1.37 g/cc to the final mud weight of 1.44 g/cm^3. While drilling this section, the downhole MWD (measurement while drilling) tool displayed indications of "stick and slip" and high torque conditions were also seen on the surface indicators. It was determined that these were originating from the adverse weather conditions that included large wave heights. This required the rig to activate its heave compensator to minimize the vertical movement due to high sea state, which resolved the problems.

This section also encountered a couple of conditions requiring well control actions. One occurred at the target depth while circulating from the bottom up that resulted in a 3.9 bbl mud pit gain and controlled mud weight of 1.49 g/cc. Another event occurred during a short trip to the shoe with a pit gain of 1.28 bbl and 6,300 ppm of gas, controlled with mud of 1.59g/cc. During the tripping of the 13 ⅝-in casing, 109 m^3 of fluid losses were recorded.

12 ¼-in x 14 ¾-in—9 ⅝-in casing

A rotary steerable BHA with a hydraulic hole opener was used to drill the 12 ¼-in x 14 ¾-in section. The LOT was performed with a 1.59 g/cc mud weight and pressures were recorded with a downhole APWD tool with a resulting EMW leak-off test of 1.74 g/cc. The wellbore was vertically drilled using the rotary steerable tool from the 13 ⅝-in casing shoe to kick off point located 67 m below the shoe. The well was deviated to the programmed azimuth and inclination achieving the required dog leg severity (DLS) of 3.03°/30 m. The remaining long tangent section was drilled to the total depth with a mud weight of 1.67 g/cc without experiencing any hole stability issues. The mud logging information with continuous mud property tracking identified sandy intervals filled with water that affected the oil to water ratio (67/33) that required raising the mud weight to control the water influx. An additional dedicated trip was implemented for the hole enlargement of the pilot hole with a 14 ¾-in Rhino* integrated borehole enlargement system reamer. The 9 ⅝-in casing running operation experienced partial mud losses of 5 m^3 and additional 13 m^3 of partial losses while pumping/cementing.

8 ½-in—Openhole section

The directional drilling of the 8 ½-in hole was conducted with a 1.69 g/cc mud weight. Due to loss circulation problems in the previous sections from induced hydraulic fracturing, an extended leak off test (ELOT) was conducted 13 m below the 9 5/8-in casing. Analysis of the large volume of fluid pumped and shut in was used to determine the fracture closure pressure. The results included closure pressure EMW of 1.86g/cm3, total volume pumped of 10.7 bbls with 2 bbls injected to the formation. (See Figure 8)

Drilling continued increasing mud weight to 1.73 g/cc to account for small changes in the oil-to-water ratio. Drilling continued through the clay stone interbedded with limestone while maintaining the hole inclination at 25.4°.

The calcium carbonate addition was increased to 60 kg/m3 in the mud system to prevent mud losses. Drilling continued in the Lower Eocene formation and the mud weight was increased to 1.77 g/cc before tripping out of the hole. The well was suspended and cement plugs to abandon were placed.

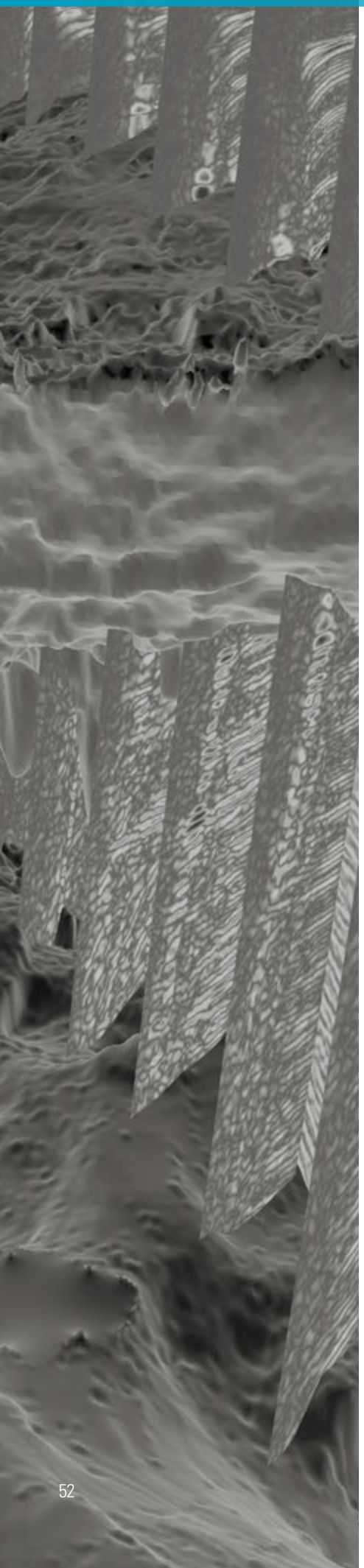

BHA	IN (m)	OUT (m)	DESCRIPTION
Stage I - Conductor 36" & 20" Casing (765m-1533.5m)			
1	763	1533.5	Tricone Bit 28" + Motor F. 9 5/8" (C/stb 27 3/4", BH=0) + Valve C.P. 9 1/2" + Stab 9 1/2" x 28" + ARC-9" (LWD) + TELESCOPE 9" (MWD) + SonicVISION 9" (LWD) + Stab 9 1/2" x 28" + DC Monel 9 1/2" + 2 DC 9 1/2" + combination 7 5/8" Reg-P x 6 5/8" Reg-C + 2DC 8" + 2Drill Ahead Tool.
Stage II - Casing 16" (1533.5m-2132m)			
2	1533.5	2132	PDC Bit 17 ½" + Power Drive 17 ½" + Comb. 7 5/8" Reg (P) x 6 5/8" Reg (C) + stab 17 3/8" + LWD/APWD (ARC) 8" + TeleScope (MWD) 8" + sonicVISION 8" + seismicVISION 8" + Stab 8 x 17 1/2" + 1 DC 8" + Stab 8 x 17 1/2" + Hole Opener Rhino Reamer 20" c/VCP + 1 DC 8" + Stab 8" x 17 1/2" + 4 DC 8" (4 joints) + Jar 8" + 1 DC 8" + Combination 6 5/8" Reg P x 5" XH C + 3 DC 6 1/2" + 3 Ling. TP HW 5" + 60 DP 5" S-135, 25.6 lb/ft
Stage III - Casing 13 5/8" (2132m - 3402m)			
3	2132	3402	PDC Bit 14 1/2" + PowerDrive 14 1/2" + Stab 14 3/8" + ARC-8 (LWD / APWD) + Telescope 8" (MWD) + sonicVISION 8" + SeismicVISION 8" + stab 14 1/2" + 1 D.C. Monel 8" + stab 14 1/2" + Hole opener RhinoReamer 17 1/2" c/VCP, (Tob 2x8) + 1 Drill Collar 8" + stab 8" x 14 1/2" + 2 Drill Collars 8" + Jar 8" + 1 Drill Collar 8" + Comb. 6 5/8" Reg P x 5" XH C + 3 Drill Collars 6 1/2" + 9 HWDP 5".
Stage IV - Liner 9 5/8" (3402 - 4565 m)			
4	3402	4565	PDC Bit 12 1/4" + PowerDrive 12 1/4" C/Gamma-Ray + ReciverPD Stab 12 1/8" + ARC-8 (LWD / APWD) + Telescope 8" (MWD) + sonicVISION 8" + ADN-8 w/stab 12"+ 1 D.C. Monel 8" + stab 12 1/4" + hole opener Rhino @ 14 3/4" c/VCP + 1 Drill Collar 8" + stab 8" x 12 1/4 + 2 Drill Collars 8" + jar 8" + 1 Drill Collar 8" + Comb. 6 5/8" Reg P x 5" XH C + 3 Drill Collars 6 1/2" + 9 HWDP 5"
Stage V - Open Hole (4565 - 5350 m)			
5	4565	5350	PDC Bit de 8 1/2" + PowerDrive de 6 3/4" c/Gamma Ray + Receiver Liso c/VCP + EcoScope 6 ¼ c/Estab. 8 1/4" + MWD de 6 3/4" + SonicVISION + stab 8 1/2" + 1 DC Monel de 6 3/4" + 2 DC de acero 6 1/2" + 9 TP HW 5" + Jar 6 1/2" + 9 TP HW 5"

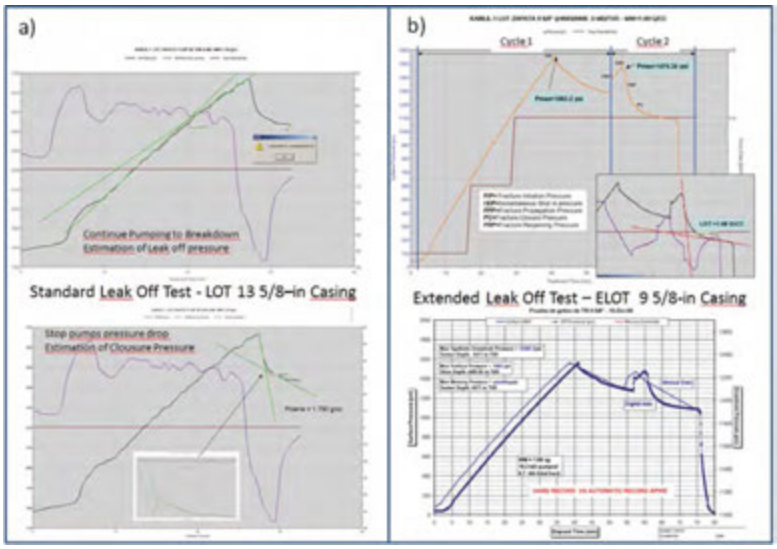

Figure 8: a) Standard LOT 13⅝-in casing shoe b) Extended LOT 9⅝-in casing shoe. Both tests were recorded with APWD. With this deepwater operation, the ELOT provided more accurate fracture pressure detection, thereby mitigating loss circulation problems.

Logging while drilling

Seismic vision while drilling (SVWD): Real-time VSP

In an effort to mitigate some of the challenges and uncertainties identified in the predrill planning of this subsalt well, the seismic while drilling service was implemented to acquire depth-velocity information in real time. A real time look-ahead-of-bit check shot and VSP was acquired in the interval between 1,500 m to 2,200 m, (16-in casing) and a salt proximity survey was conducted in the 13⅝-in casing section. The results obtained in the feasibility study confirmed that seismic-while-drilling can be a valuable tool for resolving drilling uncertainties. Different source positions were tested with several azimuths to identify the best position in which to confine the ray path to a 2D plane (to constrain the inversion) to guarantee that the energy will transmit through the salt and arrive at the sensors. Based on the results obtained through this exercise, it was determined that the optimal source was at 2,700 m with an azimuth of 270° (Figure 9).

Before recommending the seismic-while-drilling technology to resolve the uncertainties of drilling this complex well, it was necessary to perform a feasibility study. This study consisted of simulated data acquisition with the information available and building a 3D model with geological information such as: interpreted horizons, velocity from surface seismic, density values, and the well deviation. The study was performed for two different applications: 1) salt detection below the drill bit and 2) determine salt proximity to the well trajectory. Full technical descriptions of these models can be found in Sanchez, A et al. (2010).

Checkshot and VSP look-ahead-of-the-bit 16-in section

The proposed seismic-while-drilling technology was implemented for drilling the interval between 1,500 m to 2,200 m that corresponds to the 16-in casing section.

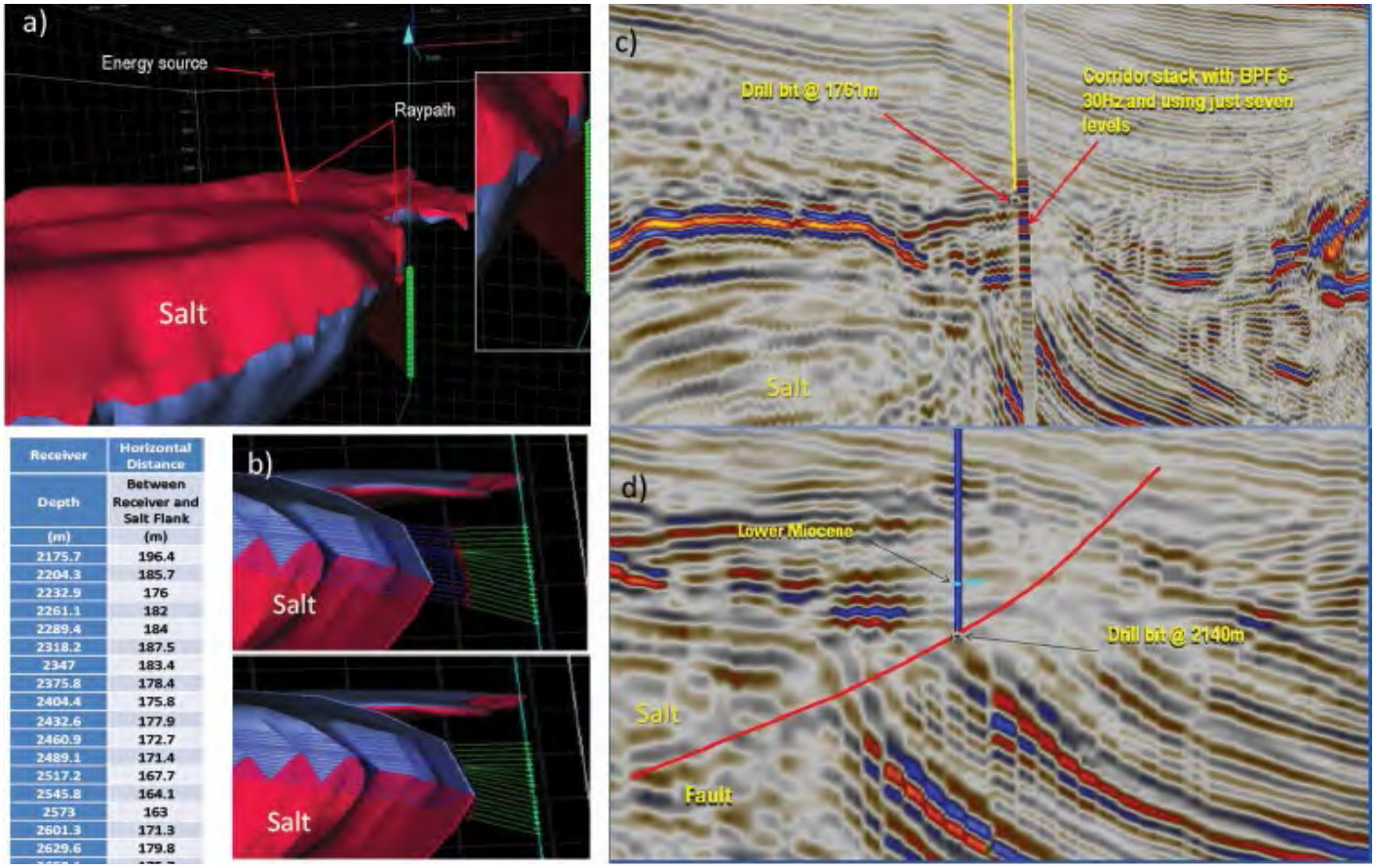

Receiver Depth (m)	Horizontal Distance Between Receiver and Salt Flank (m)
2175.7	196.4
2204.3	185.7
2232.9	176
2261.1	182
2289.4	184
2318.2	187.5
2347	183.4
2375.8	178.4
2404.4	175.8
2432.6	177.9
2460.9	172.7
2489.1	171.4
2517.2	167.7
2545.8	164.1
2573	163
2601.3	171.3
2629.6	179.8

Figure 9: a) Salt proximity results (red dots) vs. model interpretation. Salt flank from interpretation vs. salt proximity. b) Interpreted salt was moved to adjust with salt proximity results. The table shows the distances between salt flank and well position for each recorded station. c) Surface seismic section showing the match with the real-time VSP and the drill bit position. d) Defining the fault position for setting the 16-in casing before drilling the sediments with upward dips.

Real-time checkshots analysis (time-to-depth relationships) were conducted to update the drill bit position on the seismic map. Transmitting the first five levels in real time made it possible to initiate the VSP processing and look ahead to obtain a corridor stack below the drill bit. The VSP data below the drill bit showed homogenous reflections and not the strong amplitude expected for salt presence, identifying a sequence of clastic sediments (not very strong amplitude changes) instead of the salt body.

The drilling continued and the next challenge was to set the 16-in casing at the right position just below the expected fault plane. The real-time checkshot made it possible to accurately map the drill bit position on the seismic section and with the measured velocities it was possible to estimate the distance from the current drill bit position to the fault plane (Figure 9). When the drilling resumed, the fault zone was estimated to be located at 2,080 m and the sequence of sediments dipping upward was estimated to be at 2,140 m. This information was shared with the drilling engineers and was used to decide when to stop drilling for the 16-in casing and to avoid encountering drilling problems crossing the mapped fault plane on the seismic section. The mud weight was another consideration because it had reached its maximum allowable weight and did not leave any room for increasing mud weight contingency if the formations below the faults were of subsequent higher or abnormal pressure.

Salt proximity survey: 13 5⁄8-in section

The suggested acquisition interval for the entire section was between 2,200 m and 3,400 m. A total of 18 levels/shots between 2,175 m to 2,658 m were acquired. To perform the inversion and compute the salt flank location, the 3D velocity model was constrained with the new information available.

The salt velocity was assumed to be 4,500 m/s from previous measurements of salt bodies; the water velocity used of 1,500 m/s; and the velocity for the sediments above the salt dome were determined from the check shot survey acquired in the previous section using the seismic-while-drilling tool. The results obtained showed that the well was closer than expected to the salt dome with an approximate minimum distance of 200 m.

Real-time logging while drilling

LWD tools were selected for initial formation evaluation and real-time pore pressure prediction using LWD resistivity and sonic data. Sonic was added to the logging suite to measure the formation velocity for seismic correlation with the seismic model.

Real-time petrophysical modeling

In order to provide optimal decision making in real time, a formation evaluation logging suite was implemented in the 9 ⅝-in and 8 ½-in openhole sections. Petrophysical information provided by the LWD tools was the basis for decisions on whether further data acquisition was required for each target zone. The coring schedule was amended when the zone was determined non-feasible. The adnVISION* azimuthal density neutron service and the EcoScope* multifunction logging-while-drilling service were included in the BHA3 and BHA5 (Figure 10) to acquire resistivity, porosity, and lithology petrophysical information, and for calibration of the geomechanics model. The density image was obtained from the measurements and the detailed images identified sand/shale sequences, heterogeneous formations, structural dips, and formation washouts. The ultrasonic and bulk density measurements were used to determine the hole diameters.

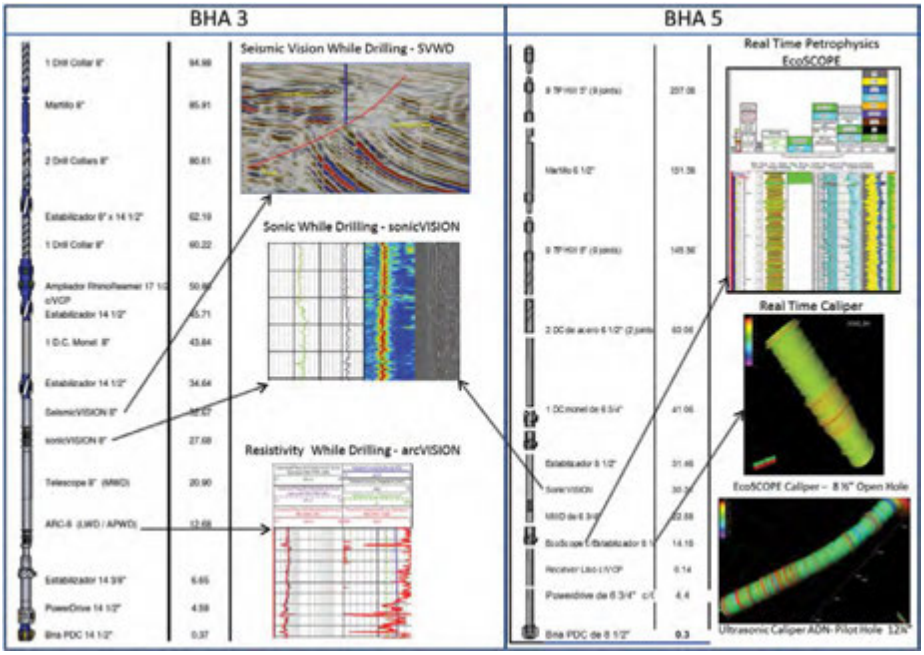

Figure 10: Example of the BHA3 and BH5 designed to obtain a complete suite of LWD measurements useful to provide formation evaluation and real-time geomechanics surveillance.

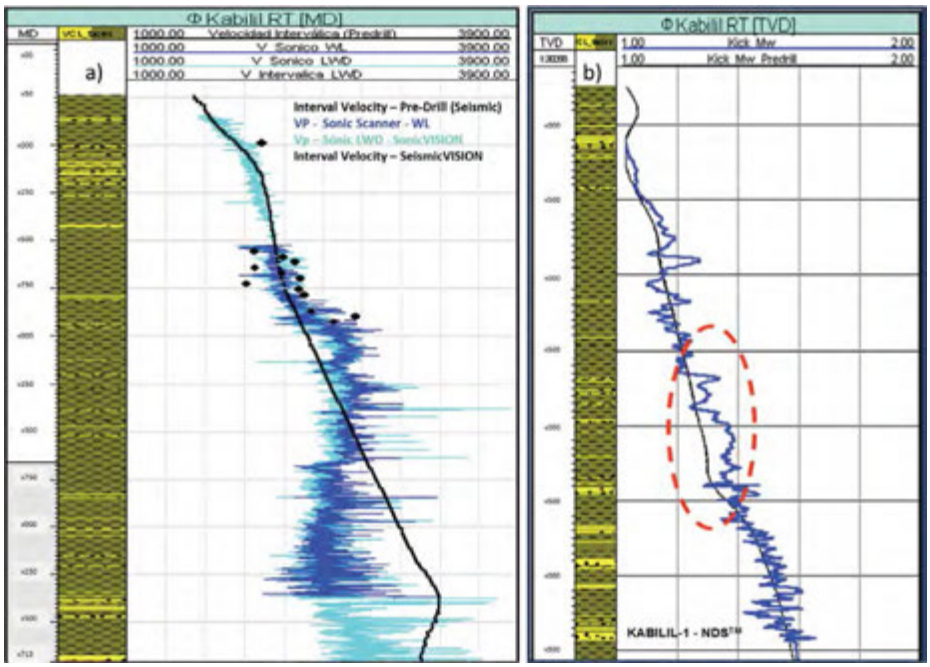

Figure 11: a) Four distinct sources of interval/acoustic velocity were acquired in the predrill phase and in real time. b) Pore pressure profile calculated in the pre drill model (black curve) vs the final pore pressure (blue curve) estimated in real-time. Notice some discrepancies that were not reproduced in the initial model.

Real-time sonic modeling

Compressional transit time derived from LWD sonic was used to calculate the pore pressure profile based on the sonic log using the Eaton and Bower´s methods. The shear transit time was obtained from wireline Sonic Scanner* acoustic scanning platform logs and empirical relationships were created for the well location in the predrill model. Four sources of sonic data were available in the predrill and real time phase: the interval seismic velocity extracted from the prestack velocity model, the interval velocity derived from the seismic-while-drilling tool, the LWD sonic velocity, and the wireline sonic velocity acquired by the Sonic Scanner platform. This information, and the LOT/ELOT pressure tests performed in the well, allowed the geomechanics engineers to calibrate the MEM and calculate a complete wellbore stability model that included a reliable collapse pressure (breakout). This complemented the 3D modeling work that was performed in the predrill planning stage.

Conclusions

In summary, the Pemex Kabilil-1 well results demonstrated the ability to drill a challenging subsalt well that faced many potential drilling problems. The application of new technologies, effective predrill modeling, workflows, and real-time monitoring resulted in exceptional drilling performance. The lessons learned and the new teamwork achieved with this first subsalt Mexican well have improved working performance between the operator, rig contractor, and the service companies. PEMEX has drilled 18 wells in deep water and 4 wells in ultradeep water where water depths are approaching 3,000 m.

References

Aguilera, L.E. et al., "Geomechanics and Pore Pressure Considerations for Successful Deep-water Exploration Drilling," paper SPE WVS 040 South American Oil and Gas Congress, organized by the SPE Western Venezuela Section, held in Maracaibo, Venezuela, between October 18–21, 2011.

Sanchez, A, Mora, A. Aguilera, L.E, Gaitán, R., "Minimizing Drilling Risks for Exploration Well in Deep Water Using Seismic While Drilling Technology," in Rio Oil & Gas Expo and Conference 2010, held in in Rio de Janeiro, Brazil between September13–16, 2010.

Plazas, L, "Implementation of No Drilling Surprises (NDS) Services in Deep Water Mexican Gulf of México," internal Schlumberger GFE Project 1 April 2010, Mexico City-Mexico, 2010.

P.R. Roller, "Using Conventional and Unique Methods to Drill a Technically Demanding Shallow Flow Zone," Paper presented at the SPE/IADC Drilling Conference, February 27–March 1 2001, Amsterdam, Netherlands, SPE/IADC 67773-MS

T.J. Akers, "Jetting of Structural Casing in Deep Water Environments: Job Design and Operational Practices," March 2008. SPE-102378.

Victor Gerardo Vallejo A (Pemex), Epitacio Solis Fuentes, (Pemex), Aciel Olivares, (Pemex), Leonardo E Aguilera G, (Pemex), Manuel E. Torres V, (Schlumberger), Luis Felipe Gonzalez, (Schlumberger)

Find out more at
www.slb.com/deepwater

Schlumberger regularly sends e-mail updates
on a wide range of domain and technical challenges.
Sign up at www.slb.com/stay_informed